MINIATURE HOMOGENEOUS CHARGE COMPRESSION IGNITION FREE-PISTON ENGINE COMPRESSOR

A DISSERTATION

SUBMITTED TO THE FACULTY OF

UNIVERSITY OF MINNESOTA

BY

LEI TIAN

IN PARTIAL FULFILLMENT OF THE REQUIREMENTS

FOR THE DEGREE OF

DOCTOR OF PHILOSOPHY

ADVISORS:

DAVID B. KITTELSON

WILLIAM K. DURFEE

JUNE 2013

Acknowledgements

This research was supported by the Center for Compact and Efficient Fluid Power, a National Science Foundation Engineering Research Center funded under cooperative agreement number EEC-0540834.

Abstract

Utilizing the high energy density of hydrocarbon fuels, an internal combustion engine based free-piston engine compressor is a promising solution as a power supply for miniature size mobile fluid power applications. A free-piston engine is a type of engine without crankshaft, and piston motion depends on force balance instead of mechanical constraints. Homogeneous charge compression ignition (HCCI) is a combustion mode in which homogeneous fuel air mixture is compressed to the point of auto-ignition. The objective of the thesis work is building a miniature size engine compressor to work as a compact fluid power supply, while combining the HCCI and free-piston engine configuration.

Mathematical models for components were calibrated and verified by components testing. The overall engine compressor model correlated well with testing results of a proof-of-concept prototype. Although the prototype only achieved 0.6% overall efficiency from fuel energy to cooled compressed air because of poor compressor efficiency and high fuel short circuiting loss, the miniature free-piston engine compressor showed the potential to be a high energy density, compact fluid power supply.

Table of Contents

List of Tables ---------- vi

List of Figures ---------- v

Nomenclature ---------- xii

1 INTRODUCTION 1

1.1 Motivation 1

1.2 Project objective statement 3

1.3 Significance of work 4

2 LITERATURE REVIEW 5

2.1 Free-Piston Engine 5

2.2 Homogeneous Charge Compression Ignition 13

3 DESIGN CONCEPT AND PRELIMINARY MODELING 20

3.1 Free-piston engine configuration design 20

3.2 Preliminary design concept 22

3.3 Preliminary simulations 23

4 MODEL ENGINE COMPONENT TESTING AND MODELING 44

4.1 Relevance of model engine testing 44

4.2 Brief overview of model engines 46

4.3 Test setup 48

4.4 Test results and component models 53

4.5 Conclusions 73

5 FREE-PISTON ENGINE COMPRESSOR MODELING AND MODEL BASED DESIGN 75

5.1 Free-piston engine compressor sub-models 76

5.2 Engine compressor overall model 80

5.3 Using models to determine target engine speed 81

5.4 Free-piston engine parameters 82

5.5 Simulated engine operation 83

6 PROTOTYPE TESTING AND MODEL VALIDATION 87

6.1 Generation I engine prototype 87

6.2 Prototype generation II design 89

6.3 Prototype testing and model validation 93

6.4 Conclusion 112

7 SUGGESTED FUTHER WORK 114

REFERENCES 116

Appendix A ..... Review of two-stroke engines 126

Appx. A.1 Engine cycles: Two stroke & four stroke 126

Appx. A.2 Two stroke engine charging methods 128

Appx. A.3 Two stroke engine scavenging systems 130

Appx. A.4 Implications of two stroke engines in this project 132

Appendix B ..... Prototype hardware problems 133

Appx. B.1 Piston-cylinder clearance, and piston scuffing and wear 133

Appx. B.2 Fuel delivery during start up 136

Appx. B.3 Rubber bumper fatigue and crack 138

Appx. B.4 Compressor valve fatigue 140

Appx. B.5 Spring sag 141

Appendix C ..... List of materials and parts in experiments 142

Appendix D ..... Pictures of test benches 145

Appendix E ..... Prototype standard operating procedure 148

Appx. E.1 Standard operating procedure: background: 148

Appx. E.2 Standard operating procedure: experimental Procedures: 149

Appx. E.3 Standard operating procedure: hazard Identification: 150

Appx. E.4 Exposure Assessment: 152

Appx. E.5 Control Plan: 152

List of Tables

Table 1-1 Design metrics of Test Bed 6 1

Table 3-1 Model diesel fuel content 33

Table 3-2 Free-piston HCCI engine compressor ballpark parameters determined by preliminary simulations 35

Table 3-3 Crankcase induction reed check valve parameters 37

Table 4-1 Specifications of AP .09 model aircraft engine 49

Table 6-1 Combustion analysis results of three cycles 104

Table 6-2 Modeling results of four cycles with different HCCI ignition threshold .. 112

List of Figures

Figure 1-1 CCEFP Ankle Foot Orthosis (CCEFP, 2012) 1

Figure 1-2 Actuator power/weight ratio and energy source energy/weight ratio comparison (Krivts & Krejini, 2006) 2

Figure 1-3 Efficiency target of engine compressor (based on Riofrio & Barth 2003, Barth & Riofrio 2004)) 4

Figure 2-1 Crankshaft two stroke engine operation 7

Figure 2-2 Generalized free-piston two stroke engine operation 8

Figure 2-3 Single piston configuration 8

Figure 2-4 Dual piston free-piston engine 9

Figure 2-5 Opposed Piston free-piston engine configuration 10

Figure 2-6 Spark ignition 14

Figure 2-7 Compression ignition 15

Figure 2-8 HCCI combustion 16

Figure 3-1 Mechanical spring fatigue strength (Lesjofors 2009) 21

Figure 3-2 Design concept of the engine 22

Figure 3-3 Speed, compression ratio and cylinder bore when aspect ratio = 1 25

Figure 3-4 Compression ratio, aspect ratio and bore size when engine speed = 300Hz 26

Figure 3-5 Actual versus geometric compression ratio for several engine speeds ... 30

Figure 3-6 CHEMKIN simulation result of HCCI ignition in different compression ratio and inlet temperature, at engine speed 18000 rpm 31

Figure 3-7 Ignition curves for various rules showing the compression ratio required to ignite as a function of engine speed. 33

Figure 3-8 Operating range for model diesel fuel in HCCI mode 34

Figure 3-9 Reed check valve induction system for a model engine 36

Figure 3-10 Reed valve vibration simulation at full lift 38

Figure 3-11 FLUENT mesh for reed valve flow simulation.....39

Figure 3-12 FLUENT simulated flow coefficient related with reed valve lift 39

Figure 3-13 CFD simulated pressure on reed valve sealing surface, left: during inflow into the crankcase, right: during backflow from the crankcase.....40

Figure 3-14 Reed valve response in a two stroke crankshaft engine at 18000rpm.....41

Figure 3-15 Delivery ratio and engine power of a two stroke engine with reed check valve induction system 42

Figure 4-1 AP .09 model aircraft engine cut-away view 46

Figure 4-2 Model engine dyno test bench with data acquisition (DAQ) system.....52

Figure 4-3 Model engine motoring test bench for leakage measurement.....53

Figure 4-4 Pressure trace versus crank angle degree in seven consecutive cycles (A crank angle of 0 indicates TDC) 54

Figure 4-5 Engine characteristics with carburetor on 4.5 turns and wide open throttle55

Figure 4-6 Model engine indicated efficiencies at different carburetor needle valve setting.....55

Figure 4-7 Engine indicated efficiency and power output related with A/F ratio 56

Figure 4-8 Cyclic variation related to the start of combustion 56

Figure 4-9 Model engine air induction versus engine speed 57

Figure 4-10 Motoring pressure trace at various speeds to study leakage 58

Figure 4-11 logP-logV plot for engine motoring 59

Figure 4-12 Leakage model and comparison with experimental data from engine motoring 60

Figure 4-13 Mechanical efficiency of the engine 61

Figure 4-14 Crankshaft speed based friction model and experimental data comparison 62

Figure 4-15 logP-logV plot of a cycle, at 10236 rpm, carburetor 4 turns 64

Figure 4-16 Comparison of mass fraction burned calculated from heat release analysis and burn rate analysis, at 10236 rpm, carburetor 4 turns 65

Figure 4-17 Comparison of start of combustion from simulation, and from combustion analysis of experimental data 67

Figure 4-18 Combustion duration at various speeds 68

Figure 4-19 Comparison of model engine heat release experimental data and model results, carburetor at 4 turns 69

Figure 4-20 Simulation and experimental results of model engine scavenging 70

Figure 4-21 Distribution of charging efficiencies of 181 cycles 72

Figure 5-1 Model components in the engine compressor 76

Figure 5-2 Engine Compressor overall model in SIMULINK 80

Figure 5-3 Trade off of several efficiencies with engine speed 81

Figure 5-4 Simulation of engine compressor starting and operating 84

Figure 5-5 Simulation of engine compressor piston position trace in consecutive cycles.....84

Figure 6-1 Pro-E design cutaway and fabricated prototype gen I 88

Figure 6-2 Prototype gen I components.....88

Figure 6-3 Free-piston engine compressor design cutaway and prototype gen II 89

Figure 6-4 Some components of prototype gen II 89

Figure 6-5 Double-jaw seal plates for sealing against connecting rod 91

Figure 6-6 Design of prototype compressor side intake and output check valves.....91

Figure 6-7 Rubber bumper in prototype gen II.....92

Figure 6-8 Pistons and connecting rod assembly of prototype gen II with dead weight.....92

Figure 6-9 Experimental testing apparatus 94

Figure 6-10 Startup behavior of miniature free-piston engine (TO: transfer port open) 95

Figure 6-11 Prototype engine compressor charging up a 530mL reservoir.....95

Figure 6-12 Engine operating frequency with different piston assembly mass, at 4.8 bar compressor output pressure 96

Figure 6-13 Piston position-speed diagram of 9 consecutive cycles at engine startup 98

Figure 6-14 Piston position-speed diagram of a typical cycle of experimental data at steady state running, compared with modeling result of free-piston engine and a crankshaft engine 99

Figure 6-15 Compressor output flow rate at various output pressure and comparison with the model.....100

Figure 6-16 Energy balance in free-piston engine compressor at 4.5 bar compressor output (model results) 101

Figure 6-17 Analysis of bumping in the free-piston engine compressor prototype ..102

Figure 6-18 Heat release analysis result of three cycles.....104

Figure 6-19 Pressure volume log-log diagram of three cycles 104

Figure 6-20 Cycle thermal conversion efficiency related with Mass fraction burned at TDC, of 570 cycles, with 34.3 grams piston assembly at 4.8 bar compressor pressure output.....105

Figure 6-21 Pressure volume log-log diagram for 12 cycles in free-piston engine compressor with 34.3 grams piston assembly at 4.8 bar compressor output, and comparison with crankshaft engine 106

Figure 6-22 Pressure volume diagram for glow ignition free-piston engine experimental result and model prediction, with 34.3 grams piston assembly at 4.8 bar compressor output.....107

Figure 6-23 Pressure volume diagram from glow ignition and HCCI model results109

Figure 6-24 Compression ratio versus mass fraction burned at TDC of 570 cycles, with 34.3 grams piston assembly at 4.8 bar compressor output 110

Figure 6-25 P-V log-log diagrams of four cycles with different ignition timing in a HCCI free-piston engine.....111

Figure 6-26 Compression ratio versus ignition timing in a HCCI free-piston engine, modeling results (EC: exhaust port closed) 111

Nomenclature

η	Efficiency
η_{ch}	Charging efficiency
$\eta_{fc,i}$	Indicated fuel conversion efficiency
η_{m}	Mechanical efficiency
Λ	Delivery ratio
τ	Ignition delay time
ρ	Density
ρ_{i}	Inlet air density
Φ	Equivalence ratio
μ	Viscosity
σ	Boltzmann constant
a	Vibe function coefficient
A_C	Combustion chamber piston area
A_R	Rebound chamber piston area
A_{CC}	Heat transfer area
A_{reed}	Reed valve surface area
c_p	Specific heat capacity at constant pressure
c_v	Specific heat capacity at constant volume

e_C	Lower heating value of fuel
F_L	Load on engine piston set
F_O	Fourier number
F_P	Pressure force on reed valve
F_{spring}	Rebound spring force
F_S	Stoichiometric fuel air ratio
$\tilde{h}$	Convection heat transfer coefficient
k	Thermal conductivity
L	Characteristic length
m	Vibe function coefficient (in 3-10)
$m_{c.v.}$	Mass inside control volume
m_p	Piston mass
r	Compression ratio
P_{BR}	Brake power of engine
P_{cc}	Combustion chamber pressure
P_c	Crankcase pressure
P_{comp}	Compressor chamber pressure
P_{atm}	Atmosphere pressure
ΔP	Pressure difference
R	Gas constant

S	Stroke
T	Combustion chamber temperature
T_{atm}	Atmosphere temperature
t_o	Ignition time (start of combustion)
Δt	Combustion duration
$\dot{Q}$	Heat transfer rate
U_P	Piston speed
V_{swept}	Swept volume
W	Engine power
$\dot{W}$	Work transfer rate
x_{reed}	Reed lift
x	Fuel consumption percentage
x_{piston}	Piston position

rpm	revolutions per minute
cpm	cycles per minute
AFO	Ankle foot orthosis
ATDC	After top dead center
BTDC	Before top dead center
BDC	Bottom dead center
BMEP	Brake mean effective pressure

CFD	Computational fluid dynamics
CAD	Crank angle degree
CCEFP	Center for Compact and Efficient Fluid Power
CI	Compression ignition
CNC	Computer numerical controlled
EGR	Exhaust gas recirculation
EO	Exhaust port open
EC	Exhaust port closed
HAL	Hybrid Assistive Limb
HCCI	Homogeneous Charge Compression Ignition
IMEP	Indicated mean effective pressure
KE	Kinetic energy
PE	Pressure potential energy
SI	Spark ignition
TB6	Test bed 6
TDC	Top dead center
TO	Transfer port open
TC	Transfer port closed

1 INTRODUCTION

1.1 Motivation

CCEFP is a seven university research consortium headquartered at the University of Minnesota. The vision of CCEFP is to transform fluid power so that it is compact, efficient and effective. This will benefit the technology community by significantly reducing energy consumption and spawning new industries.

CCEFP is developing a compact, untethered ankle foot orthosis (AFO) as a test bed for new technologies in tiny fluid power (Figure 1-1). The ankle foot orthosis is a medical assistive device that can provide the torque necessary to enable or facilitate movement of the patient's impaired ankle for normal walking.

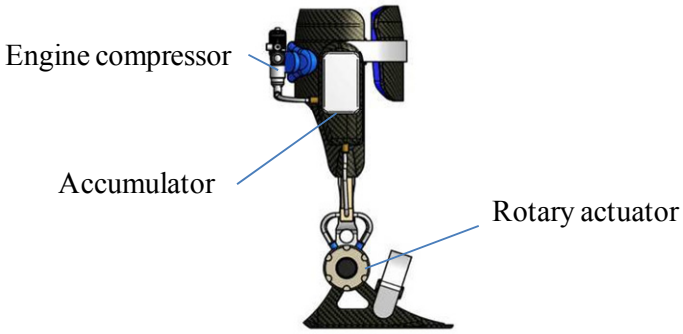

Figure 1-1 CCEFP Ankle Foot Orthosis (CCEFP, 2012)

1.1.1 Different design matrices of Test Bed 6

The CCEFP Test Bed 6 team had specified several goals of the development of TB6 as listed in Table 1-1.

Table 1-1 Design metrics of Test Bed 6

Metric #	Design aspect	Goal
1	Power applied	10-100 W

2	Weight	System < 1 kg
3	Untethered run time	2 hr

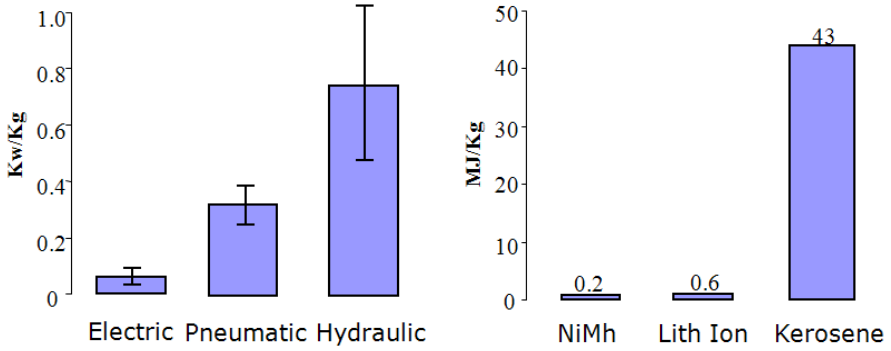

Figure 1-2 Actuator power/weight ratio and energy source energy/weight ratio comparison (Krivts & Krejini, 2006)

Figure 1-2 is a comparison of actuator power/weight ratio and energy/weight ratio for typical electrical and fluid power systems, which shows that fluid power actuators have more potential in realizing compact high power actuation and that hydrocarbon fuels have far more superior energy density than existing batteries. As a result, compared with battery-motor package which is the major competing technology with the project, a fuel-engine-compressor package has potential advantages of lighter weight of actuators, longer run time, simpler transmission and better packaging. Disadvantages include heat, noise, emission and vibration problems associated with engines.

Test Bed 6 team's investigation concluded that for satisfying design matrices of Test Bed 6, internal combustion engine-fluid power package is promising to achieve the weight and run time requirements.

1.2 Project objective statement

The objective of this thesis project was to develop a compact, low power fluid power supply that can be used for the a portable ankle foot orthosis (AFO) and other miniature size low power mobile fluid power devices.

Specifically, the goal was to develop a compact, high efficiency air compressor that provides about 20 W of continuous pneumatic power. The power source is a free-piston engine operating in a homogeneous charge compression ignition (HCCI) two stroke cycle, integrated with a free-piston air compressor.

The major advantages of the fuel-engine compressor package include high power-weight ratio and energy weight ratio. Thus the package will help the Test Bed 6 meet its metric 2 (weight < 1kg). Specifically, the engine compressor, fuel and fuel tank are expected to weigh less than 400 grams. The size of the engine compressor is expected to be smaller than 50 mm by 50 mm by 150 mm.

As the Test Bed 6 requires about 10 W power on average on the ankle (Winter, 2005), the power requirement of the engine compressor depends on the efficiencies of actuators. In this project, the actuator efficiency was assumed to be around 50%. Thus, the engine compressor fluid power output target was set to be about 20 W, in cooled compressed air form.

The lower efficiency of fuel - engine compressor - fluid power package compromises its high energy density advantage over battery motor package. The efficiency of the proposed engine compressor package should be better than a target value to deliver considerably better energy density than battery motor package.

A comparison of the system to a battery motor package determines the target efficiency of the engine compressor to be 4.6%, from fuel energy to pressure energy of cooled compressed air (Figure 1-3).

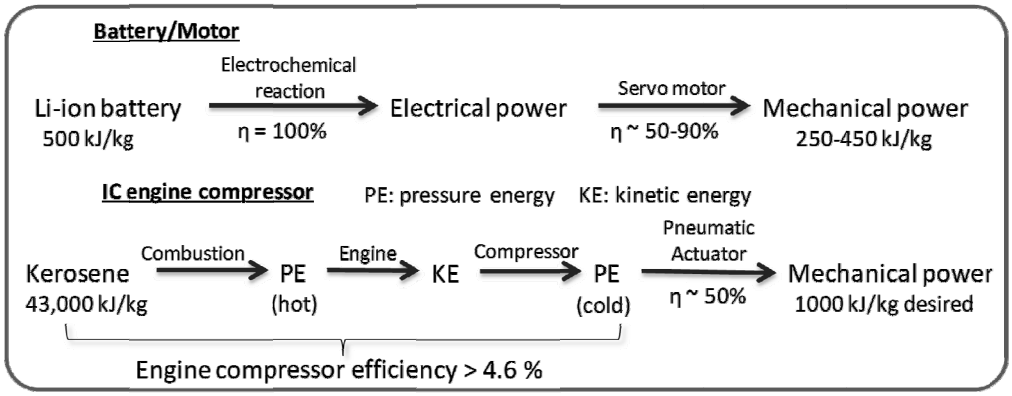

Figure 1-3 Efficiency target of engine compressor (based on Riofrio & Barth 2003, Barth & Riofrio 2004))

1.3 Significance of work

The thesis work investigated the area of internal combustion engines in small scale (about 1 cc displacement). Unique characteristics of tiny engines were investigated by theoretical research, modeling and experiments. The research is beneficial for areas related to small scale engines.

The project explored the possibility of compact, tiny scale pneumatic power supply, which is essential for tiny fluid power systems such as CCEFP Test Bed 6. The fluid power – internal combustion engine pneumatic power supply package was proved with potential to provide much higher power and energy density than battery-motor package, and enable mobile fluid power devices to be more compact and run longer.

2 LITERATURE REVIEW

An internal combustion (IC) engine is a type of engine in which fuel oxidation and energy release occur in a combustion chamber which is an integral part of the working fluid flow (Heywood 1988). Classified by method of ignition, IC engines include spark-ignition, compression-ignition and homogeneous charge compression ignition (HCCI) engines, which are reviewed in section 2.2. By working cycles there are four stroke and two stroke engines which are reviewed in Appendix A. The free-piston engine is a unique engine internal mechanism design which is reviewed in the next section.

2.1 Free-Piston Engine

A free-piston engine is a type of internal combustion engine that has no crankshaft. Without the kinematic constraint of a crankshaft, the movement of the piston is dynamically driven by pressure in the combustion and compressor chambers, and rebound spring force. A rebound device such as a gas spring, metal spring or hydraulic accumulator is used to store energy for next cycle's in-cylinder charge compression of the engine side. Two-stroke cycle combustion is usually used.

Compared to a crankshaft engine, the free-piston configuration is more compact and simpler, with fewer moving parts and no side thrust between piston and cylinder wall. Large free-piston engine air compressors were developed before, for example, by Pescara (1928), Neumann (1935), and Braun (1973). The biggest challenge for free-piston engine is precisely controlling the piston motion to ensure efficient scavenging, correct compression ratio and ignition timing (Milkasen & Roskilly 2007).

Recently, attention had been paid to developing small free-piston engines. Riofrio, et. al (2002) designed and prototyped a free liquid-piston engine compressor targeting at 100 W fluid power output. Aerodyne Research Inc. designed and manufactured 10 W and 500 W miniature engine-generators, which are two-stroke free-piston engines coupled to linear alternators (Annen et. al 2006). Their tests showed 16% thermal efficiency. Aichlmayr, et. al. proposed a miniature free-piston engine coupled with homogenous charge compression ignition (HCCI) combustion, and experimentally demonstrated that HCCI can occur in a 3 mm bore cylinder, circumventing the flame quenching problem in small space (Aichlmayr 2002).

The engine compressor in this project utilizes free-piston engine configuration for two reasons. (1) Friction is one of the dominant effects in small engines. The free-piston engine configuration is much simpler and results in less friction, compared to crankcase-engine-compressor design. (2) Free-piston engine coupled with HCCI is a good solution for miniature size engine for its simplicity and easy hardware implementation, as discussed in the review on HCCI in later chapter 2.2.

2.1.1 Free-piston engine versus crankshaft engine: operating principle

In a crankcase engine the piston's motion is converted to rotating motion by the connection rod – crankshaft mechanism, to drive work machines with shaft power output. In contrast, the free-piston engine is a combustion engine whose piston reciprocating motion directly drives a work machine, thus the piston is free of kinetic restraint of the crankshaft (Braun 1973, Achten 1994).

In a two stroke crankshaft engine, the piston is connected to a crankshaft and a flywheel which stores some energy during the powering stroke when the piston moves from top dead center (TDC) towards bottom dead center (BDC). During scavenging and compression, the stored energy powers the piston, and the cycle can

be completed, as shown in Figure 2-1. The engine outputs energy to load devices via shaft work at the crankshaft.

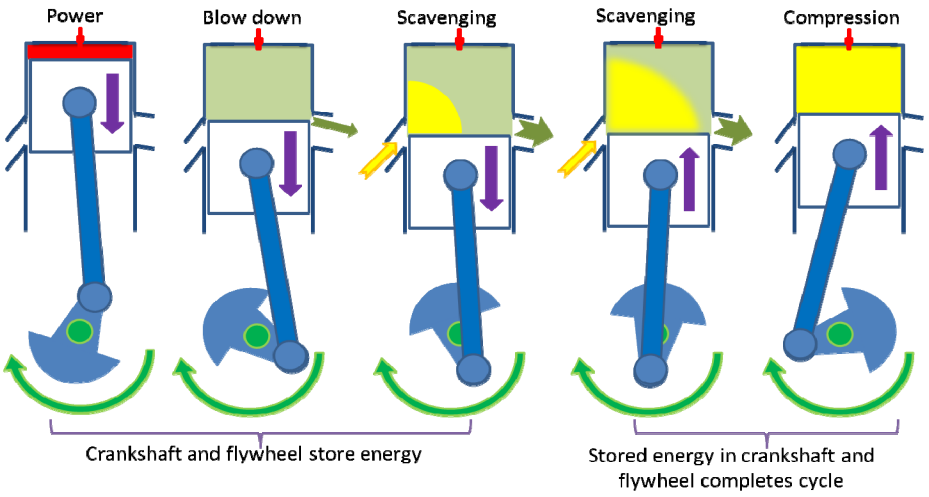

Figure 2-1 Crankshaft two stroke engine operation

Figure 2-2 illustrates how a free-piston engine works. In a free-piston engine a mechanical or air spring harvests some energy when the piston moves down and powers the scavenging and compression processes.

In free-piston engine, the piston is free because it does not have the kinematic constraint of a crankshaft, and its motion is determined by the forces acting on the piston. As a result, the piston doesn't have fixed dead end positions, in contrast to a crankshaft engine where the piston motion is defined by the crankshaft-connecting rod mechanism and the piston has fixed top dead center (TDC) and bottom dead center (BDC) positions.

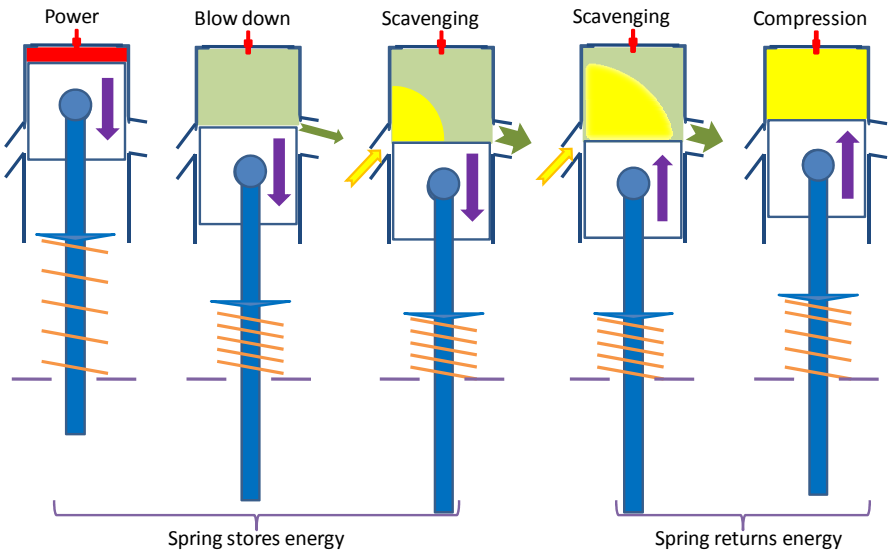

Figure 2-2 Generalized free-piston two stroke engine operation

2.1.2 General configurations

The most common free-piston engine configurations are single piston, dual piston and opposed piston.

Single piston

The single piston configuration consists of a combustion cylinder, a rebound device and a load device, as shown in Figure 2-3.

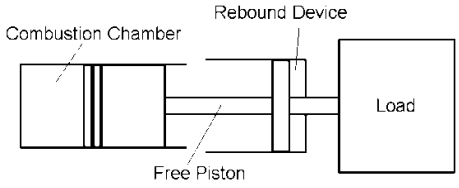

Figure 2-3 Single piston configuration

The advantages of single piston configuration are that it is simple and compact; it is also more controllable because the separate rebound device can enable better control of the piston movement. Disadvantages are that it is imbalanced, and valves must be used if uniflow scavenging scheme is used. Synchronizing of valves is

difficult, thus single piston engines typically use piston controlled ports scavenging (Mikalsen & Roskilly 2007). A brief review of two stroke engines scavenging systems is compiled in appendix section Appx. A.3.

Dual piston

This configuration uses the expansion stroke in the opposite combustion chamber to provide the rebound force reciprocally, in place of rebound chambers (Figure 2-4).

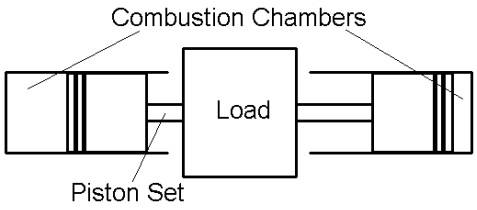

Figure 2-4 Dual piston free-piston engine

Without rebound devices, this configuration yields a more compact engine. However, controlling the stroke length and compression ratio is more difficult (Aichlmayr 2002). Variations of the expansion energy are difficult to be corrected by control devices, thus resulting in a variation of the compression energy for the next stroke, hence a variation of compression ratio (Achten 1994). Seppo Tikkanen et. al (2001) showed that the operation of the dual free-piston engine is sensitive to differences between ends and this was seen as asymmetric operation.

Opposed piston

The opposed piston configuration consists of two pistons using one common combustion chamber. A linkage is needed to synchronize the phase of two pistons (Figure 2-5).

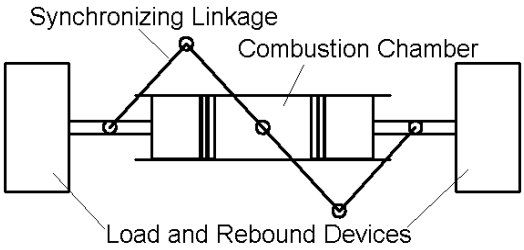

Figure 2-5 Opposed Piston free-piston engine configuration

Advantages include that it is intrinsically balanced and vibration free, and ports on the side of the cylinder enable uniflow scavenging, resulting in high scavenging efficiency (Neumann 1935). For the single and dual piston configurations, uniflow scavenging is only possible when valves are installed. The shortcomings are the need for a synchronization linkage, which increases the complicity and bulkiness of the engine and the mass that must be accelerated every stroke (Achten 1994).

2.1.3 Starting a free-piston engine

Crankshaft IC engines are sometimes started by the revolving motion of a conventional DC motor. In the case of a model aircraft engine, manual rotating the propeller is used to start the engine. These simple starting systems are not viable for free-piston engines. A free-piston engine must start on the first stroke and special techniques must be employed to do this. Generally it is started by placing the piston at an extremity of its travel and delivering an impulse (Noren & Erwin 1958). Some methods for accomplishing this include igniting a fuel-air mixture in the combustion chamber, releasing a wound spring (Farmer 1947), and pre-charging the rebound device. Farmer (1947) stated that the third technique is the only practical method for starting large free-piston engines. If using air compressor as a load, pre-charging the rebound device can be done using the stored compressed air.

For hydraulic pumps, pressurized fluid in accumulators is used for starting. For free-piston alternators, the alternator can be used as a linear motor to start the first

cycle of the engine (Hansson et. al 2005). However, special control scheme is needed to direct the current in the linear motor according to the piston motion, so that the piston can achieve desired back and forth motion for starting.

2.1.4 Free-piston engine applications

Air compressor

Air compressor is a common application of the free-piston engines (Pescara 1928). This is the most straightforward use because the stiffness of the elastic systems i.e., the combustion chamber and load, are nearly constant. Hence the engine operates at a natural frequency that is nominally fixed and the system is self-regulating.

When using air-compressor as the load, the air in the clearance volumes of the compressor can serve as part of the source of rebound energy (Aichlmayr 2002).

The Braun free-piston engine compressor is representative of free-piston air compressors. Developed by Braun and Schweitzer (Braun 1973), this machine delivers 2.94 kg/min of compressed air at 690 kPa. It is a fixed-output machine with air retained in the compressor clearance volume providing the rebound force. At full load, the machine operates at 1350 cycles/min and it develops an indicated power of 16kW. The Braun machine employs spark ignition combustion, loop scavenging, single piston, and air cooling. A spark plug ignites the premixed charge and electronic controls enable it to be triggered by piston velocity (Braun 1973).

Starting is done by compressed air stored in the air tank. Only 35 kPa is required to move the piston into starting position. The piston is driven by this pressure, and moves towards inner center to start the first cycle (Braun 1973).

Hydraulic pump

In free-piston hydraulic pump applications, a hydraulically driven rebound device may be applied, and in that case the rebound hydraulic accumulator is the bounce chamber of the free-piston engine. Hydraulics provides flexibility in the control of free-piston engine. The compression ratio may be adjusted by controlling the rebound hydraulic circuit (Achten 1994, Achten et. al 2000), and rebound action can be delayed, to control the frequency (Achten et. al 2000, Hibi & Ito 2004) or to hydraulically synchronize the pistons in the opposed piston configuration (Beachley & Fronczak 1992, Hibi & Hu 1993). The ability to control the working frequency hydraulically is a key advantage because it enables precise regulation of output flow rate and pressure for partial load operating conditions.

The Chiron Free-piston engine developed by Innas B.V. is a single piston, diesel powered, port controlled loop scavenging, hydraulic free-piston engine (Innas B.V. 2008). The Chiron engine was developed as a power source for off-highway mobile machinery such as lift trucks, excavators. The hydraulic pump's maximum hydraulic pressure is 30 MPa and net effective hydraulic power is 30 kW (Somhorst & Achten 1996). The Chiron free-piston engine hydraulic pump was used in a Steinbock Boss folk lift truck (Achten et. al 2000), with common pressure rail hydraulic system. Braking energy and energy of lowering the load are recuperated. This, combined with power management, made it possible to reduce the installed engine power by 30% compared to engine-pump combination (Innas B.V. 2008).

Gas generators

The gas-generator is a free-piston air compressor that has been modified to deliver high-pressure exhaust to turbines. This is accomplished by directing the output of the compressor to the air box of combustion chamber. Following combustion and

the opening of the exhaust ports, the exhaust enters a receiver and expands in a turbine. Shaft work is the output.

The gasifier-turbine plant can only achieve efficiency comparable to conventional engines. Furthermore, the attempt to use gasifier for automotive propulsion system failed because of poor part load efficiency (Beachley & Fronczak 1992). Consequently gas-generators were largely abandoned in 1960s.

Linear alternator

Free-piston alternators have the potential to be the primary power unit in hybrid electric vehicles (Hansson 2006). The electric alternator can be used as a motor to start or stop the piston-alternator unit, and to control the piston motion (Hansson et. al 2005).

Researchers in West Virginia Univ. developed a prototype free-piston linear alternator and engine system for use as an auxiliary power unit in hybrid electric vehicles (Cawthorne et. al 1999). The engine was gasoline fueled, spark-ignited, 36.5mm bore and 50mm maximum stroke, with a natural frequency of 1500 cycles per minute without load. It achieved approximately 780 W of net power output when friction load was applied, and achieved 316 W at 23.1 Hz with an air-core, brushless, permanent magnet linear alternator, whose entire translator assembly weighted 2.9 kg (Cawthorne et. al 1999).

2.2 Homogeneous Charge Compression Ignition

In conventional engines, ignition is triggered by a spark (as in a gasoline engine) or fuel injection event (as in a diesel engine). HCCI is a combustion mode in which fuel air mixture is compressed until it auto-ignites, thus ignition timing is determined by chemical kinetics instead of a timed ignition trigger. The engine compressor described here is intended to use HCCI combustion, for three reasons.

First, in tiny dimensions, spark plugs or a fuel injector cannot be used because they are too large. Second, the precise timing required for spark or diesel ignition is impossible without a crankshaft or engine piston position sensor. Third, HCCI is an excellent match to a free-piston because the compression ratio will automatically adapt to the onset of HCCI combustion (Aichlmayr 2002).

HCCI has various advantages including higher efficiency, ability to run in miniature scale and simple implementation. The disadvantage for HCCI in conventional crankshaft engine is its complicated ignition control. However, coupling with a free-piston engine is a potential solution for this problem. For these reasons, this project use HCCI combustion.

2.2.1 Illustrations of engine cycles: SI, CI, HCCI

Spark ignition is illustrated in Figure 2-6. The working fluid in the cylinder before ignition is fuel and air mixture. When piston approaches top dead center (TDC), the mixture temperature has risen because of compression heating; however, the temperature is not high enough for the mixture to explode. In a appropriate timing, a controlled spark releases from the spark plug, triggering the combustion. Then flame propagates approximately as an enlarging sphere through the combustion chamber (Heywood 1988).

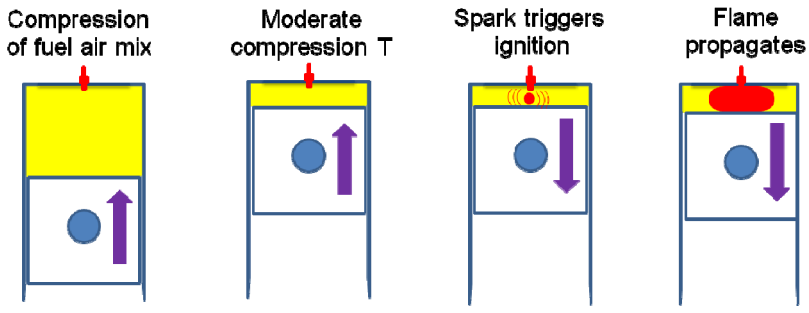

Figure 2-6 Spark ignition

In a compression ignition (CI) sequence as Figure 2-7, the working fluid being compressed before ignition is air. The compression ratio in a CI engine is much higher than a SI engine, which yields a much higher temperature after compression. At this high temperature, a fuel air mixture burns quickly. At an appropriate time, the fuel injector on the top of combustion chamber injects fuel as a fine spray. After a short delay the fuel air mixture ignites. Combustion continues as fuel is injected in a diffusion flame.

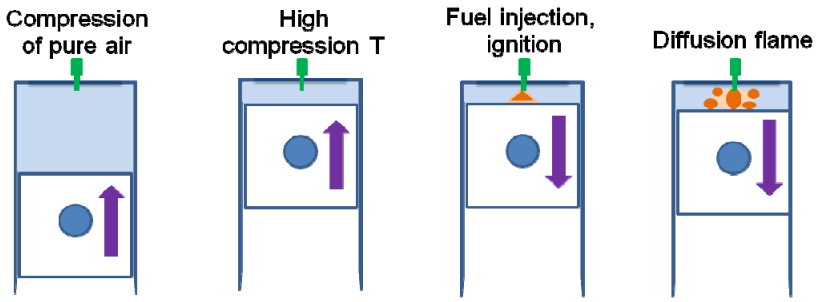

Figure 2-7 Compression ignition

Homogeneous Charge Compression Ignition (HCCI) mode is illustrated in Figure 2-8. The working fluid before ignition is fuel and air mixture, as in SI engines. However, the compression ratio is higher than SI engines. As a result, near TDC the fuel air mixture which is compressed nearly adiabatically to high pressure and temperature auto-ignites. The fuel is consumed rapidly, as multiple sites of auto-ignition enables short duration combustion throughout the charge volume (Epping et. al 2002), instead of a flame-propagation (SI engine) or diffusion flame (CI engine).

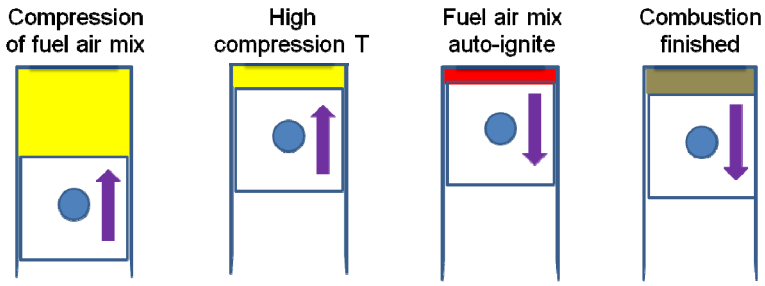

Figure 2-8 HCCI combustion

2.2.2 Features of HCCI

Efficiency benefit

Modern SI engine in automobiles can achieve an engine brake efficiency of about 30-37% (Muta et. al 2004, Heywood 1998), while modern automotive CI engine's efficiency is around 35-42% (Heywood 1998, Stock & Bauder 1990). HCCI can approach CI engine's efficiency.

SI engine utilizes premixed fuel air mixture and a throttle to control the engine load. The throttle controls the orifice area of intake charge flow, thus controls how much charge goes into the engine. This process involves pumping loss for charge intake at part load.

The compression ratio for SI engines is lower (6-11) than CI engines (12-22) (Heywood 1988). CI engines' higher compression ratio yields higher efficiency than SI engines. Also, CI engines control the load by altering how much fuel is injected into the combustion chamber, thus throttling of intake charge is not needed, saving the pumping loss. These factors contribute to the high efficiency of CI engines.

In HCCI, a high compression ratio is needed to enable auto-ignition of fuel air mixture. Also, HCCI utilizes lean burn strategy since mixture has to be lean to avoid excessive pressure rise rates. At the same time, load control is achieved through air

fuel ratio control. With this said, it can be seen that HCCI has the potential to reach diesel like efficiency (Epping et. al 2002).

Ability to operate in tiny scale

As engine scale goes down, the surface area goes down with the square of dimensions, while the volume goes down with the cube. Thus the surface to volume ratio goes up considerably, and this yields much easier heat dissipation. This has the implications for ignition, since the flame may lose heat faster than it gain from the ignition process, which yields flame quenching (Lewis & Elbe 1987). For example, Drost et. al. (1997) conducted experiments and found that the quenching distance of water cooled steel plates was 3.2 mm, and quenching diameter of a natural convection cooled aluminum tube was 1.6 mm inner diameter (with 3.2 mm outer diameter).

However, even in small scale, HCCI ignition can occur in the core area of the compressed charge. Experimental work by Aichlmayr et. al (2003) demonstrated the ability to run HCCI in 3 mm bore cylinder. In HCCI, there is no flame propagation process as in conventional cycles; instead, multiple auto-ignition sites occur throughout the charge mixture which is consumed almost instantly. Thus, the quenching distance of a propagating flame doesn't apply to HCCI combustion. The limit in HCCI, which is the heat loss through heat transfer near the wall, is significantly higher than propagating flame as the almost instantaneous combustion has a higher heat release rate. Experimental and computational study of Hultqvist et. al (2001) found that the thermal boundary layer in an HCCI engine is on the order of 1 mm thick, in which the combustion reactions are delayed but not quenched. Liu & Karim (2008) carried out 3D simulation on flame quenching in the piston crevices in an HCCI engine, and suggested that in piston crevices the quenching distance for n-heptane auto-ignition is smaller than 1 mm.

2.2.3 Control of HCCI ignition timing

One of the most significant barriers in implementing HCCI is controlling the start of combustion. Lacking the trigger for combustion, which is spark in SI engines or fuel injection in CI engines, HCCI engines requires delicate control of the timing of auto-ignition. An early ignition causes extremely high pressure rise rate which is detrimental to the engine. Late ignition would result in worse engine efficiency. Szybist and Bunting (2007) concluded that an early HCCI ignition increases combustion chamber heat transfer loss which compromises efficiency, and that a HCCI engine has highest thermal efficiency when CA50 (crank angle degree when 50% of fuel energy is released) is about 8 degrees after TDC.

Methods for control of HCCI ignition timing

In crankshaft HCCI engines, controlling of the ignition delay enables the control of combustion event. The strategy for precise control of start of combustion at different speeds and loads is one of the main targets of HCCI engine research. Methods for controlling HCCI ignition timing include thermal conditioning the intake air (Aleiferis et. al 2005), changing exhaust gas content in the cylinder with exhaust gas recirculation (EGR) (Najt & Foster 1983), altering fuel composition (Aroonsrisopon et. al 2002) and changing compression ratio (Christensen et.al 1999).

Intake air thermal conditioning involves precisely controlling the temperature of the fresh charge, thus controlling the HCCI timing. Steady state heating via resistive elements has been used extensively in research; however this would be ineffective under the changing conditions of real world engine operation, due to the high thermal inertia of the elements and hence slow response in engine transient

operations. A faster approach has been described using a fast response intake air thermal management system based on mixing separate hot and cold streams of intake air to allow rapid adjustment hot and cold proportions with closed loop feedback (Martinez-Friaz et. al 2002, Flowers et. al 2005).

Exhaust Gas Recirculation (EGR) is another means to control the HCCI timing. The EGR serves to provide some thermal energy, and also serves to limit the pressure rise since exhaust gas is comprised of high specific heat content such as water and CO2 (Thring 1989). To implement external EGR control of HCCI combustion, mixing valves need to be incorporated to control the mixing ratio of exhaust gas and fresh charge.

Free-piston engine and HCCI combustion timing control

Compared with all the control schemes used to regulate the ignition timing in a crankshaft HCCI engine, which are difficult to implement in tiny scale, the combustion timing control problem in a free-piston HCCI engine is solved naturally. In a free-piston engine, the piston keeps compressing the in-cylinder charge until it reaches auto-ignition, after which the cylinder pressure rises drastically and pushes the free-piston back. In this regards, there is no fixed TDC position nor fixed compression ratio in a free-piston engine, which solves the HCCI timing problem since the timing does not need to be controlled as long as the compression energy is high enough to trigger the auto-ignition.

3 DESIGN CONCEPT AND PRELIMINARY MODELING

3.1 Free-piston engine configuration design

For the free-piston engine compressor in this project, a single piston configuration was chosen among single piston, dual piston and opposed piston. This was due to the consideration of simplicity of this configuration, and ease of modeling and experimental research. Also, for certain desired power, dual piston or opposed piston would yield even smaller piston size, which could be an issue since the engine was already miniature.

Second, the project required pneumatic power as the engine output thus a free-piston air compressor was appropriate. As the ankle foot orthosis application required small amount of fluid power, utilizing a hydraulic system would result in small components such as pump, pipelines, valves and actuators, all of which were problematic for hardware implementation.

Third, the rebound spring should be chosen to be either a mechanical spring or a pneumatic spring (an air rebound chamber). Pneumatic spring exerts a perfectly symmetric force on the piston, as the pressure in the rebound chamber is uniform. A mechanical spring may have the problem of unsymmetrical force which may cause friction and wear problems. In the Aerodyne free-piston alternator (Annen et. al 2003), this problem was addressed by using a double-helical spring so that the asymmetry of the two helical springs can cancel each other.

Mechanical springs have fatigue problem, especially considering that the engine was designed for high frequency operation. Figure 3-1 shows the relationship between mechanical spring fatigue limit and stress applied. It can be concluded that

keeping the spring stress much lower than its limit will solve this problem since the number of pulsations increase drastically as stress decreases below certain value.

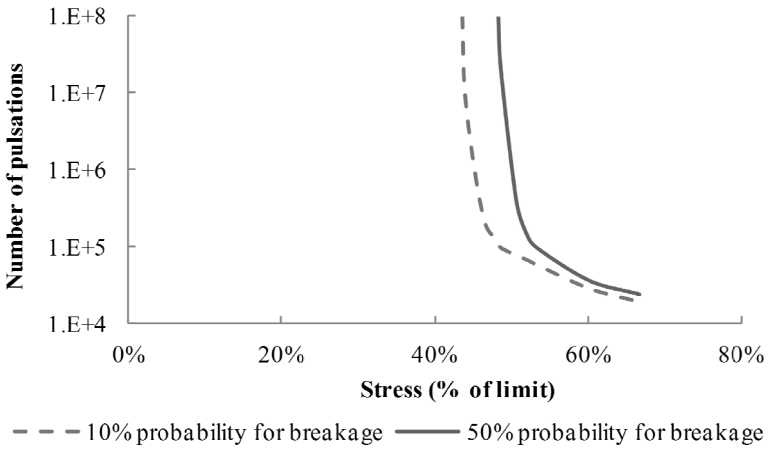

Figure 3-1 Mechanical spring fatigue strength (Lesjofors 2009)

Pneumatic spring has leakage problem. In high speed application proposed for the present project, piston cylinder seal was difficult to implement for friction consideration, which further deteriorated the problem. Also, miniature size yields much more severe leakage problem (see section 3.3.2).

Pneumatic spring has the advantage in terms of collision prevention. As piston approaches cylinder dead center, the pressure increases dramatically, i.e. the spring constant goes infinitely large. This will serve as bumper for a mechanical collision.

With these comparisons in mind, a pneumatic spring was suitable for conventional full scale free-piston engine applications. However, the leakage problem in miniature scale eliminated this option, especially for consideration of starting the engine. Thus, a mechanical spring configuration was chosen, and fatigue and force asymmetry problems needed to be considered. Also a collision prevention device needed to be properly designed.

3.2 Preliminary design concept

The preliminary design concept of the proposed miniature HCCI free-piston engine compressor was based on the reviews and considerations of two-stroke, free-piston, and model engines, HCCI combustion, Aichlmayr (2002), and the preliminary simulations described in later sections. The proposed design had these features: air cooled, two-stroke, crankcase compression, loop Schneurle type scavenging, carburetor fuel air mixing, reed valve induction system, HCCI, mechanical rebound spring, and single-piston free-piston engine directly coupled to a free-piston air compressor. The design concept is illustrated in Figure 3-2.

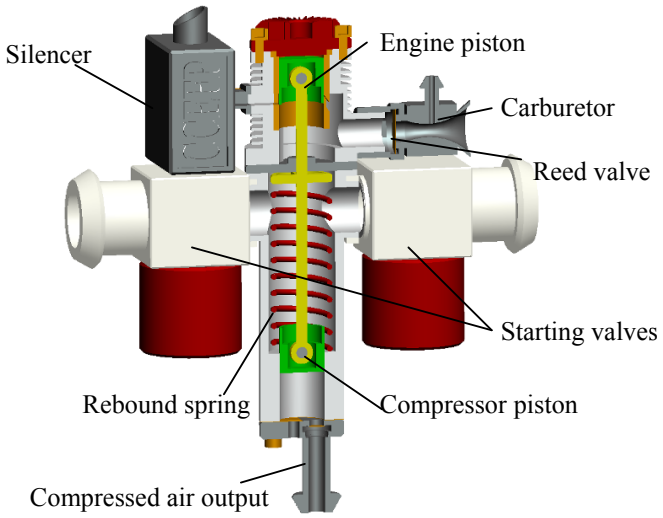

Figure 3-2 Design concept of the engine

Two starter valves were designed to start the engine, as a special starting system was necessary for a free-piston engine. The starting scheme was proposed as the following. One of the solenoid valve is connected to the high pressure air tank which the compressor supplies during normal operation; once the starting solenoid valve opens, the chamber behind the compressor piston is pressurized quickly, driving the free piston set to engine's BDC position and loading the spring. Then that valve closes, a second valve which connects to the ambient air opens, causing a fast

pressure release. The free piston is then driven to the engine's TDC position by the loaded spring. After several cycles of these sequences, the engine is expected to start. A detailed control scheme of the starting solenoid valves needed to be developed. Simpler hand start scheme was used in the proof-of-concept prototypes for simplification.

3.3 Preliminary simulations[1]

The purpose of the preliminary simulations was to set approximate operating parameters such as engine cylinder size and operation speed. These simulations were carried out before any experimental investigation or hardware implementation, thus assumptions were made for models based on literature review of existing knowledge. The preliminary modeling set a foundation for experimental and modeling work in later chapters.

3.3.1 Overall performance estimation

Performance estimation based on the approach used by Aichlmayr et. al (2002a) was used to characterize the major engine parameters. The engine power can be determined by

$$P_{BR} = \rho_i SN\left(\frac{\pi}{4}\right)^{\frac{1}{3}}\left\{\frac{(r-1)V_t}{rR}\right\}^{\frac{2}{3}} F_S \phi e_c \eta_{fc,i} \eta_m \eta_{ch} \quad (3.1)$$

Where P_{BR} is the brake output power of the engine, which is related to:

[1] This section is based on the paper, 'Miniature HCCI Free-piston Engine Compressor for Orthosis Application' (Tian et. al 2009), Copyright © SAE International and SAE of Japan. Reprinted with permission.

(1) The inlet air and fuel properties: ρ_i is the inlet air density, F_S is the stoichiometric fuel air ratio, ϕ is the equivalence ratio, e_c is the lower heating value of the fuel

(2) Engine parameters: S is the stroke, N is the engine speed (Hz), V_t is the volume of cylinder, and R is the stroke to bore aspect ratio

(3) Efficiencies: $\eta_{fc,i}$ is the indicated fuel conversion efficiency, η_m is the mechanical efficiency and η_{ch} is the charging efficiency.

In performance estimation calculation, several rough approximations were made, including the two stroke engine scavenging efficiencies model in Taylor (1985).

$$\Lambda = \frac{r-1}{2r} \qquad \eta_{ch} = \frac{1+\Lambda-e^{-\Lambda}}{2} \tag{3.2}$$

where Λ is delivery ratio which describes how much fresh charge is delivered to the engine, r is the compression ratio and η_{ch} is the charging efficiency, which is the indication of how well the cylinder is refreshed by fresh charge. That scavenging model is a rough guess on the efficiencies during a two-stroke engine scavenging process. A brief introduction on two stroke engine scavenging process and definition of efficiencies is presented in appendix section Appx. A.3.

Average piston speed was assumed to be constant

$$\widetilde{U_P} = N \cdot 2S = 10 m/s \tag{3.3}$$

That assumption was based on observations that for both miniature size engines and full scale engines, average piston speed was almost always in 8-15 m/s range, as dictated by mechanical stress, lubrication and gas motion dynamics limitations (Heywood 1988).

Mechanical efficiency η_m was assumed to be 70%. Although as described in later section in this thesis, mechanical efficiency in a miniature engine depends

strongly on engine running speed, constant value was assumed for rough performance estimation calculation.

In the calculation engine brake power output target was set to be 20W.

From the performance estimation calculation, Figure 3-3 shows the relation between speed, compression ratio and cylinder bore, to achieve the 20W power target, with aspect ratio (engine stroke to bore size ratio) of 1. It demonstrated that the engine could be chosen to be big and slow, or small and fast. The faster the engine would operate, the less fuel air mixture would be needed to be burned each cycle, thus smaller engine displacement. This demonstrated that approximate engine operating speed needed to be specified, so that approximate engine size could be calculated. Once approximate engine size was established, experimental and mathematical study can be carried out to investigate operating characteristics of engines in that specific size range.

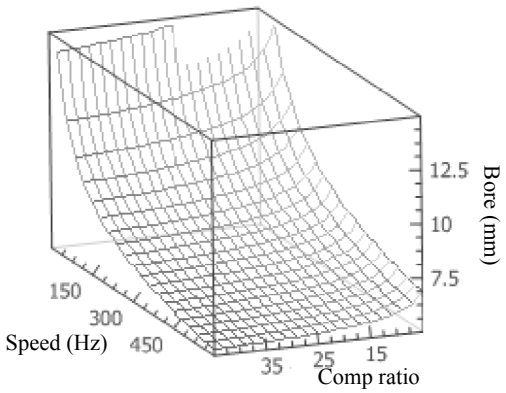

Figure 3-3 Speed, compression ratio and cylinder bore when aspect ratio = 1

Another example of how performance estimation could be used to determine approximate operating parameter is shown in Figure 3-4. Assuming the engine operates at 300Hz, to achieve 20W of brake power output, the engine stroke could be quite long if aspect ratio is more than 3. Thus to avoid a long and slender free-piston engine compressor which would be challenging to fabricate, aspect ratio

needed to be lower, i.e. smaller stroke to bore size ratio. The analysis in Figure 3-3 and Figure 3-4 is similar to Aichlmayr (2002), but with different constraints including different speed limits and size range.

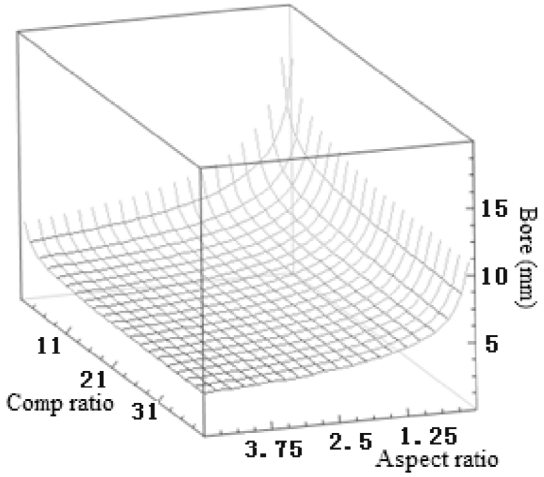

Figure 3-4 Compression ratio, aspect ratio and bore size when engine speed = 300Hz

3.3.2 Leakage simulation

As the engine gets smaller the charge leakage through the cylinder-piston gap becomes the dominant factor affecting the efficiency of the engine (Sher et. al 2009). This is because the leakage gap is determined by machining tolerances and stays the same with different engine sizes. As a result, with smaller engines, higher percentage of the in-cylinder charge leaks through the gap. In this simulation, the combustion chamber was modeled as a control volume. Leakage was simulated with a simplified scenario, in which the in-cylinder fuel air mixture was assumed to be compressed at a specific compression ratio. Retention efficiency was calculated in each simulation to indicate how much mixture was retained inside the cylinder instead of leaking out.

Simulation model setup

Cylinder state was derived from first law of thermodynamics. Consider the combustion chamber as a control volume

$$dE_{C.V.} = \delta Q + {m_{in}\overline{h_{in}}}/{M} - {m_{out}\overline{h_{out}}}/{M} - \delta W \tag{3.4}$$

The terms in the equation from left to right are control volume internal energy change, heat transfer and addition, enthalpy inflow, enthalpy out flow and work transfer. For a small calculation time step dt,

$${m_{cc}\bar{c_v}dT_{cc}}/{M} = \delta Q - \delta W + {\dot{m_{leak}}\,dt(\overline{h_{cc}} - \overline{u_{cc}})}/{M} \tag{3.5}$$

where m_{cc} is in-cylinder charge mass, T_{cc} is cylinder charge temperature and $\dot{m_{leak}}$ is in-cylinder leakage mass flow rate. Specific heat $\bar{c_v}$, enthalpy $\overline{h_{cc}}$ and internal energy $\overline{u_{cc}}$ are based on polynomial approximation as suggested in Zhu et. al (1995).

For simplification, the in cylinder gas properties were calculated as air. The fuel was assumed to combusted instantaneously at TDC. Fuel-air equivalence ratio was assumed to be 1. Heat transfer model in Sher et al (2009) was used, which assumed an average convection coefficient $\tilde{h}$:

$$\tilde{h} = {\tilde{a}K}/{B}\left({\rho U_p B}/{\mu}\right)^{\tilde{b}} \tag{3.6}$$

Heat transfer rate $\dot{Q}$ between in-cylinder charge and cylinder walls was calculated by heat convection plus heat radiation

$$\dot{Q} = -A_{cc}\tilde{h}(T_{cc} - T_{wall}) - \tilde{c}\sigma(T_{cc}^4 - T_{wall}^4) \tag{3.7}$$

where K, μ, σ and A_{cc} are heat conductivity, fluid viscosity Boltzmann constant and combustion chamber surface area. $\tilde{A}$, $\tilde{b}$ and $\tilde{c}$ are constants, which were assumed to be 0.5, 0.7 and 0.3 accordering to Sher et. al (2009).

Sutherland's formula was used to derive the dynamic viscosity μ of an ideal gas as a function of the temperature

$$\mu = \mu_o \, {T_o + C}/{T + C} \left({T}/{T_o}\right)^{1.5} \tag{3.8}$$

where μ_o is the reference viscosity at reference temperature T_o. For air, at T_o =291.15K, viscosity μ_o=18.27e-6Pa*s, and Sutherland's constant C=120K.

Piston cylinder gap was assumed to be 20 micrometer, as suggested by Sher et. al (2009). An orifice flow model was used to calculate flow rate through the piston-cylinder gap

$${dm}/{dt} = C_d A_o P_{o1} \sqrt{{2}/{R_m T_{o1}}} \times \Psi \tag{3.9}$$

For sub-sonic flow

$$\psi_{sub-sonic} = \sqrt{{\gamma}/{\gamma - 1}\left[\left({p_2}/{p_{o1}}\right)^{2/\gamma} - \left({p_2}/{p_{o1}}\right)^{\gamma+1/\gamma}\right]} \tag{3.10}$$

For sonic flow

$$\psi_{sonic} = \left({2}/{\gamma + 1}\right)^{1/\gamma - 1} \sqrt{{\gamma}/{\gamma + 1}} \tag{3.11}$$

A_o is the reference intake channel area. C_d is the flow coefficient and γ is ratio of specific heats. Subscripts 1 and 2 indicate upstream and downstream pressure. Subscript o indicates stagnant parameters.

At the time of the preliminary simulation, no experimental results were available to determine the flow coefficient C_d, which usually needs to be experimentally characterized. As a result a C_d value was fitted to approximately repeat mathematical derivation results of Sher et. al (2009). To repeat their derivation result, the flow coefficient for gap flow should be set to about 0.12. However, Sher et al's derivation possibly exaggerated the leakage, for following reasons.

First, they did not consider the lubricant oil in the gap, which can have an effect of reducing the gap width;

Second, consider COX .010 engine, whose displacement is 0.16 cc and engine speed is up to 30000rpm. Results of Sher et al (2009) basically showed that COX .010 engine could not run. However, this engine is known to run consistently and is used by hobbyists in small model airplanes.

That is why 0.06 instead of 0.12 was used for flow coefficient to consider the effect of the lubricant oil in the piston-cylinder gap.

Simulation results

The leakage simulation results are shown in Figure 3-5. The actual compression ratio was calculated by equivalent isentropic compression and is always lower than geometric compression ratio of the engine because of the blow-by leakage. In higher speed, the in-cylinder charge has less time to escape from the gap, thus the leakage effect is alleviated. For example, at a slow 1000rpm operation, the engine barely achieved any effective compression ratio, no matter how big geometric compression ratio is, because most of in-cylinder charge just leak through the cylinder-piston gap. The simulation showed that the engine needs to be run at high speed to minimize the effect of leakage. However, when engine operation speed exceeds 12000 rpm (200Hz), the fuel retention benefit from raising engine operation speed gets

insignificant, i.e. 200Hz should be adequately fast enough in the purpose of reducing fuel air mixture leakage.

In each simulation, fuel air mixture retention efficiency was calculated. Results were combined with chemical kinetics simulation which will be shown in the following section.

It should be noted that although the leakage simulation was based on a crankshaft engine for simplicity, the results apply to free-piston engine as well. At the same engine speed and geometric compression ratio, a crankshaft engine and a free-piston engine have similar level of leakage.

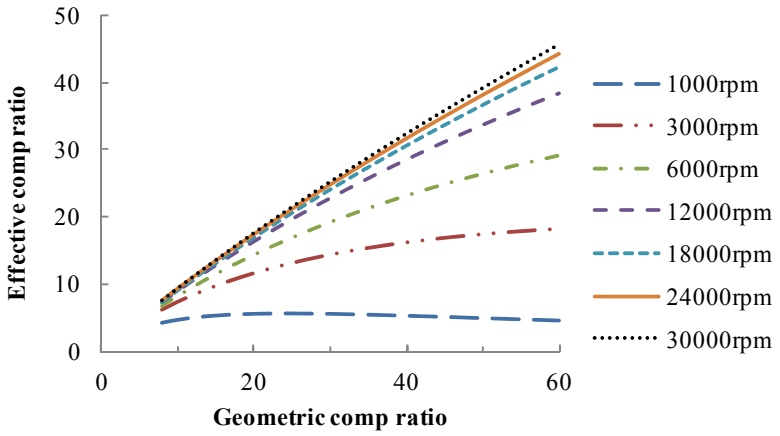

Figure 3-5 Actual versus geometric compression ratio for several engine speeds

3.3.3 HCCI chemical kinetics simulation

Since the onset of HCCI combustion is determined solely by chemical kinetics during the compression process, the compression process must be simulated properly to determine the operation characteristics of the HCCI engine. Simulation package CHEMKIN is capable of simulating the chemical kinetics during engine compression by solving detailed chemical reaction kinetics equations. In those simulations, the engine was assumed to be adiabatic with bore and stroke sizes of 8 mm. Intake equivalence ratio was assumed to be 1. Chemical kinetics mechanisms

published by Lawrence Livermore National Laboratory (LLNL) (available on LLNL official website) were used.

An example of CHEMKIN simulation results at constant engine speed of 18000rpm is shown in Figure 3-6. Simulated cycles with different inlet temperature and compression ratio resulted in HCCI ignition (marked with Y) or no HCCI ignition (marked with N). As a result the boundary between the Y and N line is the required compression ratio to ignite the fuel air mixture in HCCI mode. The results showed that with higher inlet temperature, less compression ratio is generally required for HCCI ignition. However with two stage ignition long carbon-chain hydrocarbon fuels such as the n-heptane, this was not necessarily the case as shown by the curved ignition line of n-Heptane. The results also showed that n-Heptane is easier to ignite in HCCI mode than propane, due to its larger molecule and lower Octane number.

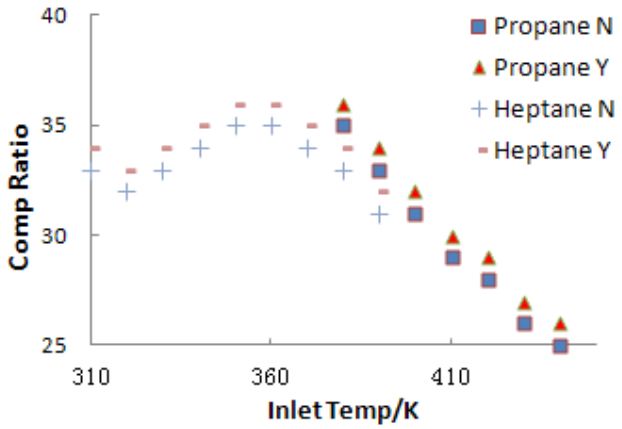

Figure 3-6 CHEMKIN simulation result of HCCI ignition in different compression ratio and inlet temperature, at engine speed 18000 rpm

The CHEMKIN simulation results in Figure 3-7 further showed that the required compression ratio to ignite the fuel increases with the engine speed, with intake

temperature of 330K. This can be interpreted from the ignition delay theory for HCCI combustion. As the engine speed increases, the HCCI ignition delay must be decreased to keep up with shorter cycle times, thus a higher compression ratio is needed.

Propane and n-Heptane ignition curves in the chart were CHEMKIN simulation results, while the model diesel fuel ignition curve in the chart was a guess instead of simulation results, since reaction mechanisms of complicated hydrocarbon fuels were not available. The guess was based on the observation that existing model diesel engines run in HCCI mode at 200-300Hz and has compression ratio of 12 to 20. Model diesel fuel is a type of fuel used in a diesel model aircraft engine which is essentially an HCCI engines, since it has a flat cylinder head without a glow plug, and compresses fuel air mixture to auto-ignite in HCCI mode. The content of model diesel fuel is listed in Table 3-1. Kerosene has a similar power density with gasoline, and much lower octane rating (about 25) which means it is easier to auto-ignite. Diethyl ether also helps the auto-ignition with its high Cetane number, thus easier ignition, and serves as a solvent to blend the contents together. Amyl nitrate is a chemical used in full-scale diesel engines as ignition improver, to increase the Cetane number of diesel fuel. Due to the ease of ignition of model diesel fuel, it will require lower compression ratio, and the engine will be easier to start when cold. Castor oil and synthetic oil are lubrication oil contents.

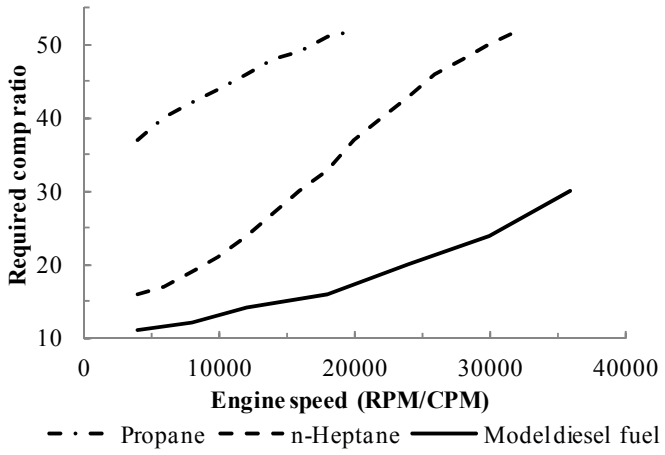

Figure 3-7 Ignition curves for various fuels showing the compression ratio required to ignite as a function of engine speed.

Table 3-1 Model diesel fuel content

Kerosene	48
Diethyl ether	30
Amyl Nitrate	2
Castor oil	10
Synthetic oil	10

The chemical kinetics simulation results were combined with leakage simulation results to reveal compression ratio requirement and engine cycle efficiencies related with operation speed.

The viable engine operating speeds for different fuels could be determined from the data shown in Figure 3-5 and Figure 3-7. While higher speed was needed for reducing leakage, the higher speed made it harder to ignite the fuel in HCCI mode. For example, it is impossible to utilize propane as fuel in HCCI mode in the current leakage level. At lower engine speed, leakage level is high and effective compression ratio is low even with high geometric compression ratio. At high

engine speed, effective compression ratio can be raised due to less leakage, but cannot catch up with the rising requirement of compression ratio for HCCI ignition due to higher engine speed. As a result, there is not any operating speed and compression ratio combination at which the engine can run in HCCI mode.

An easily ignitable fuel such as previously mentioned model diesel fuel should be used for the miniature HCCI engine so that the speed could be high enough to minimize leakage, but the fuel could still ignite in HCCI mode.

Based on the ignition curve of model diesel fuel shown in Figure 3-7 and the leakage simulation results in previous section, required effective compression ratio, needed geometric compression ratio, fuel retention efficiency and overall indicated efficiency are related to engine running speed in Figure 3-8. It can be seen that at higher speed efficiency gains from less fuel air mixture leakage and higher compression ratio. However at speeds higher than 10000rpm, the efficiency only benefits marginally from increasing engine speed.

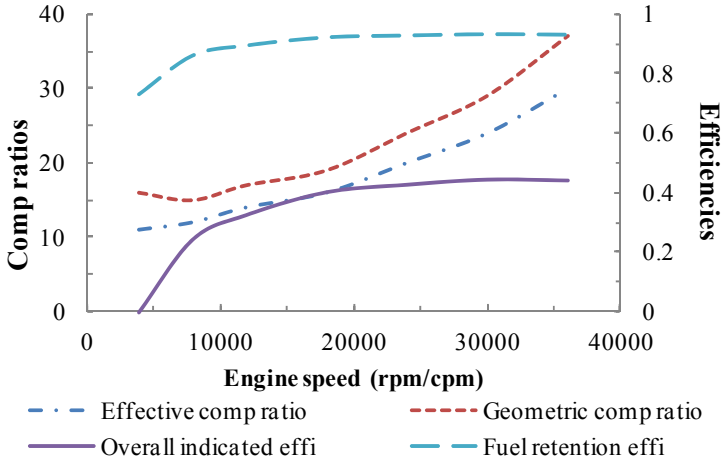

Figure 3-8 Operating range for model diesel fuel in HCCI mode

From these preliminary simulations of cylinder-piston blow-by leakage and chemical kinetics, a ballpark approximate optimum speed range could be set for a 10-20W pneumatic power output HCCI free-piston engine compressor at 5000 – 20000 rpm/cpm (about 80 – 330 Hz). (As free-piston doesn't have revolutions of a crankshaft, cycles per minute (cpm) is usually used instead of revolutions per minute (rpm)). Using this speed and assumptions listed in the performance estimation section, approximate engine bore was calculated to be about 7-12 mm. These parameters are listed in Table 3-2.

Table 3-2 Free-piston HCCI engine compressor ballpark parameters determined by preliminary simulations

Engine power	20-40 W
Pneumatic power output	10-20 W
Engine speed	80-330 Hz
Engine bore size	7-12 mm
Engine compression ratio	10-20

It should be noted that friction had not been characterized and calculated in preliminary simulations. Inclusion of speed related friction may shift the trade off to lower speed range. Also, the leakage level needed to be experimentally characterized instead of calculated from roughly estimated simulation parameters, so that more accurate models could be constructed to set target speed. These concerns were addressed in later experimental work as described in the chapter 4. The preliminary simulation did set ballpark parameters, so that later experimental work can be targeting at components in that size range, i.e. 7-12 mm bore size internal combustion engine.

3.3.4 Reed valve response simulation

A reed check valve was chosen to trap the fuel air mixture inside the crankcase chamber, based on review of different two-stroke engine induction systems in Appendix A. The valve needs time to open and close and its response is also affected by valve deformation dynamics. At higher speeds, the reed lags when opening and closing and reduces air flow through the reed check valve. In this section, reed check valve response is modeled to characterize its restriction to air induction and thus engine speed.

A reed check valve used in model engines is shown in Figure 3-9. The valve is a thin piece of stainless steel which seals against intake channel when crankcase (right side of the graph) volume is under pressure. Measured parameters of the stainless reed valve are listed in Table 3-3. When the crankcase is under vacuum, the valve opens under pressure difference and enables fuel air mixture induction. The simulation model needed to capture the interaction of valve motion dynamics and the fuel air mixture flow.

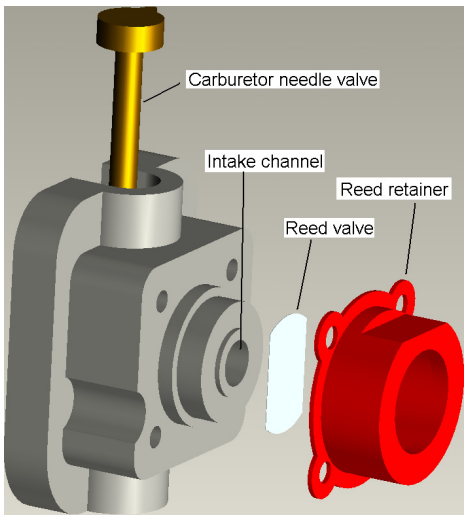

Figure 3-9 Reed check valve induction system for a model engine

Table 3-3 Crankcase induction reed check valve parameters

Weight	28.62 mg
Thickness	0.05334 mm
Material	Stainless steel
Density	7214.58 kg/m3
Reed stroke	0.381 mm

Reed valve dynamics model setup

When moving between the intake duct sealing surface and the reed retainer, the reed check valve was modeled as a rigid body. At full lift when the reed collides with the reed valve retainer, it deforms and vibrates. The valve deformation affects both the valve motion and the effective flow orifice area, thus needs to be modeled.

The valve deformation was simulated as a cantilever beam with an equivalent spring-mass-damper system, as illustrated in Figure 3-10. The differential equation describing movement of center point of the reed is

$$m'_{reed}\frac{d^2y_{center}}{dt^2} = F_p - ky_{center} - c\frac{dy_{center}}{dt} \tag{3.12}$$

where y_{center} is the position of the center of the valve, F_p is the load to the reed due to pressure difference, k and c are the equivalent spring constant and damping factor. ANSYS finite element analysis software was used to determine the equivalent spring constant k=2120 N/m.

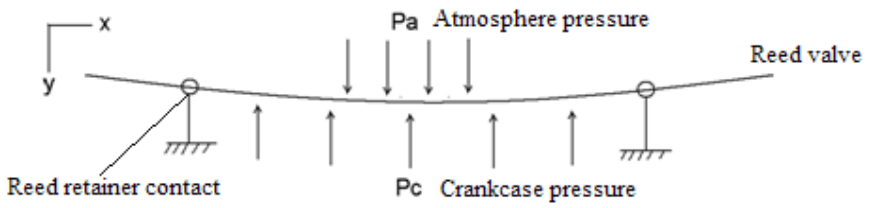

Figure 3-10 Reed valve vibration simulation at full lift

Reed valve flow rate model

An orifice flow model as described in section 3.3.2 was used to simulate the flow through the reed check valve. However, the flow coefficients needed to be determined to calculate the flow rate.

FLUENT computational fluid dynamics software was used to model the fluid flow through the reed valve and calculate the flow coefficient of the reed check valve flow channels. A mesh was constructed, with two plenums at atmosphere pressure and crankcase pressure on the two sides of the reed valve, as shown in Figure 3-11. The mesh was much denser around the reed valve due to the tiny dimensions there, and was coarser elsewhere to reduce calculation time. The FLUENT model was able to model the flow through the reed valve in different pressure difference and reed valve lift. The simulated flow coefficient versus reed valve lift is shown in Figure 3-12, and a linear equation was constructed to calculate the flow coefficient related with reed valve lift.

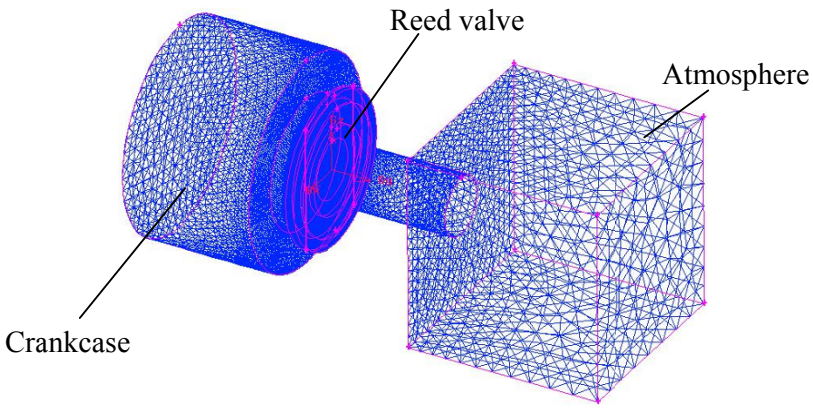

Figure 3-11 FLUENT mesh for reed valve flow simulation

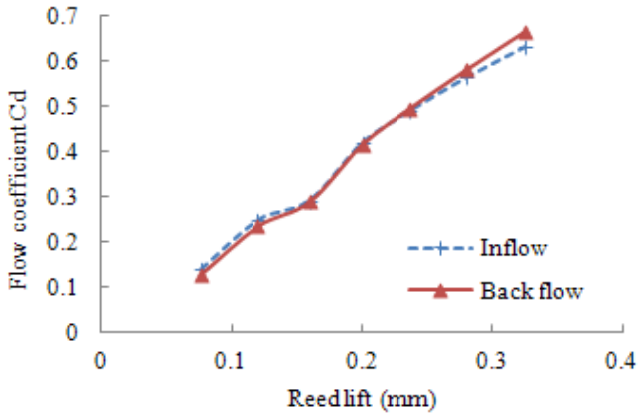

Figure 3-12 FLUENT simulated flow coefficient related with reed valve lift

Reed valve surface pressure force model

As air flows into or back from the crankcase, pressure difference on two sides of the reed valve determines the reed valve movement. A model for pressure on the reed needed to be employed to determine reed valve pressure difference force F_p. For example, Blair (1979) assumed linearly changing pressure from inlet tract pressure to crankcase pressure and Fleck et. al. (1997) assumed linear relationship fitted with a reed-lift associated pressure reduction factor. FLUENT simulation was used to simulate the pressure distribution on the reed valve. Simulation results at

0.32 mm reed valve lift and 4 kPa pressure difference are shown in Figure 3-13, for inflow into and backflow from the crankcase.

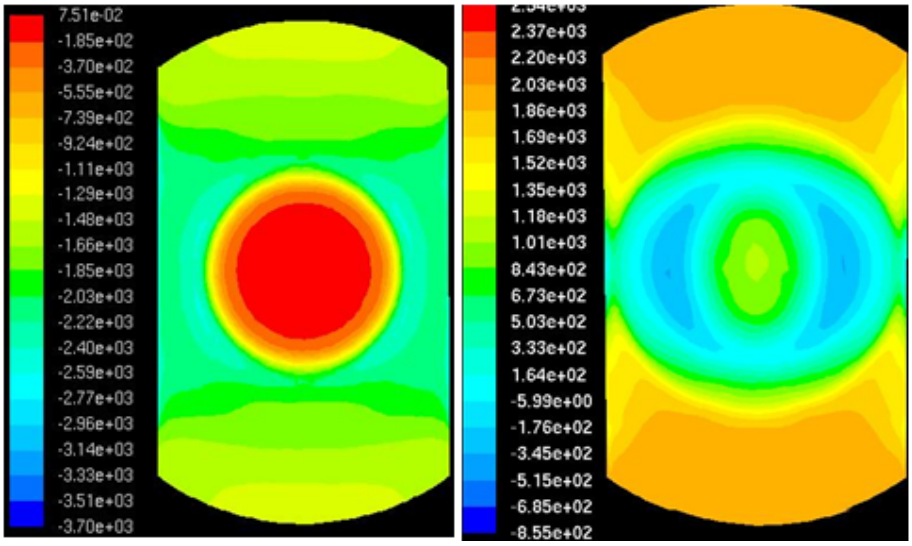

Figure 3-13 CFD simulated pressure on reed valve sealing surface, left: during inflow into the crankcase, right: during backflow from the crankcase

Based on the CFD simulation results, a model that relates pressure distribution on reed surfaces to reed lift was constructed for one-dimensional simulation. During the inflow to the crankcase, the pressure force was calculated by

$$F_p = (0.332x_{reed} + 0.213)A_{reed}\,\Delta P \tag{3.13}$$

and during the backflow from the crankcase the pressure force was

$$F_p = -(0.889x_{reed} + 0.213)A_{reed}\,\Delta P \tag{3.14}$$

where ΔP is pressure difference across the valve, A_{reed} is reed surface area, and x_{reed} is the reed lift in mm.

Reed valve induction system delivery ratio modeling

The FLUENT CFD simulation model was used to determine delivery ratio through the reed valve induction system in a two stroke crankshaft engine at various engine operating speeds. The following assumptions were made: (1) When transfer ports were closed, pressure in crankcase was reduced to atmospheric by scavenging process; (2) Stagnation pressure in the inlet duct equaled atmospheric; (3) Leakage through piston and cylinder gap was neglected; (4) Heat transfer between gas and crankcase wall was neglected. A typical simulation result of reed valve response is shown in Figure 3-14, at engine speed of 18000rpm. As the piston traveled towards TDC and transfer port closed, vacuum in crankcase opened the reed valve to maximum valve lift in about 0.3 millisecond. The extremely fast valve response time was due to the light weight of the thin stainless steel reed. After the valve reached maximum lift, the valve deformed after hitting the reed retainer. The valve deformation resulted in more valve lift as shown by the difference between the total lift and rigid lift.

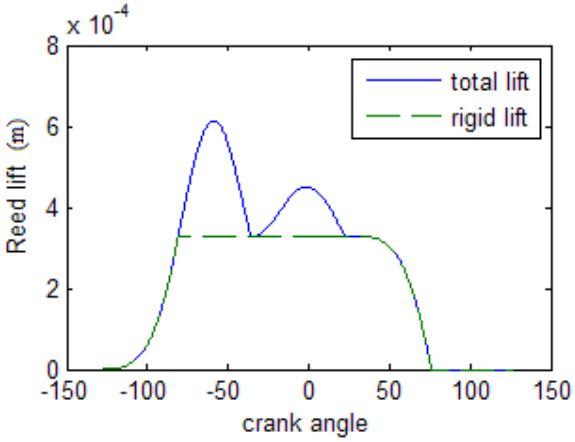

Figure 3-14 Reed valve response in a two stroke crankshaft engine at 18000rpm

Delivery ratio for a two-stroke engine is defined as

$$\mathrm{DR} = \frac{\text{mass of delivered charge into engine cylinder in one cycle}}{\text{swept volume} \times \text{ambient density}} \tag{3.15}$$

Thus delivery ratio is the indication of how much mixture is used through the transfer ports of a two-stroke engine to refresh the cylinder. The simulation results in Figure 3-15 show the delivery ratio and engine power of a two stroke engine with reed check valve induction system. It shows that the reed valve intake system did not restrict intake air flow and engine power until the engine speed reached about 50000 rpm. At higher speeds, valve response could not keep up thus reducing the engine intake flow and engine power output.

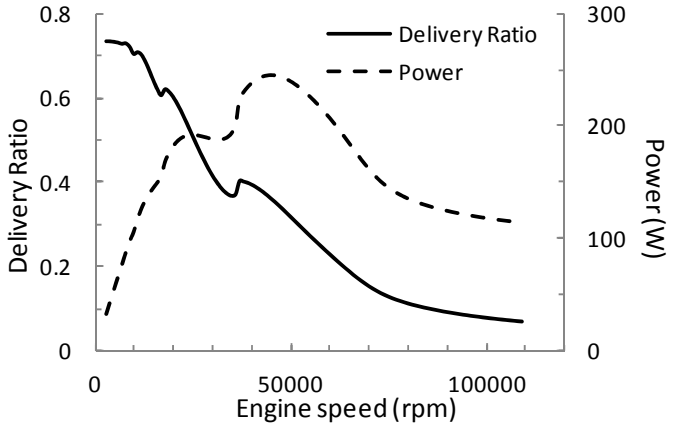

Figure 3-15 Delivery ratio and engine power of a two stroke engine with reed check valve induction system

The reed valve modeling revealed the fast response of the thin reed valve induction system, and determined that the engine intake flow would not be limited by the check valve until engine speed exceeds 50000 rpm. The simulation model of reed valve dynamics was also used in later prototype engine compressor modeling work described in chapter 5.

3.3.5 Conclusions of preliminary simulations

To operate a miniature size engine in HCCI mode, fuel needs to be easily compression ignited. With model diesel fuel, the appropriate engine operating speed

was determined to be 5000-20000 rpm/cpm, and engine bore size was calculated to be in 7-12 mm range.

Reed valve response was modeled, and the thin stainless steel reed valve used in model engines was found to have fast response and could support engine operating speed up to 50000 rpm.

4 MODEL ENGINE COMPONENT TESTING AND MODELING

Preliminary simulation results in last chapter concluded that the free-piston HCCI engine compressor should have a bore size of 7 to 12 mm, much smaller than full scale internal combustion engines. There was a need to quantitatively characterize and simulate components such as friction, blow-by leakage, scavenging and combustion in engines of this size.

As an engine gets smaller, surface effects such as friction, heat loss, and leakage get more significant (Aichlmayr 2002). To characterize those effects, test benches were built to test a 1.5 cc displacement model engine (Hornet .09, AP Engines). During motoring and firing tests, cylinder and crankcase pressures, engine brake torque, fuel flow rate, air flow rate and emissions were measured. Using experimental results, a piston-cylinder blow-by leakage model, suitable for miniature engines, was verified and calibrated. A scavenging model was developed and calibrated. Friction level was estimated by comparing indicated power calculated from in-cylinder pressure trace and brake power calculated from brake torque and speed measurements.

The tested model engine utilizes glow ignition combustion rather than spark ignition. Fuel and air are premixed and an incandescent platinum wire is used to initiate and catalyze the combustion. Combustion analysis was carried out to investigate the unique combustion process. A combustion model was established for glow ignition.

4.1 Relevance of model engine testing

To advance the development of the miniature engine compressor project, it was necessary to understand the performance characteristics of current miniature engines.

The relevance of the model engine testing to the free-piston engine project is explained as below.

The proposed free-piston HCCI engine design shared a lot of similarities with model engines. Some model engines are in the neighborhood of 10 mm bore size which is the size of the proposed engine. Both utilize two stroke, crankcase compression and Schneurle type loop scavenging. Also, to decrease the cost of fabrication, the proposed prototype was designed to utilize relatively more well developed components such as pistons and cylinder liners from off-shelf model aircraft engines.

The tests helped to characterize several components. Free-piston engines are susceptible to cycle variations which may be much worse in small scale (Ogawa & Kawaguchi 2007). Scavenging in tiny engines might be different from full-scale engines, and friction might play a bigger role. Also, piston-cylinder leakage needed to be characterized. Thus those tests were used to help validate and improve simulation models of blow-by leakage, friction and scavenging.

The tested model engine utilizes glow ignition, which behaves in manner similar to HCCI. It intakes homogeneous charge, and ignites from the chemical kinetics from the compression heat. Similar to HCCI, glow ignition doesn't need any timed ignition stimulus like spark ignition, thus would work nicely with free-piston configuration. Glow ignition is different from HCCI in that flame propagates from the glow plug after ignition occurs, while in HCCI no flame propagation is present after auto-ignition occurs. Compared with HCCI, glow ignition is much easier for cold starting the engine due to less compression ratio requirement. As a result, the first prototypes were designed to utilize glow ignition system.

4.2 Brief overview of model engines

Currently available miniature size internal combustion engines are those used in model aircraft and model cars. The smallest of them is the Cox Tee Dee .010 engine, with 6.02 mm bore and 0.163 cm^3 (0.01 in^3) displacement. The model engines that are similar in the size to the engine developed in the project, which is on the neighborhood of 1.5 cm^3 displacement, share these features: air-cooled, two-cycle, crankcase compression, loop scavenging, fuel supplied with carburetor, piston without piston rings, glow or HCCI ignition and hemispheric combustion chamber. These features result in compactness, high power density, simple components, reliability, ease of starting, easy maintenance and low cost, all of which are desired by hobbyists. Cutaway view of the AP .09 engine, the engine used in testings, is shown in Figure 4-1. Its bore is 12.5 mm, stroke is 12 mm and displacement is 1.47 cm^3.

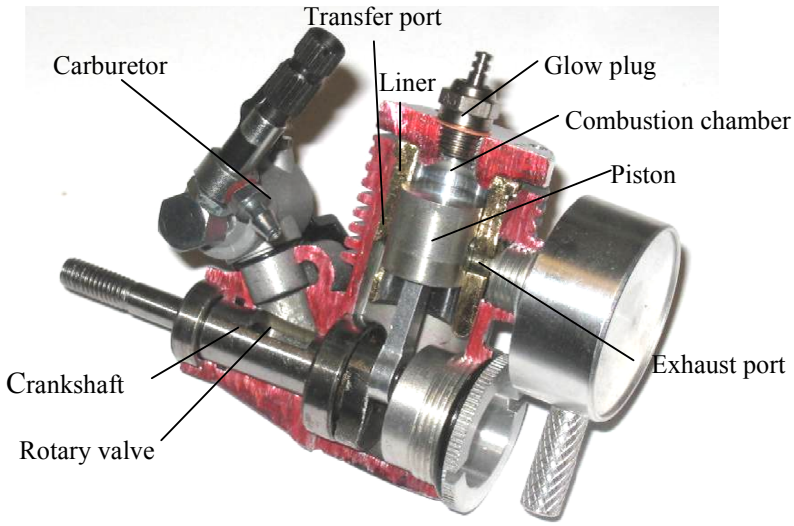

Figure 4-1 AP .09 model aircraft engine cut-away view

For small engines, it is difficult to implement spark ignition systems or direct cylinder fuel injection systems like those used in full scale SI or CI engines. The AP .09 engine utilize a glow ignition system and methanol based fuel (mixture of

methanol, nitromethane and lubrication oil). A glow plug is located on cylinder head and serves as an ignition device. The essential element of the glow plug is the platinum coil located inside the glow plug. The platinum wire which is hot and incandescent all the time during operation helps with the mixture ignition, in two ways: (1) platinum is a catalyst for methanol combustion and enables methanol to ignite at lower temperature; and (2) its high temperature during operation helps ignites the mixture.

In a glow ignition system, ignition timing is controlled by chemical kinetics, instead of being controlled by an external stimulus like a spark or fuel injection. Model engine glow ignition system is simple and no control device is needed. During operation, the glowing hot platinum wire in the combustion chamber is constantly trying to ignite the fuel air mixture through its thermal energy and catalytic effect and the resulting combustion near the surface of the wire keeps it hot while the engine runs. This combustion mode is similar to HCCI since there is no timed ignition source and ignition timing depends on chemical kinetics in the combustion chamber. The difference is that in glow plug ignition the flame propagates through the combustion chamber from the platinum wire with a gradual heat release, in contrast to the rapid heat release of HCCI.

Some of model engines replace the glow plug with a flat cylinder head with a screw to adjust the compression ratio (For example, PAW diesel model engines by Progress Aero Works). They compress the fuel air mixture until it auto-ignites, just like full-scale HCCI engines. Hobbyists often call them model diesel engines. The control of HCCI ignition timing is done by mechanically altering the compression ratio.

Being a hobbyists' area, not much data is available on performance of small model engines. Ogawa & Kawaguchi (2007) tested a four stroke, 5 cc glow ignition

engine. Cyclic variations were reported to be much larger than full scale spark ignition engines. Results included that increase percentage of nitromethane in fuel yielded a narrower range of inflammability.

Raine & Thorwarth (2004) tested a 7.4 cc two stroke, glow ignition model engine. Cyclic variation was also reported to be more severe than full scale engines. Glow plugs of different heat ranges were tested and they reported that cold heat range rating glow plugs ignites the mixture sooner, and medium rating glow plugs showed increased power with increased nitromethane content. They reported low cyclic variation at a carburetor setting at 4 turns and 0% nitromethane. (Fuel air ratio in small model engine is difficult to regulate thus is usually roughly controlled by setting the turns of carburetor needle valve.)

Ma et. al (2006) tested a 7.4 cc two-stroke glow ignition engine. Results showed that a faster combustion did not necessarily yield a higher indicated mean effective pressure since the start of combustion could shift away from its optimum value. Combustion analysis was conducted using burn rate analysis, heat release analysis, and the author's own method combining the two. Combustion duration in crank angle degrees was found to be similar to full scale engines.

4.3 Test setup

4.3.1 Test engine and fuel

The test engine is the AP Hornet 09 R/C engine shown in Figure 4-1. It is an air cooled two-stroke crankcase compression model engine with rotary valve intake system, which is the most common configuration used in model engines. The engine utilizes crankcase compression and Schneurle type loop scavenging. The specifications of the test engine are listed in Table 4-1. Geometric compression ratio was calculated by dividing BDC cylinder volume by TDC cylinder volume. Closed

cycle compression ratio was calculated by dividing cylinder volume when exhaust port is closed, by TDC cylinder volume. Closed cycle compression ratio is the effective compression ratio during compression stroke, since the in-cylinder charge does not start to build up pressure until the exhaust port is closed and the cylinder becomes a closed volume.

Table 4-1 Specifications of AP .09 model aircraft engine

Displacement	1.47 ml
Bore	12.5 mm
Stroke	12.0 mm
Geometric comp ratio	8.08
Closed cycle comp ratio	6.31
Exhaust port close/open	112 BTDC/ATDC
Transfer port close/open	121 BTDC/ATDC

The test engine ran on glow ignition model engine fuel, which is 55% methanol, 25% nitromethane and 20% lubrication oil. The fuel's density was about 0.9 g/mL and lower heating value was calculated to be 12.75 kJ/mL. In these calculations combustion of lubrication oil was neglected, for two reasons: (1) it is assumed that the lubrication oil enters the cylinder in agglomerates and would not combust well; (2) While about 5% of lubrication oil mixed in fuel is sufficient for two stroke engine lubrication (Blair 1996), model engine fuel has 20% lube oil. The excess lube oil serves as heat sink to cool the cylinder (Gierke 2007), offsetting some of the oil combustion heat.

Stoichiometric is the condition that oxygen in the fuel air mixture is just enough for fuel to completely burn. Chemical equation for complete stoichiometric burning of methanol is

$$CH_3OH + 1.5\ O_2 \rightarrow CO_2 + 2\ H_2O$$

Chemical equation for nitromethane's complete combustion is

$$CH_3NO_2 + 0.75\ O_2 \rightarrow CO_2 + 1.5\ H_2O + 0.5\ N_2$$

Each kilogram of model engine fuel contains 316.2 gram of nitromethane and 478.4 grams of methanol, thus the air mass needed to completely burn a kilogram of model engine fuel is

$$m_{air} = 316.2 \times \frac{0.75 \times 32}{61} \times 4.292 + 478.4 \times \frac{1.5 \times 32}{32} \times 4.292$$

$$= 533.95 + 3079.94 = 3613.9\ g \quad (4.1)$$

Equation for burning methanol and nitromethane mixture in 1 kilogram of model engine fuel is

$$14.95\ CH_3OH + 5.184\ CH_3NO_2 + 0.689\ Oil + 26.313\ O_2 \rightarrow 20.134\ CO_2 + 37.676\ H_2O + 2.592\ N_2 + 0.689\ Oil$$

Oil was assumed to be castol oil which was assumed to be composed of ricinoleic acid ($C_{18}H_{34}O_3$). Stoichiometric air/fuel mass ratio is

$$\emptyset = \frac{3613.9}{1000} = 3.61 \quad (4.2)$$

Nitromethane is 25% in volume in the fuel, uses 14.8% of the oxygen when the fuel combusts completely, and provides 23.4 % combustion heat. When combusted completely, nitromethane's combustion heat / utilized air ratio is 1.76 times of methanol. Furthermore, nitromethane is also able to combust as a mono-propellant. As a result more nitromethane in the fuel mixture usually results in more power.

4.3.2 Test benches setup

An engine dynamometer test bench was constructed (Figure 4-2). The intake flow rate was measured by a bubble flow meter (Gilibrator), in which bubbles went with air stream and velocity of the bubbles was measured by optical sensors. Torque and intake air flow rate were steady state measurements and were read from the scale and the flow meter screens. The fuel flow was measured by timing the fuel level dropping in the graduate cylinder. The dynamometer brake was a hysteresis type brake (HB-50m-3, Magtrol Inc.), whose brake torque was controlled by the current going through it. The engine brake torque output was measured by the reaction torque which acted on the scale through a 200 mm arm.

A pressure transducer (D-22255Q, Optrand) was installed on the cylinder head to measure the in-cylinder pressure, and an optical encoder (US Digital Inc.) with 100 pulses per revolution was used to measure crankshaft angle. Pressure transducer and encoder signals were sent into a data acquisition system, which included a data acquisition card (PCI-6143, National Instrument) and LabVIEW software. Sampling rate was 200k/s so that at least 800 data points were collected during each cycle of engine crankshaft rotation.

The engine was tested during different carburetor setting at different speeds. Adjustment of engine speed was done by adjusting dyno brake torque load. Air fuel ratio was controlled by the needle valve in the model engine carburetor. The carburetor needle valve setting was indicated by the rotations it turned from fully closed position. For example a 'Carburetor 4.5 turns' means that the carburetor needle valve was turned open 4.5 turns from fully closed position. The throttle was set in its wide open position during tests.

Fuel pressure head at the carburetor was a factor in air fuel ratio control. With the same carburetor needle valve setting, higher fuel head would result in richer mixture.

To hold the fuel head constant during the testing, a float bowl of a lawn mower carburetor was used to separate the fuel flow measurement graduated cylinder and the engine, so that when fuel level dropped in the graduated cylinder as engine consumed fuel, the fuel head at engine carburetor remained the same.

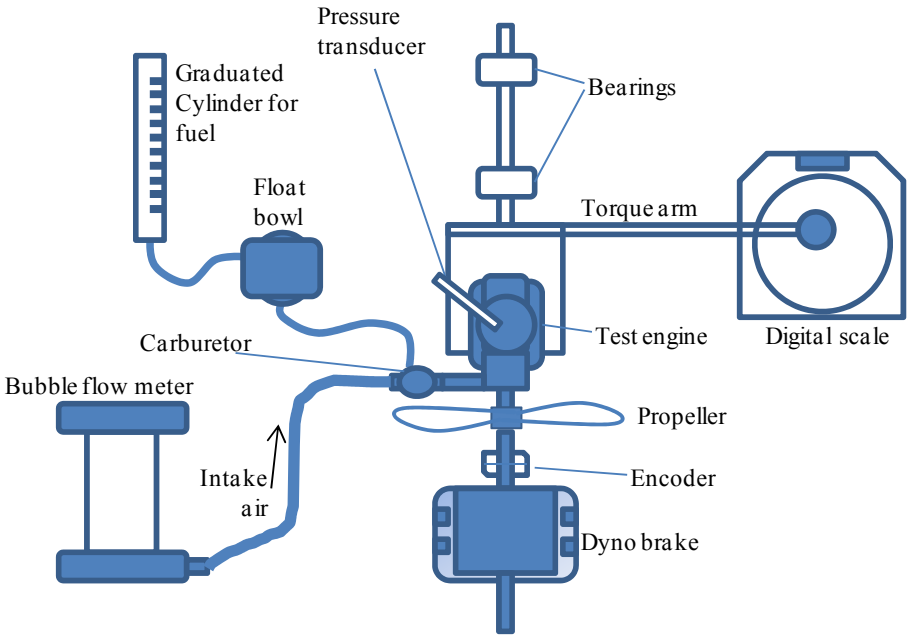

Figure 4-2 Model engine dyno test bench with data acquisition (DAQ) system

Another engine motoring bench was constructed to motor the test model engine at various speed to measure in-cylinder gas leakage level. Another AP .09 drive engine and a test engine were coupled with a shaft coupler, as shown in Figure 4-3. Pictures of the two test benches are shown in Appendix D.

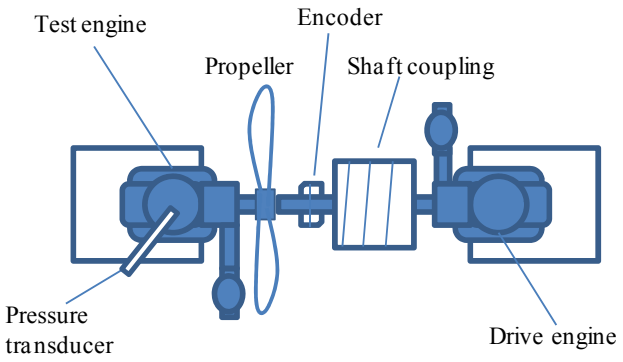

Figure 4-3 Model engine motoring test bench for leakage measurement

4.4 Test results and component models

4.4.1 Model engine general characteristics

While the model aircraft engine was running at 10200 rpm with an 8x4 propeller, pressure and encoder signal for randomly selected seven consecutive cycles were recorded and illustrated in Figure 4-4, to provide an example of acquired experimental data. Pressure traces of the 7 cycles deviated once combustion of fuel air mixture started at about 20 crank angle degrees before top dead center, indicating some cyclic variation.

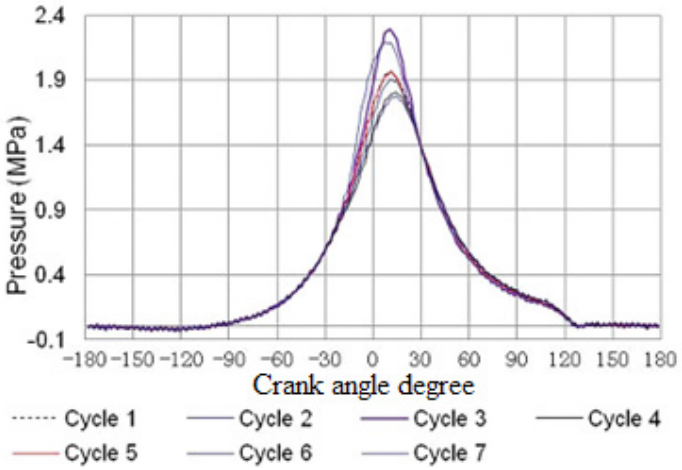

Figure 4-4 Pressure trace versus crank angle degree in seven consecutive cycles (A crank angle of 0 indicates TDC)

Engine power level can be presented by indicated mean effective pressure (IMEP), which is calculated by

$$\text{IMEP} = \frac{\text{Indicated work } \int \text{pdV per cycle}}{\text{Swept volume}} \tag{4.3}$$

The engine was bench tested with wide open throttle and the results with carburetor at 4.5 turns are shown in Figure 4-5. The engine was found to have a practical speed range of 5700 to 11500 rpm. Operating at speed lower than 5700 rpm the engine tended to stall. The power dropped rapidly after speed gets higher than around 11000 rpm. Peak IMEP was measured to be around 4 bar. Peak indicated power was around 100 W, at about 10500 rpm, while peak brake power was around 68 W at 9500 rpm.

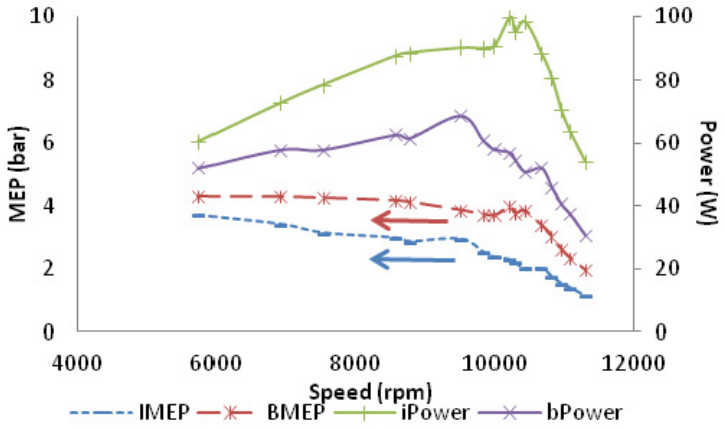

Figure 4-5 Engine characteristics with carburetor on 4.5 turns and wide open throttle

Indicated efficiency was calculated by dividing the indicated work output, which was calculated from in-cylinder pressure trace, by the energy of the consumed fuel. Engine indicated efficiency at different carburetor needle valve settings. Leaner carburetor needle valve setting generally resulted in higher cycle efficiency.

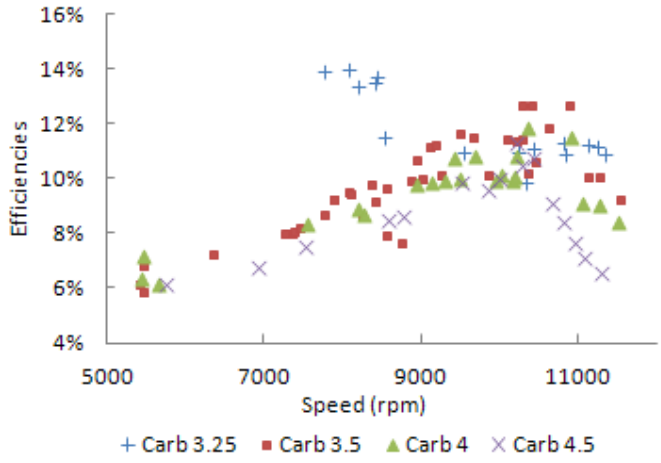

Figure 4-6 Model engine indicated efficiencies at different carburetor needle valve setting

Air fuel ratio was calculated by dividing air mass flow rate by fuel mass flow rate. Engine indicated efficiency was found to correlate with engine air/fuel ratio as shown in Figure 4-7. Engine efficiency generally increased with leaner air/fuel mixture. The fuel was a mixture of methanol, nitromethane and lubricant, which had

a stoichiometric air/fuel mass ratio of 3.61. When running the engine near stoichiometric or a little bit leaner, the engine had best indicated efficiency, while having maximum power output.

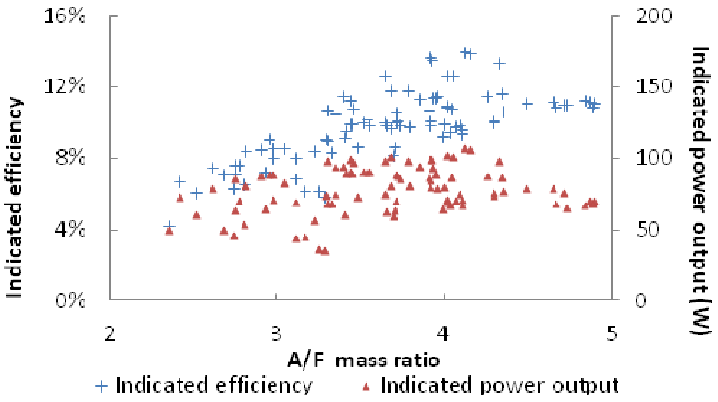

Figure 4-7 Engine indicated efficiency and power output related with A/F ratio

The engine showed quite high level of cyclic variations, which can be indicated by coefficient of variation of peak pressure or IMEP of consecutive cycles. The coefficients of variation (CoV), i.e. standard deviation/mean, were around 10% for IMEP, and around 15% for peak pressure. These coefficients were found to correlate well with start of combustion of each cycle, regardless of different air fuel ratio, as shown in Figure 4-8. Cyclic variation of IMEP was lowest at ignition timing of about 25 degrees before TDC.

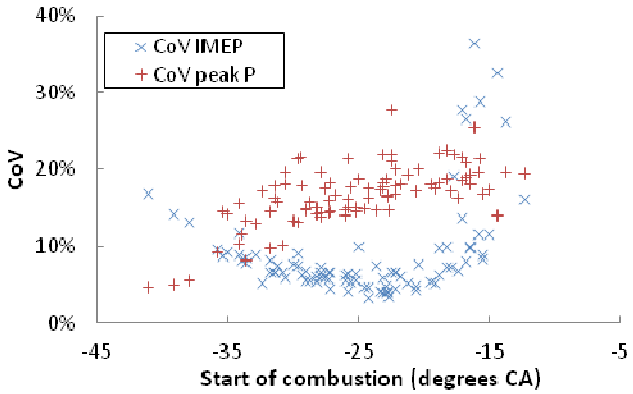

Figure 4-8 Cyclic variation related to the start of combustion

Results for engine intake air flow are shown in Figure 4-9. The model engine had a rotary valve induction system with fixed rotary valve open and close timings. As a result, timing of the rotary valve was only tuned for a range of engine speed. With the test engine, the rotary induction system was most efficient below 10000 rpm, enabling intake delivery ratio of 0.8 to 1. Delivery ratio is defined as

$$\mathrm{DR} = \frac{\text{mass of delivered charge into the cylinder}}{\text{swept volume} \times \text{ambient density}} \tag{4.4}$$

Delivery ratio is the indication of how much fuel air mixture is withdrawn into the engine through the intake valve in each cycle. When engine speed exceeded 10000 rpm, more engine speed even resulted in less air intake flow rate due to rapidly dropping intake delivery ratio, i.e. during each cycle the engine breathed in much less air since the timing of the rotary valve was not optimized for high speeds. The dropping intake air flow rate together with more friction were the reasons why the brake power output of the test engine dropped rapidly above 10000 rpm engine speed.

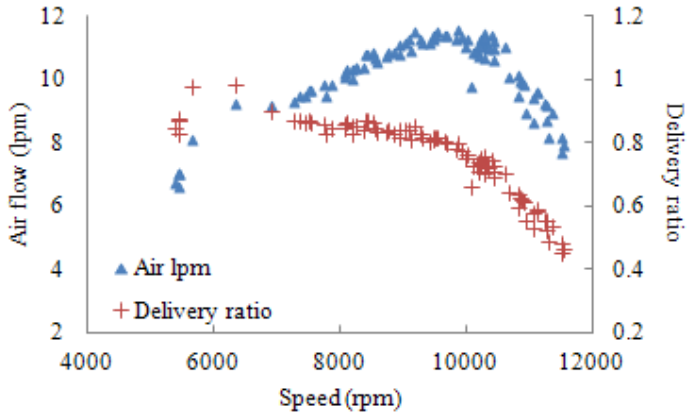

Figure 4-9 Model engine air induction versus engine speed

4.4.2 Cylinder-piston gap leakage

As the engine gets smaller the charge leakage through the cylinder-piston gap becomes the dominant factor affecting the efficiency of the engine (Sher et. al 2009). This is because the leakage gap is determined by machining tolerances and stays the same with size. As a result, with smaller engine, higher percentage of the in-cylinder charge leaks.

Experimental results

The engine was motored at various speeds on the engine motoring bench as shown in Figure 4-3. As the speed varies, different levels of leakage were observed as shown in Figure 4-10, which was the result of less time for the charge to leak down at higher speed.

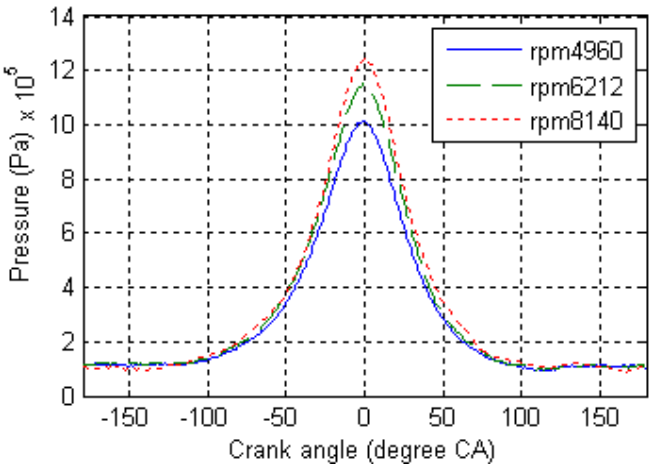

Figure 4-10 Motoring pressure trace at various speeds to study leakage

The log-log plot of the pressure traces is shown in Figure 4-11. The compression and expansion of the in-cylinder charge showed good linearity in the log-log plot, with the R-square of linear fitting bigger than 0.9999. From these data, the effect of leakage and heat transfer on the compression and expansion was linear on log-log plot, i.e. those effects can be taken into account by a polytropic index. The more

severe leakage yielded a smaller compression polytropic index, and a larger expansion one.

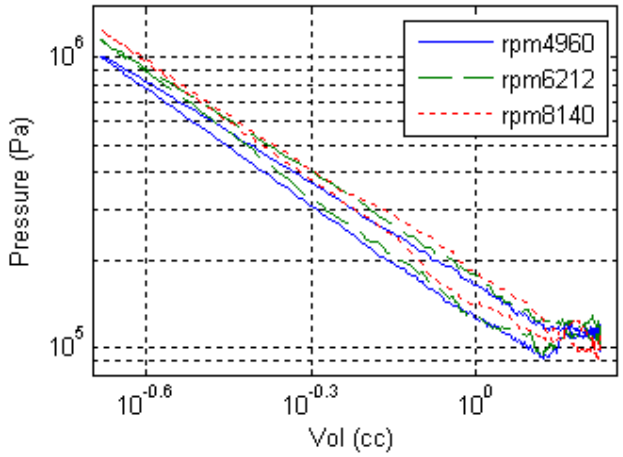

Figure 4-11 logP-logV plot for engine motoring

Leakage simulation

As discussed in 3.3.2, an orifice flow model can be used to calculate flow rate through the piston-cylinder gap. The piston-cylinder gap was difficult to measure due to the uncertainty of the temperature and thermal expansion of the piston and cylinder liner during engine operation. Thus the gap was assumed to be 20 μm as recommended by Sher et. al (2009). The flow coefficient C_d can be calibrated to fit the experimental data obtained from the motoring test, in which the test engine was motored without firing at various speeds on the motoring test stand shown in Figure 4-3.

A flow coefficient of 0.065 was determined from the fitting between the model and the experimental data. The simulation data with only heat transfer, simulation with heat transfer and leakage and experimental data are compared in Figure 4-12. The engine motoring simulation assumed ideal gas of air and used heat transfer model proposed by Annand (1963).

It can be seen that both heat transfer and leakage has the effect to decrease peak motoring pressure as engine speed decrease, i.e. while engine has more time to lose heat and lose in-cylinder mass. Without these effects, the engine would have the same peak motoring pressure at different speed. As engine speed got higher, the peak motoring pressure got closer and closer to the ideal peak motoring pressure at about 14 bar.

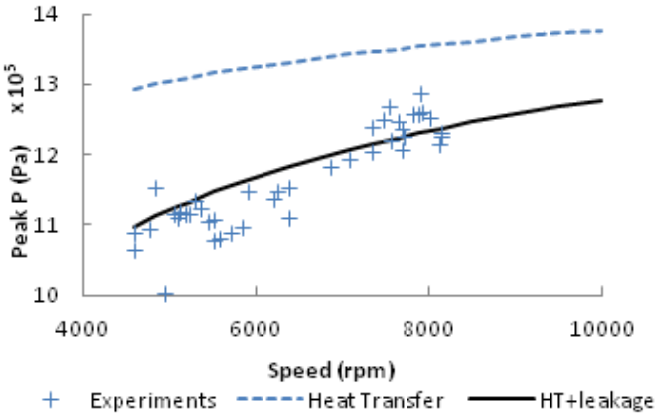

Figure 4-12 Leakage model and comparison with experimental data from engine motoring

The low flow coefficient of 0.065 generally results from the lubricant in the gap between cylinder and piston. While the flow area is calculated from the piston cylinder gap when it's dry, the gap is usually partially filled with lube oil especially because of the high percentage of lubrication oil used in model engine fuel (20%). As a result the actual flow area is much lower than the dry area, hence low flow coefficient.

4.4.3 Friction

Friction loss in a two stroke engine comes from mechanical friction between cylinder and piston, and friction in bearings. Also, crankcase scavenging engines do work to compress crankcase volume resulting in more pumping loss. In this research, the pumping loss is included in the friction loss. The friction loss in an engine causes

the difference between indicated power and brake power, hence the mechanical efficiency. The mechanical efficiency of this specific engine was around 70% in low speed, and dropped rapidly in speed higher than 10000 rpm, as shown in Figure 4-13, due to higher level of friction and decreasing brake power output above 10000 rpm, as shown in earlier sections.

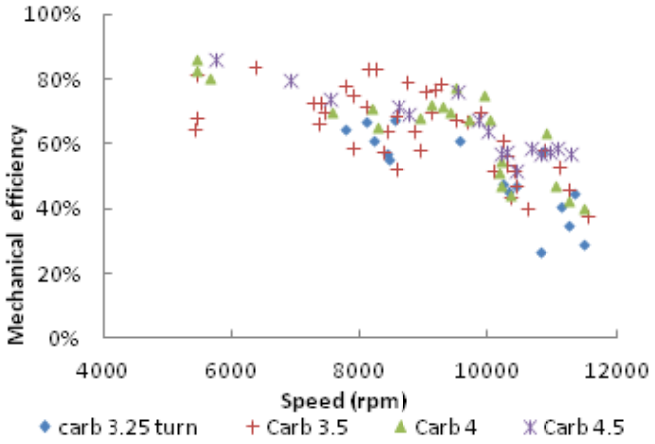

Figure 4-13 Mechanical efficiency of the engine

Friction level in an engine can be indicated by friction mean effective pressure (FMEP), calculated by

$$\text{FMEP} = \frac{\text{Friction work per cylinder per cycle}}{\text{Swept volume per cylinder}} \tag{4.5}$$

FMEP can be translated to a friction torque on the crankshaft, just as BMEP would translate to brake torque output on the crankshaft. Heywood and Sher (1999) recommend using a quadratic equation to model friction in a two-stroke engine

$$\text{FMEP} = \text{a} + \text{b}\left(\frac{\text{N}}{1000}\right) + \text{c}\left(\frac{\text{N}}{1000}\right)^2 \tag{4.6}$$

where FMEP is in kPa and engine speed N is in rpm. The term a is associated with mechanical friction, which does not change with engine speed, resulting in a

constant term in the FMEP. In a two stroke engine, the pumping work for crankcase scavenging system is included in this constant term as well. The $b\left(\frac{N}{1000}\right)$ term is associated with hydrodynamic friction due to lubrication oil in bearings and piston-cylinder gap. Hydrodynamic friction is proportional to speed gradient in the lubrication oil film, resulting in a linear term with engine speed in FMEP. The third term, $c(\frac{N}{1000})^2$, is associated with aerodynamic friction. It is quadratic with engine speed as aerodynamic drag force is in proportion to the square power of speed.

Using MATLAB polynomial fitting tool, the model was fit with experimental data. The coefficients were determined as $a = 0.2$, $b = 0.08$ and $c = 0.002$. Comparison of model and experiments are shown in Figure 4-14. The experimental and modeling results suggested that hydrodynamic friction in model aircraft engine is dominant compared to static mechanical friction, as shown by the increasing FMEP value with higher speed, and high b value in the friction FMEP model. This is due to the high lubrication oil content (20%) in model engine fuel. By design, the lubrication oil is used to lubricate bearings and piston, cool the engine, and help sealing the piston-cylinder gap especially since there are no piston rings on the piston (Gierke, 2007).

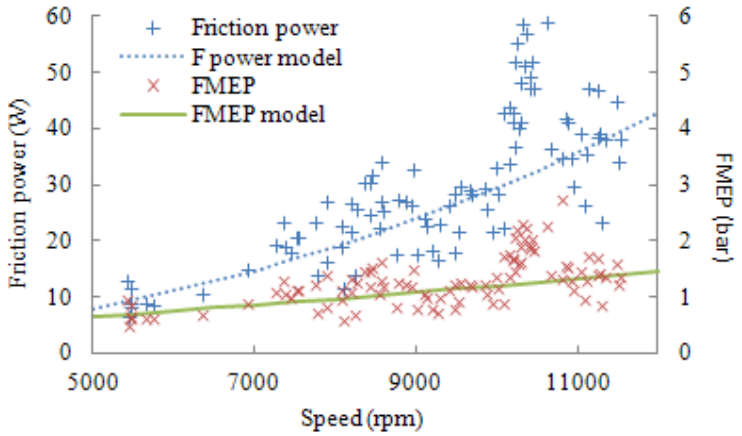

Figure 4-14 Crankshaft speed based friction model and experimental data comparison

4.4.4 Combustion analysis and glow ignition combustion modeling

Combustion analysis is the approach to obtain fuel combustion information from the experimentally measured in-cylinder pressure. Common methods used are burn rate analysis and heat release analysis.

Burn rate analysis

A burn rate analysis (Rassweiler & Withrow 1938) can be used to calculate the mass fraction burned, from the pressure data obtained experimentally. The basis of this approach is the assumption that the pressure rise is made of a pressure rise due to combustion (Δp_c) and a pressure rise due to volume change (Δp_v)

$$\Delta p = \Delta p_c + \Delta p_v = \Delta p_c + p_i \left[\left(\frac{V_i}{V_{i+1}} \right)^k - 1 \right] \tag{4.7}$$

where p is the pressure, V is volume and k is the polytropic index. Prefix Δ indicates the change. Subscripts i and $i+1$ indicate current and next time-step, as the formula is calculated in each time-step to determine Δp_c in each time-step. With the assumption that pressure rise referred to a datum volume due to combustion is proportional to the mass fraction burned (mfb), the mfb can then be calculated.

An essential aspect of this method is to determine correct polytropic index during compression and expansion. A log-log plot of in-cylinder pressure of a cycle is shown in Figure 4-15. In this plot, the engine started compressing the mixture at point A, and the mixture ignites at point B. The compression process can be seen to be a straight line in log-log plot before ignition, i.e. a polytropic process. After ignition, the pressure curve in log-log plot was no longer a straight line due to fuel combustion. But after the fuel combustion was finished at point C, the expansion process was polytropic. Thus the compression and expansion polytropic index can

be obtained from curve fitting method from data between A and B, and between C and D.

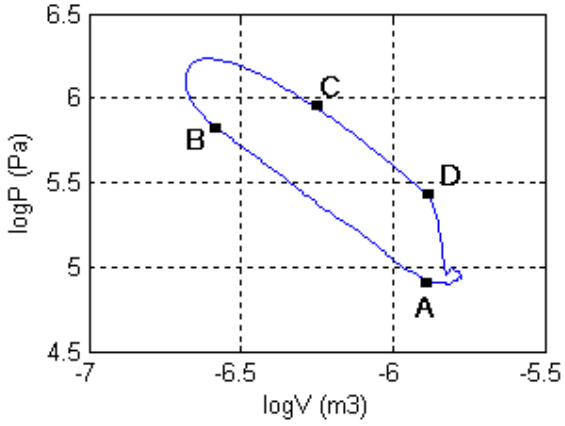

Figure 4-15 logP-logV plot of a cycle, at 10236 rpm, carburetor 4 turns

Heat release analysis, considering leakage

Heat release analysis is the approach to consider the combustion chamber as a control volume, and analysis the energy exchange in every time-step. Thus the fuel combustion heat release can be inferred from the pressure data. For this specific engine, in-cylinder mixture leakage is quite severe, thus there is some enthalpy loss associated with this. Considering this mixture leakage, the energy balance equation can be expressed as

$$m_{cv} c_v \frac{dT}{dt} = \dot{Q}_{fuel} + \dot{Q}_{HT} - \dot{W} - \sum \dot{m}_{leak} (h_{cv} - u_{cv}) \tag{4.8}$$

The terms in this equation from left to right are control volume internal energy change, fuel combustion heat, heat transfer, work output and internal energy loss due to leakage. m, c_v, T, Q, W, h and u are mass, constant volume specific heat, temperature, heat, work, enthalpy and internal energy. Subscript cv means control volume. Temperature of each time step can be calculated from measured in cylinder pressure. Heat transfer model proposed by Annand (1963) was used to

calculate the heat transfer. The leakage model was the experimentally fitted model discussed in previous section. The mass fraction burned data calculated from heat release analysis and burn rate analysis are compared in Figure 4-16. The accordance between the two calculations further validated the combustion analysis methods used.

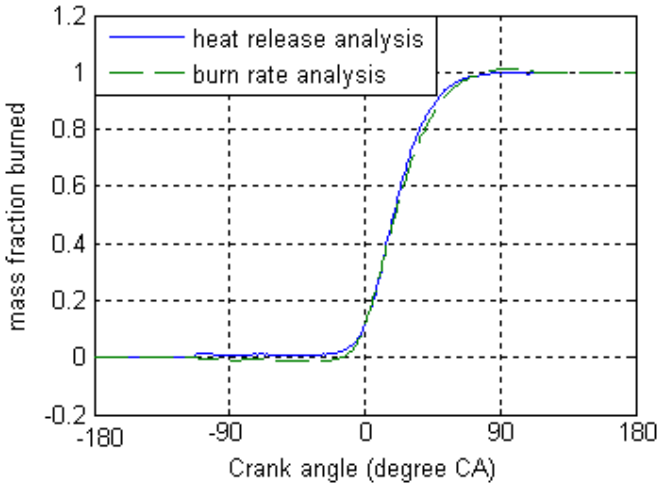

Figure 4-16 Comparison of mass fraction burned calculated from heat release analysis and burn rate analysis, at 10236 rpm, carburetor 4 turns

Combustion analysis results and glow ignition simulation

Ignition timing simulation

The engine utilizes glow ignition where the mixture ignites with the help of the glowing hot platinum wire in the combustion chamber. Since the heat is added to the glow plug during combustion period and dissipated during scavenging and compression, the platinum coil is subject to a temperature variation. Biot number and thermal time constant are used to characterize this temperature fluctuation. Biot and thermal constant τ_t can be calculated to characterize the platinum wire temperature variation. The characteristic length is the coil wire diameter, which is measured to be 0.2 mm

$$\mathrm{Bi} = \frac{hL}{k} \approx 2.8\,\mathrm{E}-4 \quad \tau_t = \frac{\rho c V}{hA} \approx 3.6 \text{ seconds} \tag{4.9}$$

With this small Biot number, heat conduction inside the wire is much faster than the heat convection away from its surface and the wire can be treated as a lumped system. Also, the time constant is much larger than the engine cycle time which is 5-10 ms for the engine which runs at 100-200 Hz. This indicates that the heat penetration through the platinum wire is slow compared to the cycle time. Thus the temperature fluctuation can be neglected and the platinum coil can be considered nearly at constant temperature during operation.

Therefore, the ignition of mixture doesn't have a 'trigger' since the platinum wire is constantly glowing. The ignition is dominated by its own chemical kinetics instead, which is similar to homogeneous charge compression ignition (HCCI) (Heywood 1988)). The mixture reacts and forms free radicals during entire compression, i.e. prepares for ignition, with the help of the glowing platinum wire. If the in-cylinder temperature and pressure are not high enough during the dynamic process of compression stroke, the mixture won't be ready for ignition at any time of the cycle, thus ignition won't occur; and vise versa. For this kind of chemical kinetics dominated ignition, ignition timing can vary widely, compared to well controlled ignition timing with a spark in a spark ignition engine, or with the fuel injection in a compression ignition engine. A time based integral was used to determine the ignition timing, similar to the model of Shaver et. al (2003). Their model was used for HCCI; however as glow ignition is similar to HCCI in that chemical kinetics during compression process determines ignition timing, the model is likely to apply to glow ignition as well. Shaver et. al (2003)'s model is a crank angle degree based integration and is not suitable for a free-piston engine which has no crankshaft. As a result a time based integral was used

$$\int_0^t C_1 T^n \exp(C_2/T)[\text{fuel}]^a[O_2]^b \, dt > Threshold \tag{4.10}$$

where T is the combustion chamber temperature, C_1, C_2, n, a and b are coefficients. The time 0 to start the integration is the exhaust port close time, the start of the closed cycle. Over time, when the integral exceeds the threshold, ignition occurs. The coefficients and threshold were adjusted to fit experimental data. C1, C2, a, b, n and Threshold were set to be 1e-16, 50, 0.1, 0, 7 and 4. The fitting of simulated ignition timing to experimental data is shown in Figure 4-17. The glow ignition timing varies widely between -40 and -10 degrees BTDC, and relates to engine speed. The model is capable of capturing this trend.

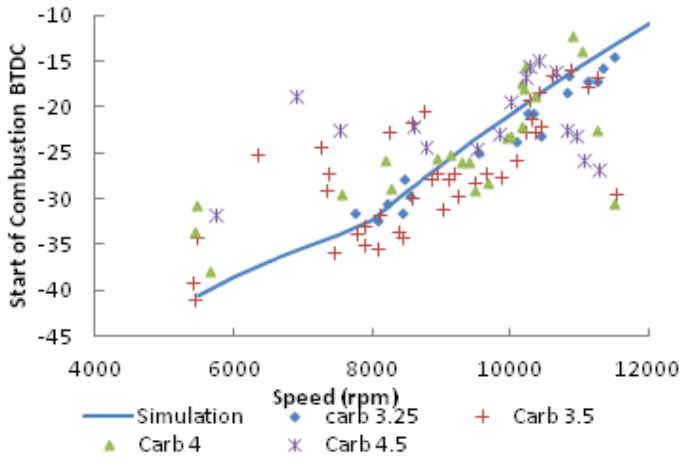

Figure 4-17 Comparison of start of combustion from simulation, and from combustion analysis of experimental data

Heat release simulation

Due to the strong catalytic effect of glowing platinum wire, the combustion in a model engine starts from the glow plug and the flame propagates through the entire combustion chamber, in a pattern similar to that of spark ignition engine. For this type of flame propagation, a Vibe function can be used to simulate the combustion process of the fuel

$$x = 1 - \exp\left[-a\left(t - t_o/\Delta t\right)^{m+1}\right] \tag{4.11}$$

where x is fuel consumption percentage, t_o is ignition time, Δt is combustion duration and a and m are coefficients for the Vibe function.

From the combustion analysis data, the combustion duration was calculated in time space, as shown in Figure 4-18. Although some fluctuation exists especially in slow engine speeds, the combustion duration generally stayed unchanged in time, with an average value of 1.43 mille-seconds, which corresponded to a flame propagation speed of about 5.2 m/s. The engine seemed to hold this flame propagation speed constant at various engine speeds, for the specific model engine fuel and at wide open throttle (WOT). As a result, in constructed combustion models this constant combustion duration assumption was made.

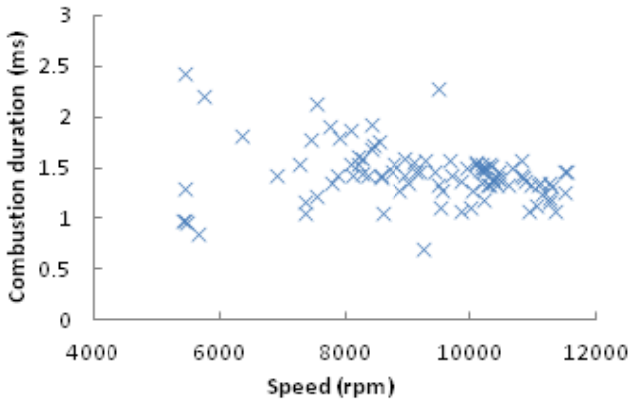

Figure 4-18 Combustion duration at various speeds

The experimental data and simulation of heat release data are compared in Figure 4-19. The model showed good correlation with experimental data in two engine speed of 8208 and 10236 rpm. This suggested that although the combustion model was experimentally fitted and should be considered an empirical calibrated model, it captured the combustion characteristics in a miniature size glow ignition two stroke

engine well, and should be able to predict combustion processes in any operation speed and engine configuration, e.g. in free-piston engine configuration.

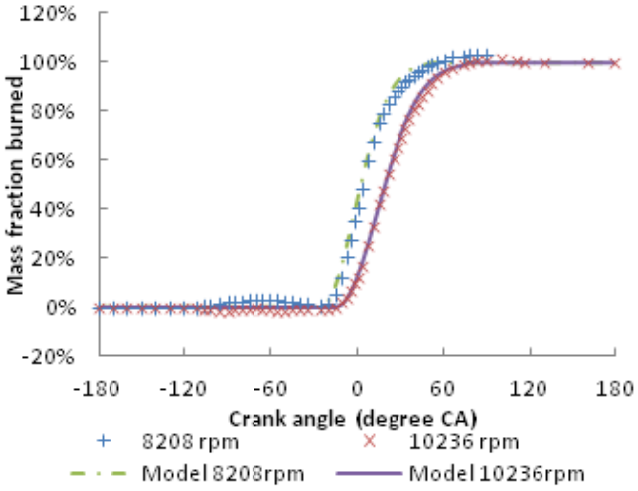

Figure 4-19 Comparison of model engine heat release experimental data and model results, carburetor at 4 turns

4.4.5 Scavenging simulation

Scavenging is the process of displacing burned exhaust gas with fresh fuel air mixture in a two stroke engine when the piston is near bottom dead center. The scavenging model for a two stroke engine needs to determine the relationship between delivery ratio and charging efficiency. Delivery ratio is defined as

$$\mathrm{DR} = \frac{\text{mass of delivered charge through transfer ports}}{\text{swept volume} \times \text{ambient density}} \tag{4.12}$$

Delivery ratio is the indication of how much fuel air mixture is spent in the scavenging process through the transfer ports to displace exhaust gas out. Charging efficiency is defined as

$$\eta_C = \frac{\text{mass of delivered charge retained}}{\text{swept volume} \times \text{ambient density}} \tag{4.13}$$

Charging efficiency is the indication of how well the cylinder is refreshed with new charge. Difference between delivery ratio and charging efficiency is that some fresh air fuel mixture goes out of exhaust port and is wasted in scavenging process, i.e. short-circuiting. Retention efficiency η_r is used to describe the percentage of fuel air mixture retained inside the cylinder after scavenging instead of short-circuiting out of exhaust port:

$$\eta_r = \frac{\text{Charging efficiency}}{\text{Delivery ratio}} \tag{4.14}$$

The retained mixture mass was inferred from the mass of burned fuel, while assuming a combustion efficiency of 75%. Experimental results of charging efficiency versus delivery ratio are shown in Figure 4-20. The engine had poor retention efficiency (around 54%), which means about half the fuel air mixture was lost during scavenging.

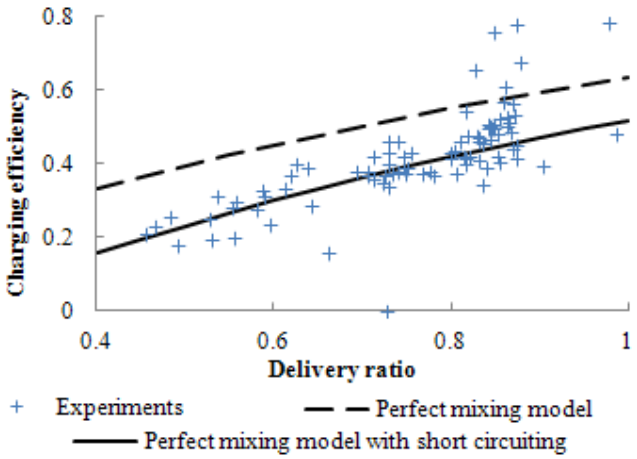

Figure 4-20 Simulation and experimental results of model engine scavenging

In a perfect mixing scavenging model, the fresh charge mixes with burned exhaust gas completely as it enters the cylinder through transfer ports. This is not good case since ideally the fresh charge should push the exhaust out without mixing

with them. In perfect mixing model, the relationship between delivery ratio λ and charging efficiency η_C is

$$\eta_C = 1 - e^{-\lambda} \tag{4.15}$$

However, the charging efficiency of the model engine was even worse than a perfect mixing model as shown in the comparison in Figure 4-20. In this miniature size model aircraft engine, the scavenging system was not optimized to retain more charge and minimize short-circuiting. A model that could fit the experimental results incorporated short circuiting with a short circuiting parameter s,

$$\eta_C = 1 - e^{-(1-s)\lambda} \tag{4.16}$$

In this model, it was assumed that the perfect mixing portion of the fresh charge (1-s) entered the cylinder and mixes with the gas content inside the cylinder instantly to form a homogeneous mixture, while the remainder of the incoming charge (s) went out of the cylinder directly.

4.4.6 Cyclic variation

Cyclic variation is the phenomenon that at a same engine setting, engine cycles present a variation in terms of the combustion strength, ignition timing, combustion duration, etc. In a free-piston engine design, the cyclic variation can be detrimental, since the piston movement is determined by the combustion process instead of by a crankshaft. Thus, a cycle with weak combustion can result in insufficient travel of the piston and ineffective scavenging for the next cycle, stalling the engine.

Two-stroke engines have more cyclic variation problems than four-stroke engines, due to the nature of the scavenging process. Slight cycle to cycle variation of the flow patterns inside the cylinder strongly impact scavenging and thus how much

fresh mixture is retained inside the cylinder. Also, as residual exhaust content is high after scavenging, and the in-cylinder gas composition is not homogeneous, variation of the composition near the glow plug leads to variation in ignition timing.

To determine the intensity of the cyclic variation, experimental data of the model engine were analyzed. Typical results are shown in Figure 4-21 which shows the frequency distribution of charging efficiency over 181 consecutive cycles at the same engine speed, load and carburetor setting.

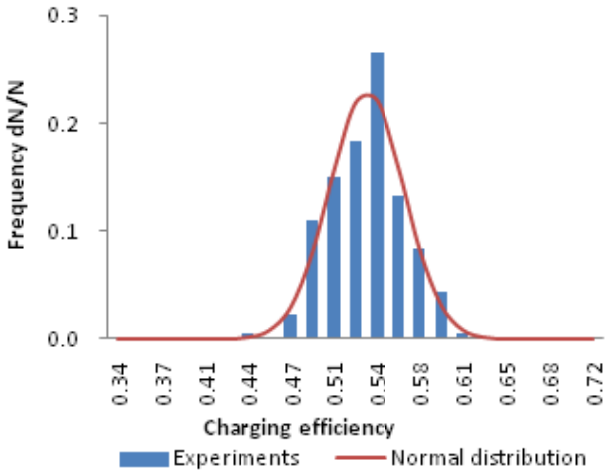

Figure 4-21 Distribution of charging efficiencies of 181 cycles

Based on the distribution of charging efficiency, the cyclic variation was modeled by the random distribution of the short circuiting portion parameter s in the scavenging model described in section 4.4.5:

$$\eta_c = 1 - e^{-(1-s)\lambda} \tag{4.17}$$

where λ is the delivery ratio, η_c is charging efficiency and s is short circuiting parameter.

In the cyclic variation model, the short circuiting parameter s was generated by a normal distribution number generator, with a probability function

$$f(s) = \frac{1}{\sqrt{2\pi\sigma^2}} e^{-\frac{(s-\bar{s})^2}{2\sigma^2}} \tag{4.18}$$

The average short circuiting ratio $\bar{s}$ was determined by the scavenging model, and parameter σ determined was by the fitting with the experimental data from model aircraft engine testing. The experimental data fit with a normal distribution with

$$\frac{\sigma}{\bar{s}} = 6\% \tag{4.19}$$

Cyclic variation in the free-piston engine compressor prototype was modeled by a normal distribution with the same $\sigma/\bar{s}$ value.

4.5 Conclusions

The miniature size two stroke model engine had an IMEP of about 3-4 bar. Cyclic variation was more severe than full scale engines. Engine indicated efficiency was found to be around 10%, mainly from the fuel lost in scavenging.

Blow-by leakage in miniature engines was severe and needed to be considered for simulations and combustion analysis. The lubrication oil helped with decreasing the blow-by leakage. A leakage model was developed and fitted to experimental data.

The miniature size model engine was found to be poorly designed in terms of scavenging and more than half the fuel air mixture comes out of exhaust port without being burned. Better port design for improving the scavenging system might increase the performance and efficiency of miniature size two-stroke engines.

Glow ignition used in model engines was modeled by a chemical kinetics dominated model which is similar to HCCI model. The ignition timing varied

widely with speed. The flame propagation can be simulated with a Vibe function method similar to spark ignition engines.

5 FREE-PISTON ENGINE COMPRESSOR MODELING AND MODEL BASED DESIGN

To further determine the parameters of the engine, models need to be established to predict the engine compressor behavior.

In chapter 4, experiments on existing engine components were conducted to characterize the blow-by leakage, scavenging, glow ignition combustion, and friction. Models were established to describe those individual components, and calibrated with experimental data. These component models could be assembled into an integrated engine compressor model for a prototype design. Some models needed to be adapted for free-piston engine configuration.

In this chapter, a comprehensive model is presented to simulate the engine compressor operation based on the design concept described in previous sections. The model was used to determine the designed engine parameters. Simulations indicated that the free-piston engine compressor was a viable compact fluid power supply. Simulation results predicted that the overall efficiency of the engine compressor is expected to be around 5% and that the package would have a much higher energy density than a battery-motor package.

The engine compressor components which needed to be modeled are shown in Figure 5-1. The engine cylinder, crankcase volume and compressor cylinder were considered control volumes. Mass, work and heat transfer with control volumes were modeled by various component models.

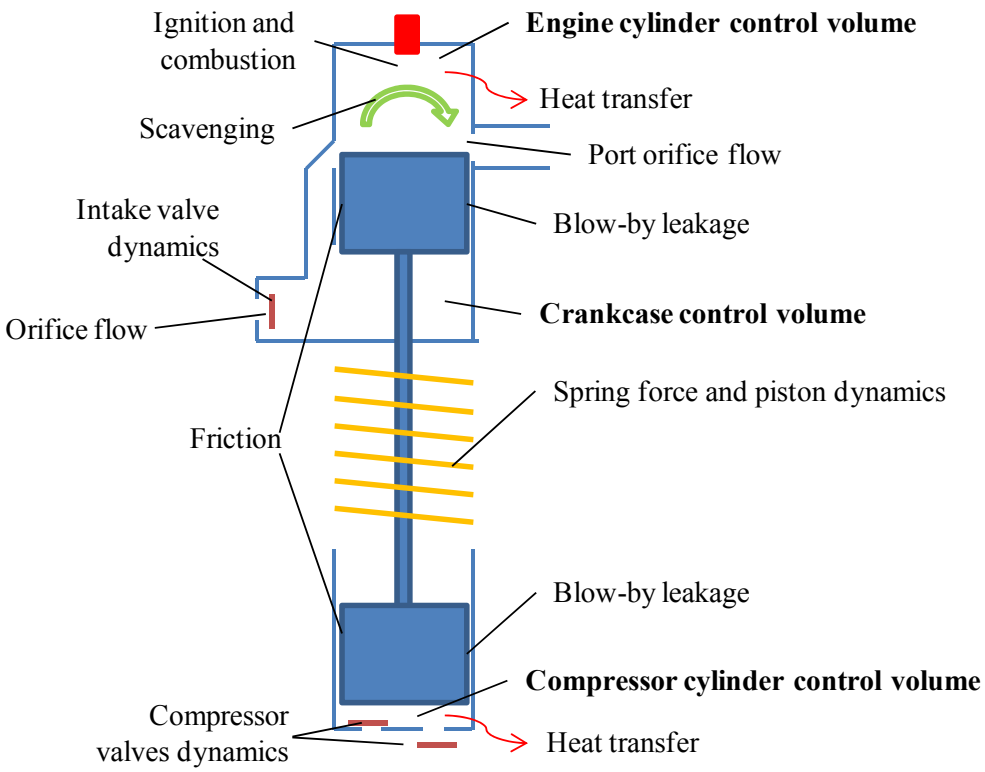

Figure 5-1 Model components in the engine compressor

In the simulations, glow ignition combustion mode was chosen instead of pure HCCI. As discussed in chapter 4, similar to pure HCCI, glow ignition has the same benefit of not needing a timed ignition source and can work well with free-piston engine configuration. Glow ignition requires less compression ratio and glow ignition engine is easier to be cold started due to less compression ratio requirement. It was a good first step towards building an HCCI engine compressor.

5.1 Free-piston engine compressor sub-models

As the tested model aircraft engine and the authors' free-piston design are both in the neighborhood of 1 cm^3 displacement, and they share several components including induction, scavenging, glow ignition and combustion systems, the model

aircraft engine component models were directly used, or adapted to be used in free-piston engine compressor prototype modeling.

5.1.1 Friction

Referring to section 4.4.3, for crankshaft engines, Heywood and Sher (1999) recommend using a quadratic equation to model friction in a two-stroke engine. However, in a free-piston engine, a correlation between friction force and piston speed is more suitable as the free-piston engine does not have a crankshaft. Linear friction force f can be correlated with piston speed v by

$$f = a + bv + cv^2 \tag{5.1}$$

where f is friction in Newton, v is piston speed in m/s, a, b, and c are coefficients which are mainly related to mechanical, hydrodynamic and aerodynamic friction, similar to Heywood and Sher (1999) model coefficients.

Using piston speed based friction model, FMEP in the model aircraft test engine could be calculated by assuming constant crankshaft angular velocity. With a fitting process, a, b and c were determined to be 1.6, 0.5 and 0.04. The fitting to experimental data was similar between piston speed based friction model, and crankshaft rotation speed based friction model in section 4.4.3.

5.1.2 Scavenging, blow-by leakage, glow ignition combustion, cyclic variation and reed check valve models

Model aircraft engine component models described in section 4.4.5, section 4.4.2, section 4.4.4 and section 4.4.6 were used directly in the free-piston engine compressor prototype modeling, as the prototype were designed to utilize off-shelf model aircraft engine piston and cylinder liner which contains scavenging passages. As a result, the scavenging, blow-by leakage, glow ignition combustion and cyclic

variation models of the model aircraft engine would be able to predict scavenging, leakage and combustion characteristics in the free-piston engine compressor prototype.

The prototype was designed to utilize reed check valve for engine crankcase intake system, compressor intake and compressor output. The reed valve model described in section 3.3.4 was used for all those check valves to model there opening and closing response.

5.1.3 Thermodynamic model for each chamber

The energy balance of combustion, crankcase and compressor chambers were determined by the first law of thermodynamics

$$m_{c.v}c_v\frac{dT}{dt} = \dot{Q} - \dot{W} + \sum \dot{m}_{in}\left(h_{in} - u_{c.v.}\right) - \sum \dot{m}_{out}\left(h_{out} - u_{c.v.}\right) \tag{5.2}$$

where m is the mass, $\dot{Q}$ is heat transfer and $\dot{W}$ is work transfer. Subscripts in and out denote inflow and outflow of the control volume. Mass transfer through crankcase included intake flow through induction reed valve and scavenging outflow into combustion chamber through transfer ports. Mass transfer through combustion chamber included scavenging inflow from transfer ports, scavenging outflow out of exhaust ports and leakage flow through piston cylinder gap. Mass transfer through compressor chamber included inflow from compressor intake check valve, output flow through compressor output check valve and leakage flow through compressor piston cylinder gap.

5.1.4 Compressor modeling

The compressor cylinder was modeled as a control volume. Intake and output check valves controlled the flow into and out of the compressor cylinder. Previous mentioned valve dynamics model was used to simulate those valves.

Leakage model was used for the compressor blow-by leakage flow in the gap between compressor piston and cylinder. Leakage flow coefficient was adjusted to account for the more severe leakage compared to the engine side, because less lubrication oil would be in the compressor piston cylinder gap to help with sealing.

5.1.5 Heat transfer model

The heat transfer model suggested by Sher et. al (2009) was used, as previously described in section 3.3.2. Sutherland's formula was used to derive the dynamic viscosity of an ideal gas as a function of the temperature.

5.1.6 Piston dynamics

The motion of the free-piston was determined by force balance of the pressure inside the engine cylinder, engine crankcase and compressor cylinder, the friction force, f, and the return spring force, F_{spring}. As a metal spring was used in the prototype design, F_{spring} could be calculated from piston position. Piston motion dynamics were

$$m_{piston}\frac{dv_{piston}}{dt} =$$

$$\left(P_{eng\,cyl} - P_{crankc}\right)A_{eng\,pist} - \left(P_{comp\ cyl} - P_{atm}\right)A_{comp\ pist} - F_{spring} - f \quad (5.3)$$

5.2 Engine compressor overall model

An overall model for the engine compressor was constructed based on the experimentally fitted and verified sub-models using the MATLAB SIMULINK tool, as shown in Figure 5-2. SIMULINK is an effective graphical interface for designing, simulating and testing time-variant dynamic systems.

The SIMULINK model for the engine compressor prototype graphically consisted of five sub-models: (1) engine cylinder thermodynamics, energy transfer and combustion dynamics (sections 5.1.3, 5.1.5, 4.4.4 and 4.4.6); (2) crankcase thermodynamics and energy transfer (sections 5.1.3); (3) compressor cylinder thermodynamics and energy transfer (sections 5.1.3, 5.1.4, 5.1.5); (4) mass transfer flow rates calculation (sections 4.4.2 and 4.4.5); and (5) piston assembly motion dynamics calculation (sections 5.1.6 and 5.1.1). Each sub-model had its own hierarchies of sub-models, some of which were the component sub-models described previously.

With the SIMULINK model, the starting and operation could be simulated with all sub-models in place. The overall model was used to examine factors the influence engine compressor performance.

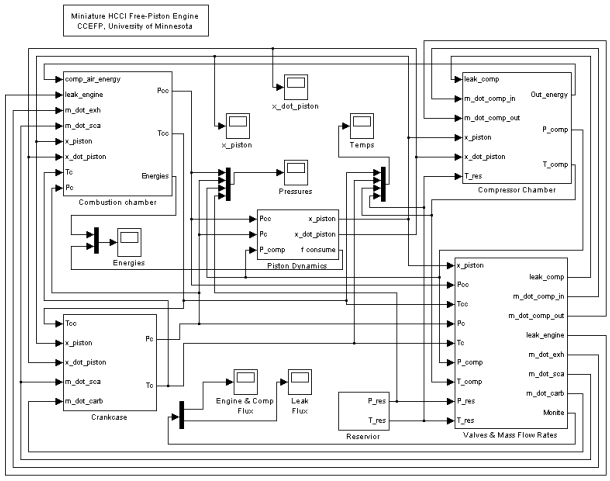

Figure 5-2 Engine Compressor overall model in SIMULINK

5.3 Using models to determine target engine speed

In previous discussion of preliminary simulation in chapter 3, a target operation speed of 80-330 Hz was set considering effects of leakage and chemical kinetics. Reed check valve response was found not to be a limiting factor in speed range. However in those simulations friction effect was not considered. As engine compressor component models were constructed and calibrated, now the target engine speed could be specified.

The trade-off between leakage, heat transfer and friction determined the optimum operating speed of the engine. The overall engine compressor model was used to determine optimum speed. High engine speed reduced leakage and heat transfer losses, but increased friction losses considerably. This trade-off was simulated and the results are shown in Figure 5-3. The retention efficiency indicates how much mixture is retained inside the cylinder without leaking through the cylinder-piston gap. It was quite low at low speed, for example at 50 Hz operation about half of the cylinder charge was lost due to leakage. On the other hand, the mechanical efficiency dropped with increasing speed. From the overall efficiency curve, the engine's optimum operating range was determined to be between 100 and 150 Hz.

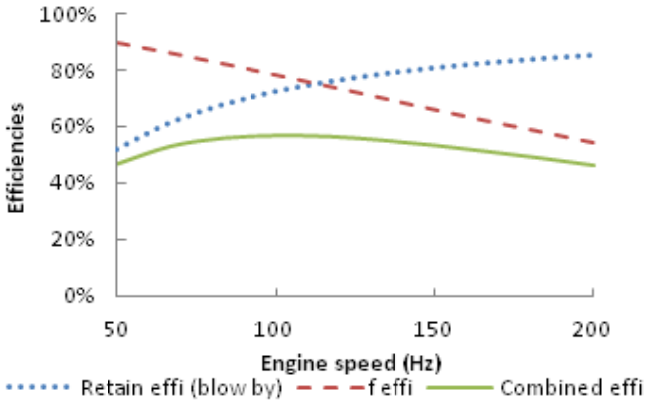

Figure 5-3 Trade off of several efficiencies with engine speed

Higher operating speed would yield more severe noise, vibration and harshness problem. As a result, the free-piston engine compressor target operating speed was chosen to be 100 Hz. It should be noted that this target speed can change if the leakage or friction level in the designed prototype changes. Currently model engine components were used which resulted in the same leakage and friction levels as in a model aircraft engine. If more optimized components were used and for example, friction level decreases, then the trade-off between leakage and friction can shift towards higher speed range.

5.4 Free-piston engine parameters

With the engine operating speed specified, the engine size could be determined because the target power output was known. This target could be met using standard components. Thus, the engine compressor was designed to utilize an AP .09 model engine cylinder linear component, which has a bore of 12.5 mm and nominal stroke of 12 mm. In free-piston configuration the stroke could be more or less than 12 mm depending on the piston motion dynamics.

The free-piston engine can be considered a damped spring-mass system consisting of the rebound spring and the piston assembly. The combustion inside the engine cylinder accelerates the mass spring system and converts expansion work to kinetic energy and potential energy in spring and air compression while friction and discharge of compressed air dissipates energy. Spring stiffness and piston assembly mass are the main parameters to determine the engine operating speed. The effective spring constant includes that of the metal spring and nonlinear components associated with gas compression and expansion in the engine and compressor. A preloaded spring with a spring constant, k=1500 N/m, and a preload of 10 N was selected to provide sufficient energy for compression of the charge. The piston

assembly mass was then adjusted to give the desired operating frequency. A piston assembly mass of 40 grams led to an operating frequency of 98 Hz.

As discussed in the cyclic variation sub-model section, the miniature size two-cycle engine showed strong cyclic variation which was detrimental for a free-piston engine. To address this problem, the free-piston engine compressor was designed to 'over-stroke' past the nominal bottom dead center (BDC) in an average cycle. Thus when a weak cycle occurs, the piston could still travel far enough to uncover the scavenging and exhaust ports enough for an effective scavenging process.

5.5 Simulated engine operation

5.5.1 Starting of engine

The scenario for starting of the engine was that the piston was pulled to the bottom position where the rebound spring is fully compressed. When the piston was released, it initiated the first cycle of combustion. Simulated pressure traces of several cycles of the engine compressor operation after starting are shown in Figure 5-4. From the simulation, the first cycle had later ignition due to cold in-cylinder temperature. After the first cycle, ignition timing was advanced due to the high temperature residual exhaust from the previous cycle. In operation, when the compressor cylinder pressure exceeded the reservoir pressure, compressor output valve opened and the compressed air was delivered to the reservoir.

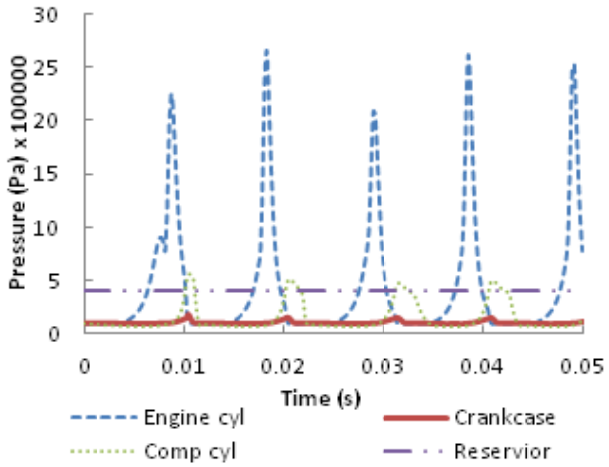

Figure 5-4 Simulation of engine compressor starting and operating

5.5.2 Cyclic variation simulation

The engine compressor cyclic variation was simulated by a random variable in the scavenging model as discussed in section 4.4.6. A trace of the piston position in several consecutive cycles is shown in Figure 5-5.

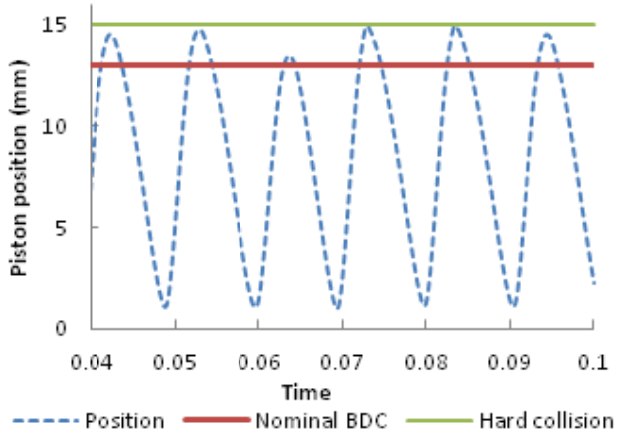

Figure 5-5 Simulation of engine compressor piston position trace in consecutive cycles

From the simulations the engine piston showed variation in the bottom dead center (BDC) position due to different combustion strengths in those cycles. However, for the simulated level of cyclic variation, the piston always passed the

nominal BDC position, enabling adequate scavenging for the next cycle. In cycles with strong combustion, the piston encountered hard collisions with a buffer at its outmost position. This lead to some energy loss; however it is necessary to ensure adequate piston travel in weak cycles.

5.5.3 Engine compressor efficiencies

The various efficiencies of the engine compressor were simulated. The engine indicated efficiency is the work done by the in-cylinder pressure divided by fuel energy consumed, i.e.

$$\eta_i = \frac{\int P_{eng}\, dx_{piston}}{e_c \int \dot{m}_{fuel}\, dt} \tag{5.4}$$

where P_{eng}, e_c and $\dot{m}_{fuel}$ are engine cylinder pressure, fuel lower heating value and fuel flow rate. The engine indicated efficiency of the engine compressor was simulated to be 14.6%.

The mixture retention efficiency indicates how much fuel air mixture is retained inside the engine cylinder and burned, instead of short-circuiting directly out of the exhaust port. The retention efficiency was simulated to be 47.4%. The low retention efficiency, i.e. waste of fuel in scavenging contributes to relative low indicated efficiency. The mechanical efficiency of the engine compressor was simulated to be 79.9%.

The compressor efficiency is the useful energy inside the compressed air output divided by the work done on the compressor. Using an analysis similar to Riofrio (2008) and taking into account that the compressed air eventually cools to ambient temperature and loses some of its energy, the energy stored in compressed air is

$$E_{comp\ air} = \frac{P_{comp} - P_{atm}}{P_{comp}} m_{air} R T_{atm} \tag{5.5}$$

where subscripts comp and atm denote compressed air and atmosphere. The compressor efficiency was simulated to be 39.1%. Inefficiencies are due to the compression heating of air, blow-by leakage between compressor piston and cylinder, and heat transfer in the compressor. With all the inefficiencies, the engine was predicted to output 17.6 W of cooled compressed air, at an overall efficiency of 4.6%.

Referring to Figure 1-3 on the efficiency target, the models predicted that the engine compressor has the potential to achieve high engine density.

6 PROTOTYPE TESTING AND MODEL VALIDATION

Based on the modeling and components testing work in previous chapters, two miniature size free-piston engine compressor prototypes were designed and fabricated. The latest prototype engine compressor combined a 12.5 mm bore two-stroke internal combustion engine and an air compressor to produce about 5W pneumatic power for small scale mobile fluid power devices.

While incorporating free-piston engine configuration, the prototypes were designed to be self-regulating with no active control of the piston motion. A model aircraft engine type glow plug ignition system was used whose ignition timing was not directly controlled, similar to homogeneous charge compression ignition.

6.1 Generation I engine prototype

A first generation prototype was designed and fabricated as shown in Figure 6-1. In this prototype, the engine cylinder liner, engine cylinder head, silencer, carburetor, engine piston and engine piston pin were components of an ‘AP Hornet .061’ model aircraft engine. The compressor piston and liner are from an ‘AP Hornet 09’ model aircraft engine. Custom components were machined by CNC machining. The model engine components and custom components are shown in Figure 6-2.

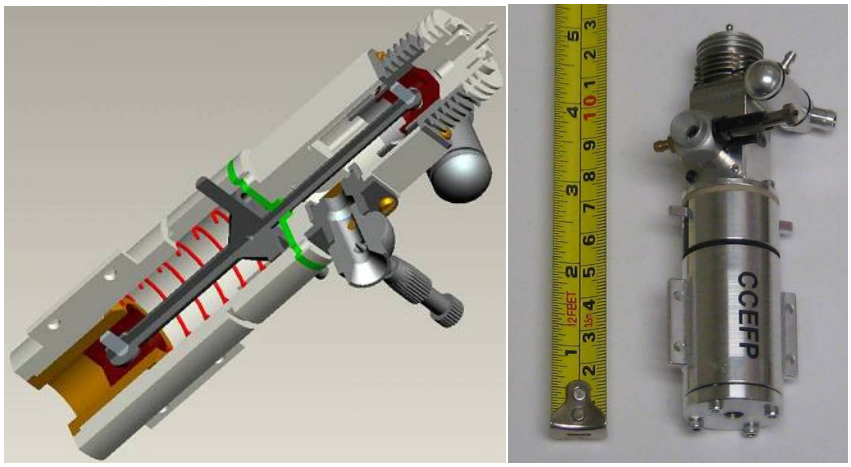

Figure 6-1 Pro-E design cutaway and fabricated prototype gen I

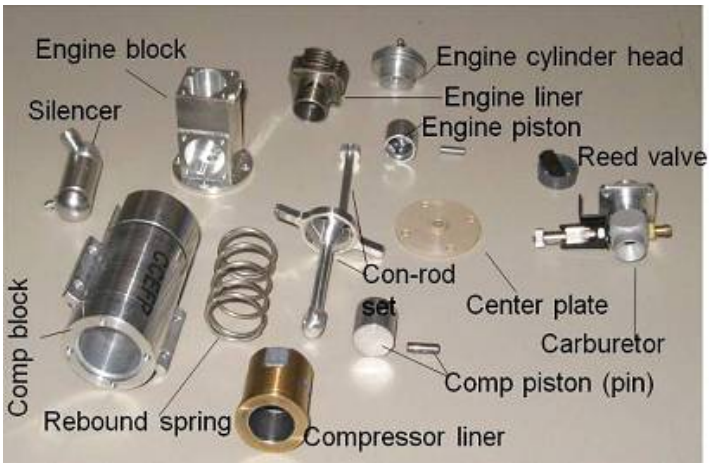

Figure 6-2 Prototype gen I components

The prototype gen I had alignment problem which resulted in excessive friction. The connecting rod of prototype I was designed to be two sections screwing together. Being miniature size and featuring slender aspect ratio, the screwed together connecting rod could not ensure the engine piston, center plate sealing surface and compressor piston to be co-axis. The alignment problem resulted in friction and made the pistons to bind, and as a result, the prototype gen I only got occasional firing in the engine piston and failed to operate continuously.

6.2 Prototype generation II design

To address the alignment and binding problem, a second prototype was designed and built as shown in Figure 6-3. Some of the fabricated components are shown in Figure 6-4.

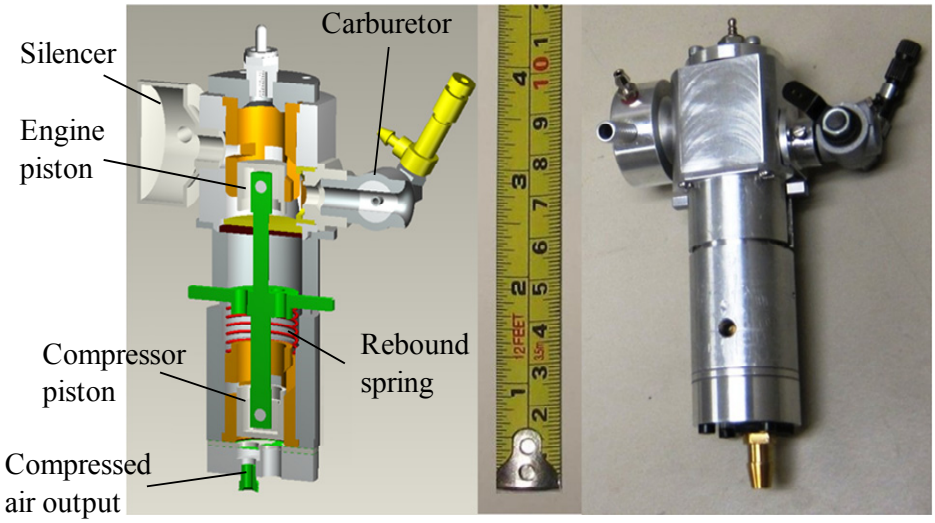

Figure 6-3 Free-piston engine compressor design cutaway and prototype gen II

Figure 6-4 Some components of prototype gen II

The device is 12 cm long and weighs 260 grams. On the engine side, the fuel air mixture induction is done by the upward motion of the piston drawing the fresh mixture from the carburetor into the crankcase through a low mass reed intake check valve. Schnuerle type scavenging is used. Downward piston motion compresses the

fresh mixture inside the crankcase, forcing it to flow around and up into the cylinder space above the piston ready for compression and combustion. On the compressor (lower) end of the device, reciprocating motion of the compressor piston intakes ambient air and supplies compressed air to the output through custom designed intake and output reed check valves. The downward motion of the piston is driven by the expanding combustion products inside the engine cylinder and the upward return motion is driven by the metal rebound spring and at the beginning of the stroke, the residual compressed air below the compressor piston. This prototype utilizes glow plug ignition instead of HCCI for easier starting and smaller compression ratio. A glow plug is located on the top of the engine's combustion chamber.

The gen II prototype features double-jaw seal plates to address the alignment problem encountered in previous prototype I, in which the connecting rod was designed to be two pieces screwing together for two reasons. First, the crankcase seal plate sealed against the middle of the connecting rod which was smaller in diameter than both ends of the connecting rod, thus two piece design enabled the assembly of the crankcase seal plate. Second, the connecting rod was slender and was difficult to machine in one piece. To address the assembly problem, double-jaw seal plates were designed to be assembled from both sides of the connecting rod sealing surface, as shown in Figure 6-5. The two jaws together sealed the crankcase against the one-piece connecting rod. Further design efforts were made to shorten the connecting rod making it easier to be machined.

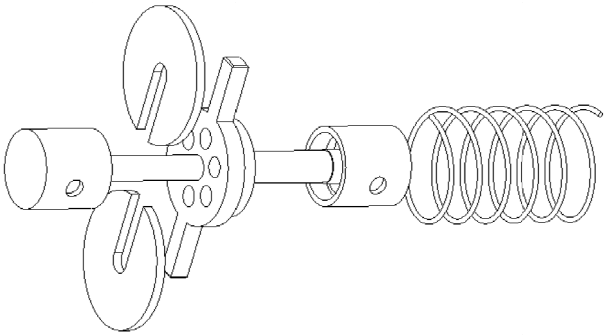

Figure 6-5 Double-jaw seal plates for sealing against connecting rod

The compressor side intake and output check valves were EDM cut from 0.004 in. stainless steel alloy foil. The compressor valves assembly was designed to yield minimum dead volume in the compressor as shown in Figure 6-6. As discussed in previous valve response simulation in preliminary simulation section, these stainless steel valves have fast response due to their light weight.

A rubber bumper was designed to cushion piston assembly motion in the case of a collision between the piston assembly and the compressor block. The two bumper rubber rod was designed to seat in two drilled holes in the compressor block, as shown in Figure 6-7, so that longer rubber section could deform more without fatigue failure.

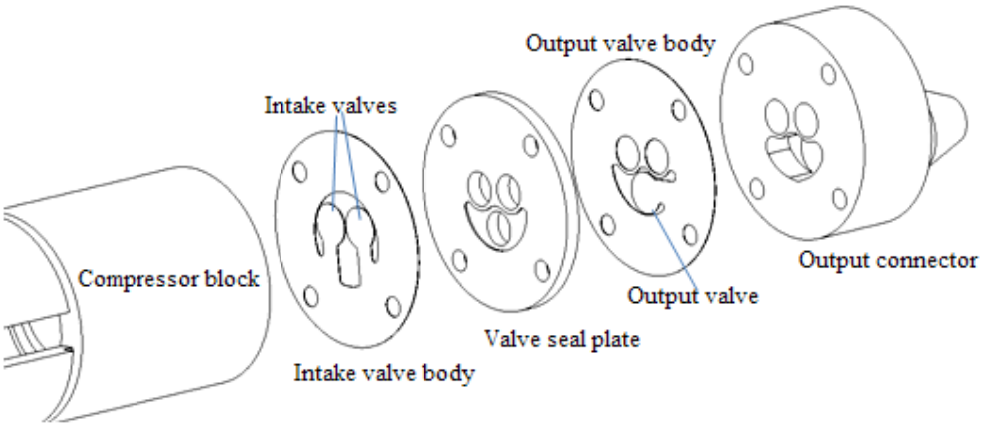

Figure 6-6 Design of prototype compressor side intake and output check valves

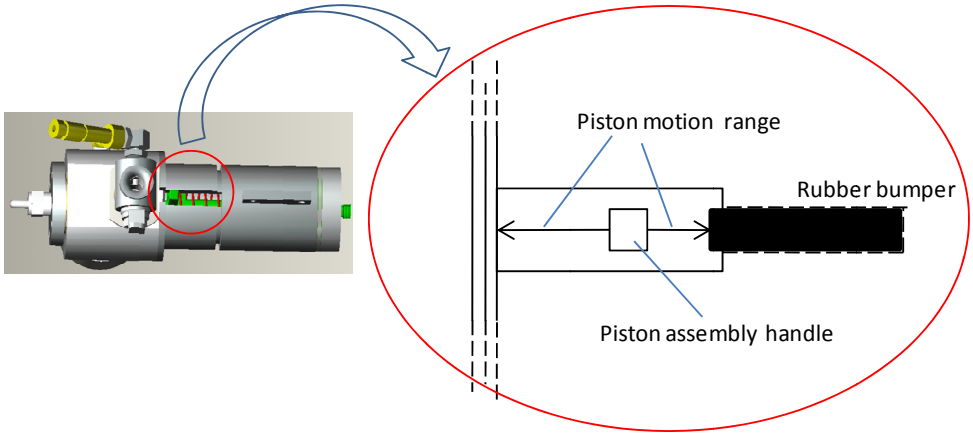

Figure 6-7 Rubber bumper in prototype gen II

The fabricated engine piston, compressor piston and connecting rod assembly, together with the double-jaw seal plates are shown in Figure 6-8. To get piston assembly weight target of 40 grams as specified in Chapter 5, a dead weight was needed. The dead weights were designed as an annular pipe piece to slide onto the connecting rod, machined out of steel or tungsten alloy, with 9.5 and 20.5 grams weight. The overall weight of the piston assembly with the dead weight was 34.3 grams with steel dead weight, or 45.3 grams with tungsten dead weight.

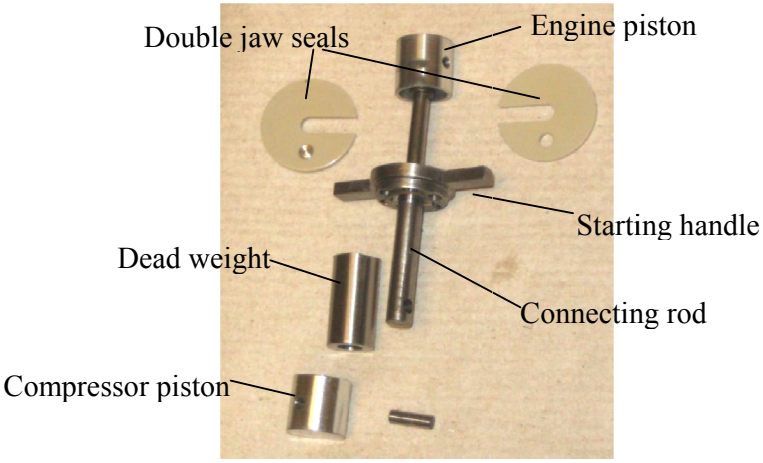

Figure 6-8 Pistons and connecting rod assembly of prototype gen II with dead weight

The testing data shown in this chapter 6 was all with prototype gen II. If not specified, 'prototype' in this chapter refers to 'prototype gen II'.

6.3 Prototype testing and model validation

6.3.1 Experimental set up

The experimental apparatus for prototype testing is shown in Figure 6-9. A picture of the test bench is also shown in Appendix D. A high bandwidth, high resolution laser triangulation sensor (MTI Instrument, model LTC-120-20-SA) was used to measure the piston position. A small optical type pressure sensor was used to measure in cylinder pressure (OPTRAND, model D22255-Q). The compressor output was connected to a 530mL air tank through an additional check valve to prevent slow leakage through the compressor output valve. The air tank pressure could be regulated with an adjustable relief valve to adjust relief pressure. The exhaust port of the relief valve had steady flow of air at ambient pressure at the same flow rate of the prototype compressor output, thus could be measured by a Gilibrator bubble flow meter.

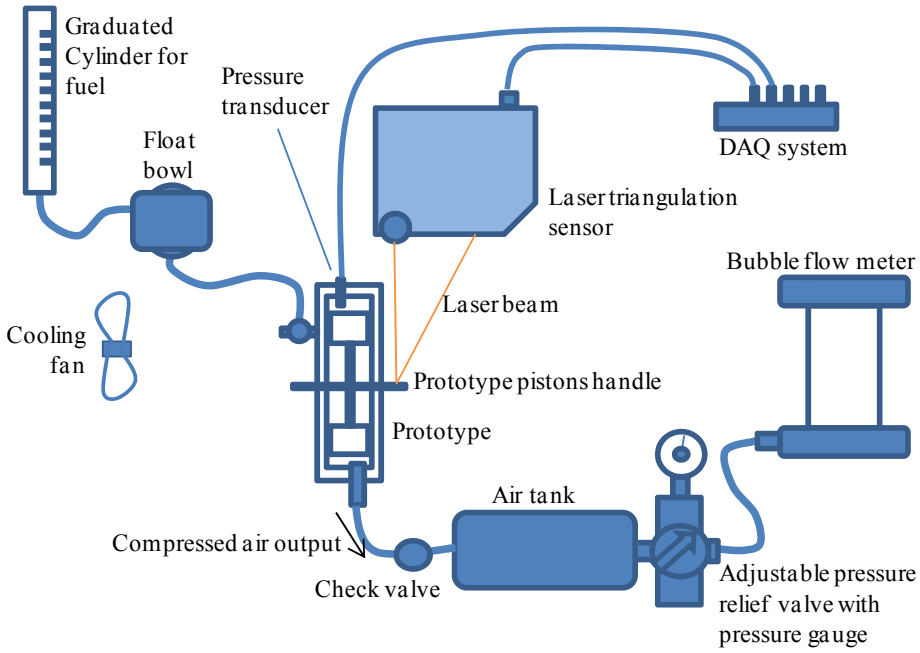

Figure 6-9 Experimental testing apparatus

6.3.2 Prototype starting and running

To start the prototype, the starting handle was pulled by hand to compress the rebound spring. After the piston reached its bottom most position with the spring fully compressed, the handle was released to initiate the first cycle. After running several cycles by hand to purge the cylinder and fill it with fresh fuel air mixture, the prototype started and entered steady state running within a few cycles. The piston position and cylinder pressure during starting are shown in Figure 6-10. The first two combustion events were weak, reaching peak pressure of about 15 bar, just enough to push the piston past the transfer port open (TO) position at 10.87mm. After the piston passed the TO position in the first cycle (at that position the exhaust port is open as well), scavenging occurred and supplied the engine with fresh fuel air mixture for the next cycle.

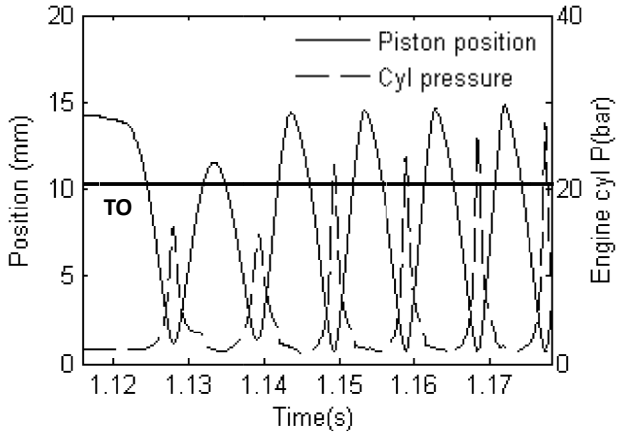

Figure 6-10 Startup behavior of miniature free-piston engine (TO: transfer port open)

Figure 6-11 shows the time history of reservoir pressure, engine operating frequency and IMEP. As the device pushed compressed air into the tank, the tank pressure rose, increasing the compressor output pressure. This in turn increased the effective stiffness of the rebound spring which changed the natural frequency of the engine. Figure 6-11 shows this increase in engine frequency with operating time. The IMEP of the engine was around 3 bar, which was lower than the experimentally measured IMEP of about 4 bar of a similar size glow ignition R/C aircraft engine. This was due to a less effective scavenging process and a lower cycle efficiency which is explained below in the section on combustion analysis.

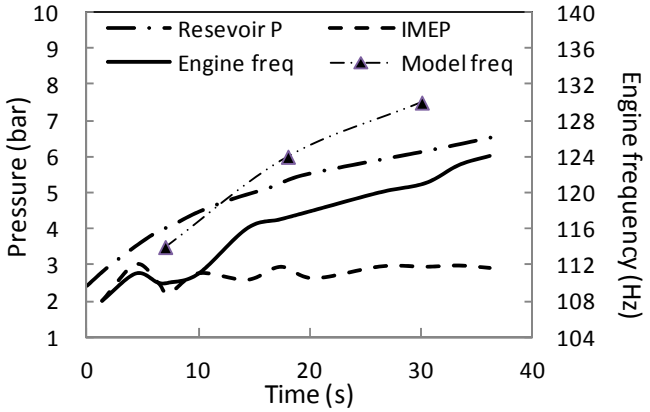

Figure 6-11 Prototype engine compressor charging up a 530mL reservoir

The measured engine frequency approximated predicted frequency, as shown by the Engine freq and Model freq curves in Figure 6-11 which are the measured and model predicted frequencies. Further data with constant 4.8 bar compressor output steady state running, but with different piston assembly weight is shown in Figure 6-12. The measured frequencies were lower than the predications because of underestimating speed related hydrodynamic and aerodynamic friction, and underestimating leakage inside the compressor.

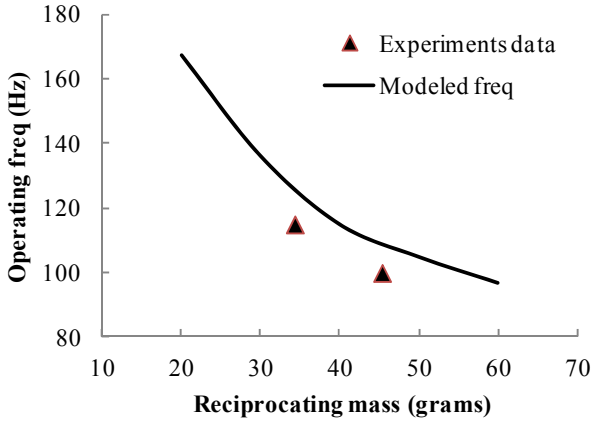

Figure 6-12 Engine operating frequency with different piston assembly mass, at 4.8 bar compressor output pressure

The amount of energy stored in compressed air was determined by calculating the amount of work it could do if expanded to atmospheric pressure adiabatically. By calculating the amount of energy stored in the air tank, the output compressed air power was estimated to be 5 W. The efficiency of converting the indicated output of the engine (~48W) to compressed air output was low at about 10% because of leakage in the compressor, compressing heating effect and friction in the engine and compressor.

Fuel flow rate of steady state running at 4.8 bar compressor output pressure with 45.3 grams piston assembly was measured to be 0.069 mL/s. From the fuel flow rate, engine in-cylinder pressure trace combustion analysis and compressor flow rate,

various tested efficiencies and power were calculated and listed as below. Engine thermal conversion efficiency

$$\eta_{\text{engine ,thermal conv.}} = {}^{\text{Engine indicated output}}/_{\text{combusted fuel energy}} = 19\%$$

Engine Indicated efficiency was

$$\eta_{\text{engine}} = {}^{\text{Engine indicated output}}/_{\text{Fuel energy}} = 6.0\%$$

Engine brake output efficiency was poor compared with engine thermal conversion efficiency because the majority of consumed fuel didn't contribute to heat release inside the engine, due to short-circuiting during scavenging process and possibly low combustion efficiency.

Assuming a 70% conversion from the indicated engine output to the brake output to drive the compressor, the compressor efficiency can be estimated as

$$\eta_{\text{compressor}} = {}^{\text{Cooled compressed air output}}/_{\text{Engine brake output}} \approx 14.3\%$$

The low compressor efficiency was suspected to be because of compression heating effect of air and the severe leakage inside the compressor, which was because that the prototype compressor check valves sealing and piston-cylinder gap sealing were not optimized.

Engine compressor overall efficiency is the cooled compressed air output energy divided by fuel chemical energy, and was

$$\eta_{\text{engine compressor overall}} \approx 0.6\%$$

It was low compared to 4.6% model prediction in chapter 5, because of the low compressor efficiency, possibly high friction, and that the engine ran rich with excessive short circuiting loss, to ensure easy starting and stable operation.

6.3.3 Piston motion analysis

In a crankshaft engine, piston motion is mechanically restrained by crankshaft and connecting rod. As the crankshaft rotates, energy converts among mixture expansion energy, crankshaft and flywheel kinetic energy and shaft work. In a free-piston engine the process is more complex as the motion of piston is determined by a force and energy balance instead of by mechanical constraint.

Figure 6-13 shows the position-velocity phase diagram for the engine. The vertical dash line in the diagrams is where the piston motion was limited by a rubber bumper. As the piston travels beyond the bumper limit, the kinetic energy of the piston and connecting rod is wasted in the collision. The speed of piston at the collision point is a good indication of how much energy is wasted in the bumper collision.

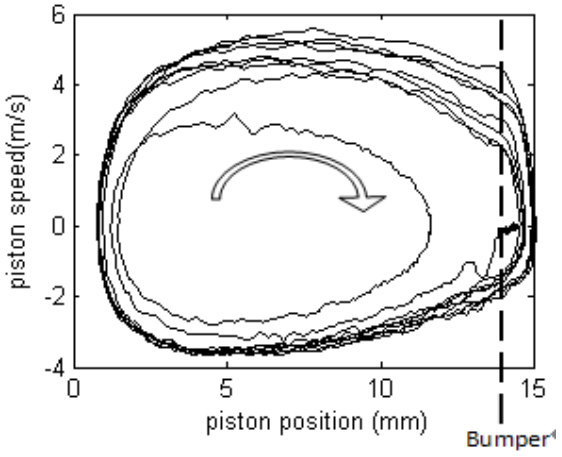

Figure 6-13 Piston position-speed diagram of 9 consecutive cycles at engine startup

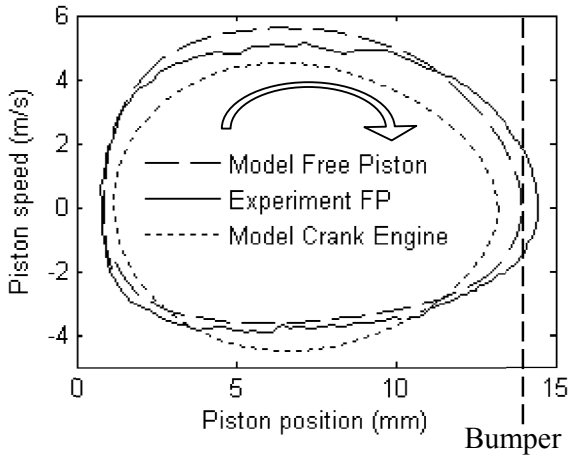

Figure 6-14 Piston position-speed diagram of a typical cycle of experimental data at steady state running, compared with modeling result of free-piston engine and a crankshaft engine

For the first few cycles, the engine compressor was running with no load while the output pressure built up. As can be seen in Figure 6-13, initially almost all energy from engine output was wasted in bumping into the bumper, which is about 0.4 J per cycle. Ignition occurred at around TDC, i.e. the left most part of the diagram. During the compression stroke which is the bottom half of the phase plot, rebound spring energy was released to accelerate the piston and overcome pressure built up in the engine cylinder.

Figure 6-14 compares the system model in section 5.2, the measured data during steady state operation and a crankshaft engine model. The free-piston engine trace is distinct from the crankshaft engine trace as the piston is free from the kinematic constraint of crankshaft and connecting rod. The model of the free-piston engine predicts the trend correctly and fits with the experimental data, indicating that the system model can accurately capture the dynamics of the free piston. Errors in the model are likely due to the simplifying assumptions used for the scavenging and combustion models.

6.3.4 Compressor output flow rate measurement

The compressor output flow rate was measured at steady state running and compared to modeling results by the engine compressor overall model described in section 5.2, with 34.3 grams piston assembly at various compressor output pressure, as shown in Figure 6-15. As discussed earlier, the prototype compressor had low efficiency due to leakage inside the compressor. The model captured these inefficiencies and predicted the trend of decreasing compressor output flow rate with increasing output pressure.

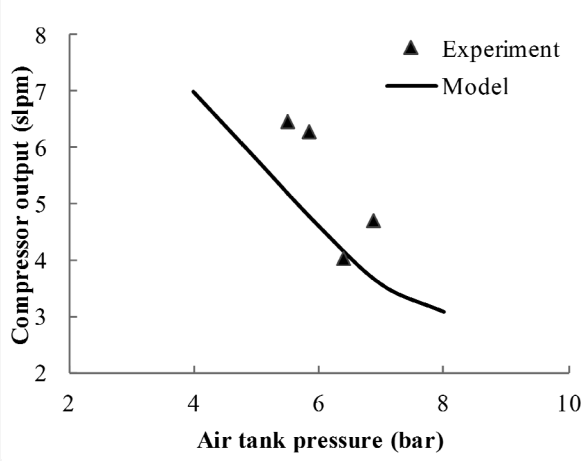

Figure 6-15 Compressor output flow rate at various output pressure and comparison with the model

6.3.5 Energy balance and self regulation with over-stroke feature and a collision bumper

The free-piston engine compressor was designed to be self-regulated without using active control. As a result, cyclic variation was a barrier to running the engine. In weak cycles, if the piston did not travel far enough to uncover the exhaust and transfer port for sufficient time, the scavenging process would be interrupted,

making the engine stall on the next cycle. In strong cycles, the piston might travel too far and encounter destructive metal to metal collision against the end stop.

To accommodate for this variation, the device was designed to have 2 mm over-stroke, which means the pistons could travel 2 mm further than nominal BDC position of a crankshaft engine. In strong cycles, the pistons would travel further than nominal BDC while the rebound spring and compressor absorbs more energy. After the piston traveled to the end of the 2 mm over-stroke, rubber bumpers would absorb extra energy if there was still any. These measures enabled the free-piston engine compressor to handle some variation in the amount of energy released from combustion product expansion. This energy balance is shown in Figure 6-16. Variation of expansion process energy release could be in a relatively wide range, while the piston travel was still long enough to enable scavenging but not so long to result in metal to metal collision.

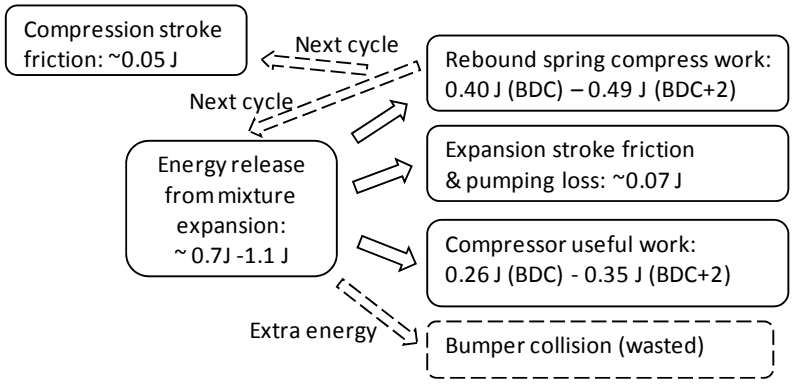

Figure 6-16 Energy balance in free-piston engine compressor at 4.5 bar compressor output (model results)

As discussed in section 6.3.3, at lower compressor output pressure, the compressor absorbed less energy and more energy was wasted in the bumper collision. When the piston position was at 14mm it collided into the rubber bumper, and it was assumed that the kinetic energy at that moment was wasted in bumper

collision. The average bumped energy was calculated by averaging about 20 consecutive cycles. The results are shown in Figure 6-17. Compressor absorbed work was calculated by assuming a polytropic compression process inside the compressor with a compression index of 1.3. Bumping avoidance efficiency was calculated by

$$\text{Bumping avoidance effi} = {}^{\text{comp work}}/_{(\text{comp work} + \text{bumped energy})}$$

At different compressor output pressure, the sum of average bumped energy and compressor work was about 0.32 J per cycle. As the load absorbing capacity of the compressor increased with output pressure, less energy was wasted in bumping, resulting in a higher bumping avoidance efficiency.

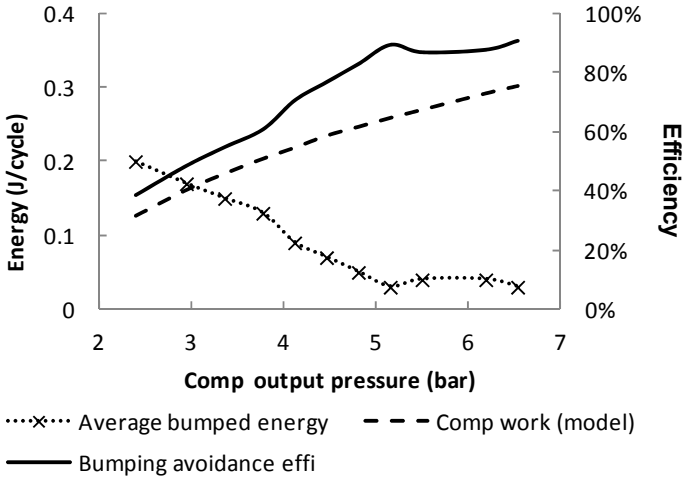

Figure 6-17 Analysis of bumping in the free-piston engine compressor prototype

6.3.6 Combustion analysis

A combustion analysis was performed to calculate heat release from cylinder pressure and piston position data, as described in section 4.4.4. Results from

combustion analysis include mass fraction burned (MFB) data, which is the time history of the mass fraction of fuel already burned.

The combustion analysis results for three cycles are presented in Figure 6-18. Ignition timing was consistent for the cycles, while combustion speed varied. In most cycles combustion was slow and lasted until the exhaust port opened. There were also some cycles with fast combustion, for example cycle 75 shown in Figure 6-18 and Figure 6-19, while combustion process finished a little past TDC. The difference in combustion speed can be explained by the cyclic variation of exhaust residue content, mixture composition and mixture motion in the combustion chamber. An internal combustion engine achieves highest possible thermal cycle efficiency if combustion happens instantaneously at top dead center, like in an ideal Otto cycle. Faster combustion process near TDC is favorable in achieving higher cycle thermal efficiency.

Figure 6-19 shows log-log pressure-volume data for the three analyzed cycles at 4.8 bar compressor output pressure with 34.3 grams piston assembly. With faster combustion, the cycle had significant pressure rise before the piston traveled to TDC. This resulted in less compression ratio[2] as the pistons were brought to stop earlier. However, as combustion process happens faster around TDC because of the higher pressure instead of lasting throughout the expansion stroke, the faster heat release offset the effects of lower compression ratio, resulting in higher cycle thermal efficiency. MFB at TDC is a good indication of how fast and how early the

[2] As the engine is a free-piston engine and doesn't have fixed swept volume, top dead center and bottom dead center, for convenience, compression ratio in this thesis is calculated by exhaust port closed cylinder volume divided by top dead center cylinder volume. This is the effective geometric compression ratio in a two-stroke engine.

combustion process occurred. The comparison of the three cycles is shown in Table 6-1.

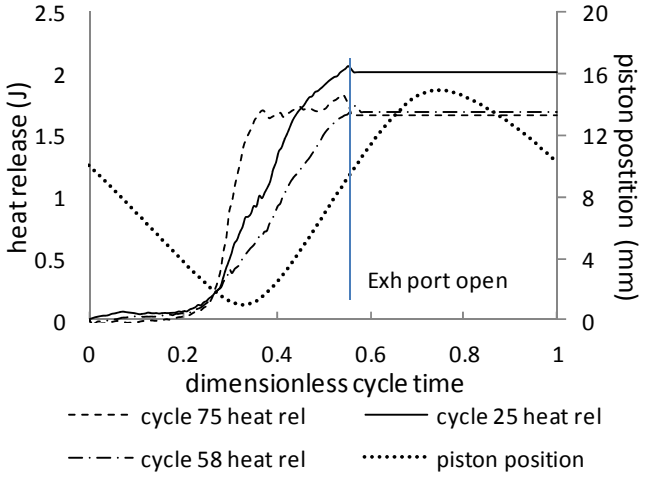

Figure 6-18 Heat release analysis result of three cycles

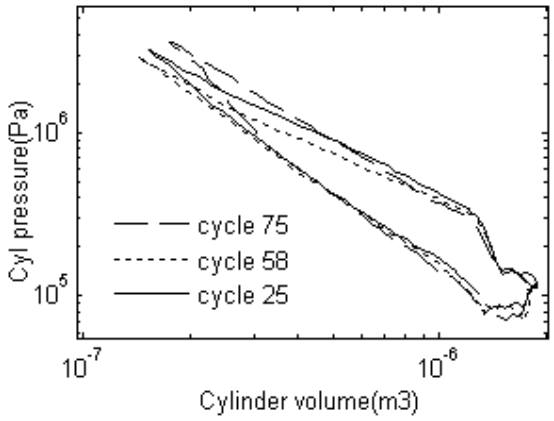

Figure 6-19 Pressure volume log-log diagram of three cycles

Table 6-1 Combustion analysis results of three cycles

Cycle	MFB at TDC	Comp ratio	Thermo conv e
Cycle 75	77.7%	7.42	22.78%
Cycle 25	37.4%	8.43	18.81%
Cycle 58	26.9%	9.05	16.84%

The correlation between cycle thermal conversion efficiency and MFB at TDC of 570 consecutive cycles is shown in Figure 6-20, further showing how thermal efficiency increases with combustion speed.

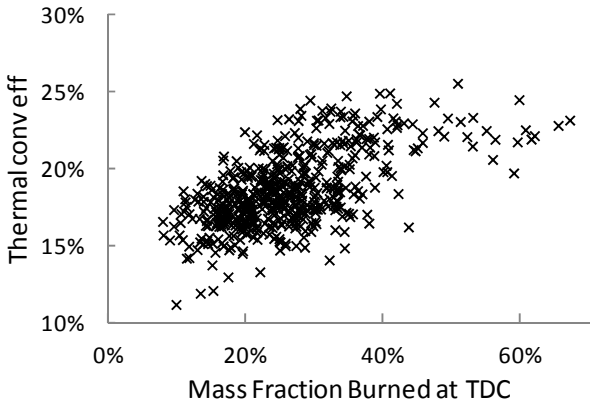

Figure 6-20 Cycle thermal conversion efficiency related with Mass fraction burned at TDC, of 570 cycles, with 34.3 grams piston assembly at 4.8 bar compressor pressure output

6.3.7 Comparison with crankshaft engine

Pressure volume data for 12 cycles of the free-piston engine is shown in Figure 6-21 along with data from its crankshaft engine counterpart. The crankshaft engine data was from experimental test of a same size crankshaft engine which utilizes the same engine cylinder and glow plug ignition system. The typical pressure volume diagram for free-piston engine compressor differs considerably from the crankshaft engine.

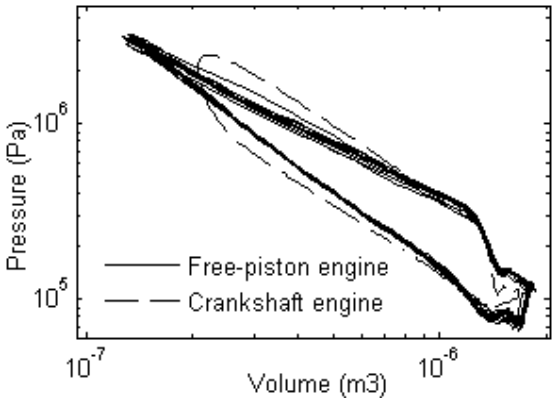

Figure 6-21 Pressure volume log-log diagram for 12 cycles in free-piston engine compressor with 34.3 grams piston assembly at 4.8 bar compressor output, and comparison with crankshaft engine

Figure 6-21 illustrates that in the free-piston engine prototype combustion continued throughout the expansion process, while the combustion in the crankshaft engine was centered about the top dead center, as can be seen by the different shapes of the pressure volume traces in Figure 6-21. This can be explained by the nature of the free-piston engine. After the mixture ignites in a crankshaft engine when the piston is around top dead center, the piston is effectively held in the top position by the crankshaft and connecting rod. In a free-piston engine the mixture also ignites around top dead center position. However, at that position the rebound spring is not exerting much force on the pistons and the compressor is not doing work since it is still in the end of intake stroke. As a result, without the mechanical restraint of crankshaft and connecting rod, the piston rapidly retracts from the TDC position, outpacing the mixture combustion process. The retraction of the piston decreases the pressure and temperature in the combustion chamber and results in increased combustion duration. Combustion analysis of the cycles shown in Figure 6-21 showed average combustion duration of about 3 ms, compared to 1.4 ms in the crankshaft engine.

The combustion process of the crankshaft engine shown in Figure 6-21 was close to that of an ideal Otto cycle in which combustion occurs instantaneously at TDC,

resulting in high thermal efficiency. With an effective compression ratio of 5.31 and leakage in the miniature engine, the crankshaft engine's average cycle thermal conversion efficiency was 22.3%. In contrast, the free-piston engine heat release process was far from ideal. With a higher effective compression ratio of around 10, the average cycle thermal conversion efficiency for the free-piston engine was 18.1%.

Model prediction and experimental result are compared in Figure 6-22. The glow ignition modeling results were from the engine compressor overall model described in section 5.2. The model of the glow plug engine was able to predict the heat release process of the glow plug ignition free-piston engine. The deviation between the curves that occurs during the compression process indicates that the free-piston engine prototype had a higher polytrophic index during compression stroke than predicted by the model. This was likely because the model was not able to estimate exhaust residue content in the cylinder, cylinder wall temperature, and the amount of lubrication oil present in the piston cylinder gap which helped sealing the gap from leakage.

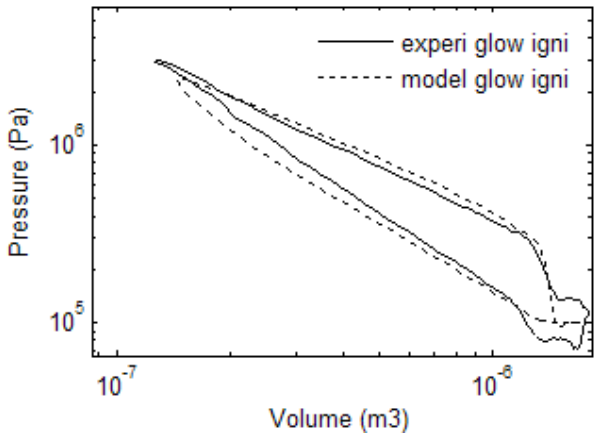

Figure 6-22 Pressure volume diagram for glow ignition free-piston engine experimental result and model prediction, with 34.3 grams piston assembly at 4.8 bar compressor output

Implementation of true HCCI should increase cycle efficiency in a free-piston engine. Aichlmayr (2002) realized HCCI in a small 3 mm cylinder, and high speed camera images showed that the HCCI combustion process duration was less than 60 μs. If HCCI is implemented in this free-piston engine, the entire combustion process will happen around TDC, yielding higher thermal efficiency. This was confirmed by the engine compressor model. An HCCI combustion model was added to the engine compressor overall model described in section 5.2, with 30 μs combustion duration. HCCI ignition model was similar to the glow ignition model in equation 4.10, with higher ignition threshold value. The engine model used a stiffer spring to achieve high enough compression ratio to enable HCCI combustion

The result of modeling HCCI in the miniature free-piston engine compressor is shown in Figure 6-23 which shows a steep rise of in-cylinder pressure due to the fast heat release. The model predicted the thermal conversion efficiency of the glow plug free-piston engine to be 25% and the thermal conversion efficiency of the HCCI free-piston engine to be 41%. Part of the efficiency gain is because of the rise of compression ratio (12.3 for HCCI compared to 9.0 for glow plug ignition), while the rest of the improvement is due to more optimal heat release. While the model over-predicts the thermal conversion efficiency as measured in the real engine, the model result that HCCI cycle efficiency will be higher than glow plug ignition can still be trusted.

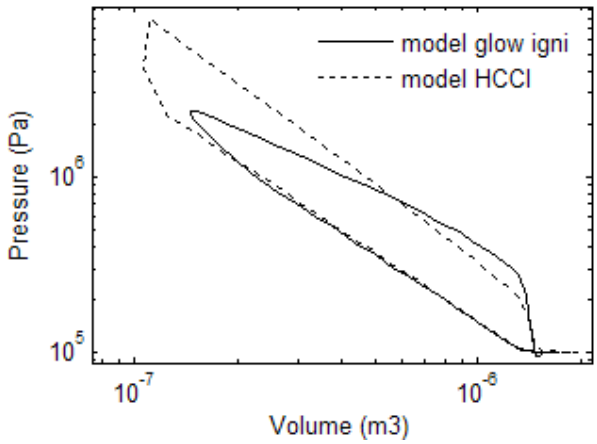

Figure 6-23 Pressure volume diagram from glow ignition and HCCI model results

6.3.8 Self-regulation of compression ratio

The free-piston engine compressor adapted its compression ratio to the combustion process as shown in Figure 6-24. This result can be explained by the higher MFB at TDC indicating faster combustion and thus more pressure build up in the compression process. As a result the pistons decelerate faster and stop earlier, yielding a smaller compression ratio. This self-regulation works well with glow plug ignition, which lacks fixed ignition timing. Compression ratios up to 11 were observed in cycles where the mixture was difficult to ignite or slow to burn, while lower compression ratios were observed in cycles with early ignition or fast burn rate, reducing peak pressure.

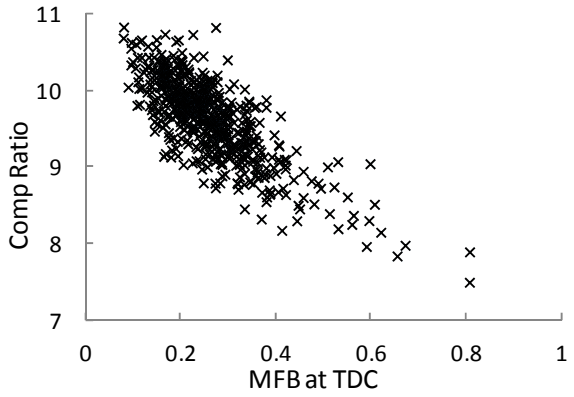

Figure 6-24 Compression ratio versus mass fraction burned at TDC of 570 cycles, with 34.3 grams piston assembly at 4.8 bar compressor output

The ability to adjust compression ratio according to combustion process is a good starting point for implementing HCCI. HCCI has ignition timing determined by chemical kinetics, just like glow ignition. Therefore, true HCCI should work well in the free-piston engine because compression ratio should automatically adjust to ensure appropriate combustion timing.

Mathematical modeling was further used to evaluate the ability to self regulate its compression ratio in a true HCCI free-piston engine. The combustion duration in the combustion heat release model was set to be 30μs. The parameter RRth in equation 4.10 was adjusted in the HCCI ignition timing model in section 4.4.4 to result in different HCCI ignition timing. P-V log-log diagrams of four cycles with different RRth parameter are shown in Figure 6-25. RRth value of 7, i.e. lower integration threshold for HCCI ignition timing model, resulted in rapid heat release and pressure rise in earlier stage of compression process. The pressure rise stops the free-piston sooner and yielded lower compression ratio. In contrast, higher RRth values resulted in later ignition timing, and the piston traveled further yielding higher compression ratio.

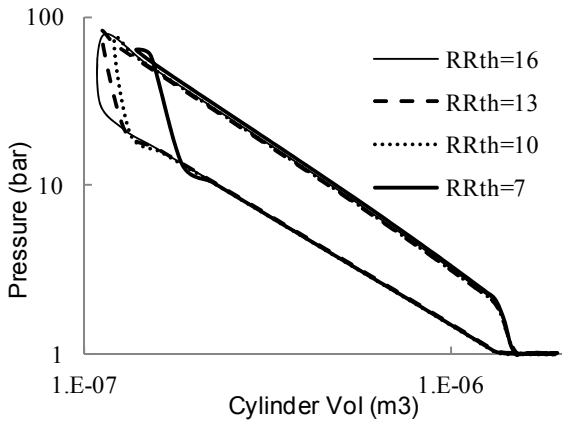

Figure 6-25 P-V log-log diagrams of four cycles with different ignition timing in a HCCI free-piston engine

The model result of correlation between compression ratio and HCCI ignition timing (time between exhaust port closed and ignition) is shown in Figure 6-26. Later ignition yielded higher compression ratio and vice versa. This showed that a free-piston engine could adapt its compression ratio automatically to HCCI combustion timing.

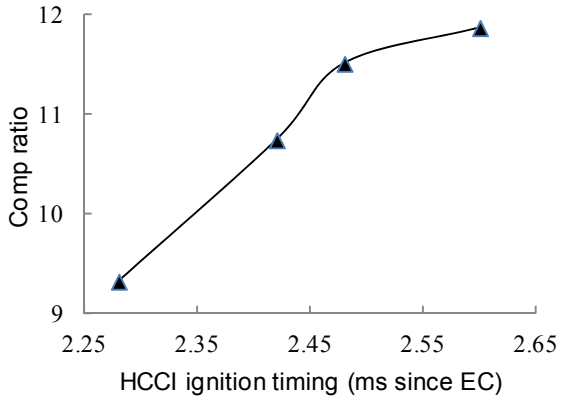

Figure 6-26 Compression ratio versus ignition timing in a HCCI free-piston engine, modeling results (EC: exhaust port closed)

More modeling results of the four cycles are shown in Table 6-2. As HCCI ignition threshold was increased, compression ratio raised which resulted in improving cycle thermal conversion efficiency and engine work output.

Szybist and Bunting (2007) concluded that in a crankshaft engine, an early HCCI ignition increases combustion chamber heat transfer loss which compromises efficiency, and that a HCCI engine has highest thermal efficiency when CA50 (crank angle degree when 50% of fuel energy is released) is about 8 degrees after TDC. However in the case of a free-piston engine, the modeling results showed that the HCCI combustion heat release process was always near TDC position. As a result, heat transfer loss was similar with different HCCI ignition timing, and played minor role in determining cycle thermal conversion efficiency, as shown in Table 6-2.

Table 6-2 Modeling results of four cycles with different HCCI ignition threshold

	RRth=7	RRth=10	RRth=13	RRth=16
Comp R	9.3	10.7	11.5	11.9
Thermal conv e	36.3%	39.4%	40.9%	41.8%
Heat trans loss	41.3W	40.9W	39.2W	38.4W
Work output	68.3W	74.1W	77.2W	78.7W
Frequency	124.4Hz	124.2Hz	124.1Hz	124.0Hz

6.4 Conclusion

The prototype produced compressed air up to 6.5 bar pressure and had an overall efficiency of 0.6% from fuel chemical energy to cold compressed air energy, compared to the predicted 4.6% efficiency. It was lower because of the low compressor efficiency, possibly high friction, and that the engine ran rich with excessive short circuiting loss, to ensure easy starting and stable operation.

The experimental data of the prototype showed that the engine compressor model captured the characteristics of the prototype quite well. Analysis of experimental data revealed that slow combustion process in the glow plug ignition free-piston engine was one of the reasons of the low cycle thermal efficiency. Faster combustion process like HCCI was found to be able to increase cycle efficiency in a free-piston engine, as predicted by modeling results. The compression ratio in the free-piston engine prototype was found to automatically adjust for combustion timing and speed. This feature was speculated to be suitable for implementing HCCI.

7 SUGGESTED FUTHER WORK

(1) Practical problems encountered with the prototype should be addressed, which include piston scuffing problem, carburetor fuel delivery at starting up, piston-cylinder sealing, scavenging loss, compressor valves sealing and compressor valves fatigue. More details about these practical problems are described in Appendix B.

Among the practical problems, the piston-cylinder sealing and scuffing problem, and scavenging loss problem could possibly be addressed by custom made piston, cylinder liner and scavenging passages with appropriate materials.

It should be noted that if components are updated and optimized, modeling of the engine compressor should be carried out again to re-establish optimized operating speed and design parameters.

(2) Consistency in starting and running need to be improved. Currently the prototype starts in a 'hit or miss' manner and could only sustain continuous run time up to about 6 minutes before stalling. The fuel delivery, scavenging and combustion during starting need to be investigated and improved for consistent starting in a free-piston engine. Wear and fatigue of engine compressor components need to be understood and addressed.

Also, an automatic starting scheme, instead of the currently used hand starting, needs to be developed such as the pneumatic starting discussed in section 3.2.

(3) Pure HCCI should replace the glow ignition system to yield faster combustion and higher cycle efficiency. Pure HCCI requires higher compression ration thus piston-cylinder leakage should be minimized to deliver high enough compression.

(4) Alternative fuel should be considered. Currently the prototype utilizes methanol based fuel to work with the simple carburetor and the platinum catalyst of glow ignition system. Dimethyl ether might be promising, because it is non-toxic, it has high Cetane number thus easier to ignite in HCCI mode, and that it is a gaseous fuel which can be stored in a compressed fuel canister. A pressurized fuel canister based system might provide more consistent fuel flow metering than the current carburetor setup.

REFERENCES

Achten, P. A. J., Johan, P. J., Oever, V. D., Potma, J., & Vael, G. E. M. (2000). Horsepower with brains: The design of the chiron free-piston engine. *SAE Technical Paper, paper number 2000-01-2545*.

Aichlmayr, H. T. (2002). Design considerations, modeling, and analysis of micro-homogeneous charge compression ignition combustion free-piston engines. *PhD Thesis, University of Minnesota, Minneapolis, MN.*

Aichlmayr, H. T., Kittelson, D. B., & Zachariah, M. R. (2002a). Miniature free-piston homogeneous charge compression ignition engine-compressor concept - part I: Performance estimation and design considerations unique to small dimensions. *Chemical Engineering Science, 57*(19), 4161-4171.

Aichlmayr, H. T., Kittelson, D. B., & Zachariah, M. R. (2002b). Miniature free-piston homogeneous charge compression ignition engine-compressor concept - part II: Modeling HCCI combustion in small scales with detailed homogeneous gas phase chemical kinetics. *Chemical Engineering Science, 57*(19), 4173-4186.

Aichlmayr, H. T., Kittelson, D. B., & Zachariah, M. R. (2003). Micro-HCCI combustion: Experimental characterization and development of a detailed chemical kinetic model with coupled piston motion. *Combustion and Flame, 135*(3), 227-248.

Aleiferis, P.G., Charalambides, A.G., Hardalupas, Y., Taylor, A.P. & Urata, Y. (2005). Modelling and Experiments of HCCI Engine Combustion with Charge Stratification and Internal EGR. *SAE Technical Paper, paper number 2005-01-3725.*

Annand, W. J. D. (1963). Heat transfer in the cylinder of reciprocating internal combustion engines. *Proceedings of the Institution of Mechanical, 177*(36).

Annen, K.D, Stickler, D.B. & Woodroffe, J., (2003). Linearly-Oscillating Miniature Internal Combustion Engine (MICE) for Portable Electric Power. *Proceeding of 2003AIAA Aerospace Science Mmeeting, Paper No.2003-1113*

Annen, K. D., Stickler, D. B., & Woodroffe, J. (2006). Glow plug-assisted HCCI combustion in a miniature internal combustion engine generator. *Proceeding of 2006 AIAA Aerospace Science Meeting, Paper No.2006-1349.*

Aroonsrispopon, T., Sohm, V., Werner, P., Foster, D.E., Morikawa, T. & Iida, M. (2002). An Investigation into the Effect of Fuel Composition on HCCI Combustion Characteristics. *SAE Technical Paper, paper number 2002-01-2830.*

Au, M. Y., Girard, J. W., Dibble, R., Flowers, D., Aceves, S. M., Martinez-Frias, J., et. al. (2001). 1.9-liter four-cylinder HCCI engine operation with exhaust gas recirculation. *SAE Technical Paper, paper number 2001-01-1894.*

Barth, E. J., & Riofrio, J. (2004). Dynamic characteristics of a free piston compressor. *2004 ASME International Mechanical Engineering Congress and Exposition, IMECE, , 11.* pp. 47-54.

Blair, G. P. (1996). *Design and simulation of two-stroke engines*. Warrendale, PA: Society of Automotive Engineers Inc.

Blair, G. P., & Hinds, E. T. (1979). Predicting the performance characteristics of two-cycle engines fitted with reed induction valves. *SAE Technical Paper, paper number 790842.*

Braun, A. T., & Schweitzer, P. H. (1973). Braun linear engine. *SAE Preprints volume 10, paper number 730185.*

CCEFP. (2012). Website [Internet]; 2012. Available from: www.ccefp.org.

Christensen, M., Hultqvist, A. & Johansson B. (1999). Demonstrating the Multi Fuel Capability of a Homogeneous Charge Compression Ignition Engine with Variable Compression Ratio. *SAE Technical Paper, paper number 1999-01-3679.*

Drost, M. K., Call, C., & Wegeng, R. (1997). Microchannel Combustor/Evaporator thermal processes. *Microscale Thermophysical Engineering, Volume 1, Number 4, 1 October 1997 , pp. 321-332.*

Eichelberg, G. (1948). Free piston generators. *Schweizrische Bauzeitung 1948,* pp 673-679.

Epping K., Aceves S., Bechtold R. & Dec J. (2002). The Potential of HCCI Combustion for High Efficiency and Low Emissions. *SAE Technical Paper, paper number 2002-01-1923.*

Fleck, R., Cartwright, A., & Thornhill, D. (1997). Mathematical modelling of reed valve behaviour in high speed two-stroke engines. *SAE Technical Paper, paper number 972738.*

Flowers, D. L., Martinez-Frias, J., Espinosa-Loza, F., Dibble, R., Kristic, M., & Bining, A. (2005). Development and testing of a 6-cylinder HCCI engine for distributed generation. *Internal Combustion Engine Division of ASME 2005 Fall Technical Conference.*

Gierke, D. (1994). *2-stroke glow engines for R/C aircraft volume 1.* Wilton, CT: Air Age Media Inc.

Gierke, D. (2005). *Radio control airplane engine guide.* Wilton, CT: Air Age Media Inc.

Gierke, D. (2007). *2-stroke glow engines vol.2 power: Beyond the basics.* Wilton, CT: Air Age Media Inc.

Gomes Antunes, J. M., Mikalsen, R., & Roskilly, A. P. (2008). An investigation of hydrogen-fuelled HCCI engine performance and operation. *International Journal of Hydrogen Energy, 33*(20).

Grinnell, S. D. (1955). Flow of a compressible fluid in a thin passage. *Transactions of American Society of Mechanical Engineers, paper number 55-BA-13*

Hepperle, M. (1979). COX TEE-DEE .010 review. *Aeromodeller magazine, October 1979 issue.*

Hepperle, M. (2008). *COX engine museum,* webpage. *Website page URL:* http://www.mh-aerotools.de/airfoils/cox_frameset.htm

Heywood, J. B. (1988). *Internal combustion engine fundamentals.* New York, NY: McGraw-Hill Inc.

Heywood, J. B., & Sher, E. (1999). *Two-Stroke Cycle Engine: It's Development, Operation and Design.* London, United Kingdom: Taylor & Francis Group.

Higley, H. (1992). *All about engines.* Baltimore, MD: Harry B. Higley & Sons, Inc.

Hinds, E. T., & Blair, G. P. (1978). Unsteady gas flow through reed valve induction systems. *SAE Technical Paper Series, paper number 780766.*

Huber, R. (1958). Present state and future outlook of free-piston engine. *Proceeding of ASME Meeting 1958,* pp. 12.

Hultqvist, A., Engdar, U., Johansson, B. & Klingmann, J. (2001), Reacting Boundary Layers in a Homogeneous Charge Compression Ignition (HCCI) Engine. *SAE Technical Paper, paper number 2001-01-1032.*

Jajcevic, D., Almbauer, R. A., Schmidt, S. P., & Glinsner, K. (2008). CFD simulation of a real world high-performance two stroke engine with use of a multidimensional coupling methodology. *SAE Technical Paper Series, paper number 2008-32-0042.*

Jajcevic, D., Almbauer, R. A., Schmidt, S. P., & Glinsner, K. (2009). Simulation of scavenging process, internal mixture preparation, and combustion of a gasoline direct injection two-cylinder two-stroke engine. *SAE Technical Paper Series, paper number 2009-32-0046.*

Kalghatgi, G., Hildingsson, L., & Johansson, B. (2009). Low NOX and low smoke operation of a diesel engine using gasoline-like fuels. *Proceedings of the ASME Internal Combustion Engine Division 2009 Spring Technical Conference.*

Kitamura, T., Ito, T., Senda, J., & Fujimoto, H. (2002). Mechanism of smokeless diesel combustion with oxygenated fuels based on the dependency of the equivalence ratio and temperature on soot particle formation. *International Journal of Engine Research August 1, 2002 vol. 3 no. 4 pp 223-248.*

Krivts, I. L., & Krejnin, G. V. (2006). *Pneumatic actuating systems for automatic equipment.* London, United Kingdom: Taylor & Francis Group.

Lawrence Livermore National Laboratory. (2009). *Combustion mechanisms. Available at URL:*
https://www-pls.llnl.gov/?url=science_and_technology-chemistry-combustion-mechanisms

Lesjofors. (2009). *Spring durability and spring fatigue. Website URL:*
http://www.lesjoforsab.com/technical-information/durability.asp

Lewis, B. & Elbe, G. (1987). *Combustion, Flames and Explosions of Gases*. Waltham, PA: Academic Press Inc.

Liu, C. & Karim, G. A. (2008), A 3D-Simulation with Detailed Chemical Kinetics of Combustion and Quenching in an HCCI Engine. *SAE Technical Paper, paper number 2008-01-1655.*

Lü, X., Chen, W., & Huang, Z. (2005). A fundamental study on the control of the HCCI combustion and emissions by fuel design concept combined with controllable EGR, part 2. effect of operating conditions and EGR on HCCI combustion. *Fuel, Volume 84*(9).

Ma, H., Kar, K., Stone, R., Raine, R., & Thorwarth, H. (2006). Analysis of combustion in a small homogeneous charge compression assisted ignition engine. *International Journal of Engine Research, Volume 7(3)*

Martinez-Frias, J., Aceves, S. M., Flowers, D. L., Smith, J. R., & Dibble, R. (2002). Thermal charge conditioning for optimal HCCI engine operation. *Journal of Energy Resources Technology, Volume 124, Issue 1, pp 67-76.*

Mikalsen, R., & Roskilly, A. P. (2007). A review of free-piston engine history and applications. *Applied Thermal Engineering, 27*(14-15), pp 2339-2352.

Murray, E. J. (1975). *A survey of scuffing in spark ignition engines.* Proceeding of Piston Ring Scuffing Conference, Institution of Mechanical Engineers, London, 13-14 May 1975.

Muta, K., Yamazaki, M. & Tokieda J. (2004). Development of New-Generation Hybrid System THS II – Drastic Improvement of Power Performance and Fuel Economy. *SAE technical paper, paper number 2004-01-0064.*

Najt P.M. & Foster D.E. (1983). Compression-Ignited Homogeneous Charge Combustion. *SAE Technical Paper, paper number 830264.*

Neumann, K. (1935). Junkers free-piston compressor. *Mechanical Engineering, 57*(4), pp 246-247.

Noguchi, M., Tanaka, Y., Tanaka, T., & & Takeuchi, Y. (1979). A study on gasoline engine combustion by observation of intermediate reactive products during combustion. *SAE Technical Paper Series, paper number 790840.*

Ogawa, T., & Kawaguchi, Y. (2007). Performance testing of 5CC glow ignition four-stroke engine. *2007 ASME/JSME Thermal Engineering Summer Heat Transfer Conference, HT 2007, July 8, 2007 - July 12, Vol 3.* pp. 807-814.

Onishi, S., Han Jo, S., Shoda, K., Do Jo, P., & Kato, S. (1979). Active thermo-atmosphere combustion (ATAC): A new combustion process for internal combustion engines. *SAE Technical Paper Series, paper number 790501.*

Pescara, R. P. (1928). *Motor compressor apparatus,* US Patent 1,657,641, 1928.

Raine, R. R., & Thorwarth, H. (2004). Performance and combustion characteristics of a glow ignition two-stroke engine. *SAE Technical Paper Series, paper number 2004-01-1407.*

Rassweiler, G. M., & Withrow, L. (1938). Motion pictures of engine flame correlated with pressure cards. *SAE Paper, paper number 380139.*

Riofrio, J. A., & Barth, E. J. (2003). A free piston compressor as a pneumatic mobile robot power supply: Design, characterization and experimental operation. *International Journal of Fluid Power, 8*(1), 17-28.

Riofrio, J. A., & Barth, E. J. (2008). Design and analysis of a resonating free liquid-piston engine compressor. *ASME International Mechanical Engineering Congress and Exposition, IMECE 2007, , 4.* pp. 239-246.

Shaver, G. M., Gerdes, J. C., Jain, P., Caton, P. A., & Edwards, C. F. (2003). Modelling for control of HCCI engines. *Proceeding of the 2003 American Control Conference 2003, Volume 1, pp. 749-754.*

Shaver, G. M., Gerdes, J. C., & Roelle, M. (2004). Physics-based closed-loop control of phasing, peak pressure and work output in HCCI engines utilizing variable valve actuation. *Proceedings of the 2004 American Control Conference (AAC), June 30, 2004 - July 2, , 1.* pp. 150-155.

Sher, I., Levinzon-Sher, D., & Sher, E. (2009). Miniaturization limitations of HCCI internal combustion engines. *Applied Thermal Engineering, 29*(2-3), pp. 400-411.

Stock, D. & Bauder, R. (1990). The New Audi 5-Cylinder Turbo Diesel Engine: The First Passenger Car Diesel Engine with Second Generation Direct Injection. *SAE Technical Paper, paper number 900648.*

Szybist, J.P., Bunting, B.G. (2007). The Effects of Fuel Composition and Compression Ratio on Thermal Efficiency in an HCCI Engine. *SAE technical Paper, paper number 2007-01-4076.*

Taylor, C. F. (1985). *The internal combustion engine in theory and practice: Volume II: Combustion, fuels, materials, design*. Cambridge, MA: The M.I.T. Press. ISBN-10: 0262700271.

Thring, R. H. (1989). Homogeneous charge compression ignition (HCCI) engines. *SAE Technical Paper Series, paper number 892068.*

Tian, L., Kittelson, D. B., & Durfee, W. K. (2009). Miniature HCCI free-piston engine compressor for orthosis application. *Proceeding of the Small Engine Technology Conference, paper number 2009-32-0176.*

Tsinoglou, D. N., Koltsakis, G. C., & Jones, J. C. P. (2002). Oxygen storage modeling in three-way catalytic converters. *Industrial & Engineering Chemistry Research, Vol. 41 (5), pp 1152–1165.*

Wilson, R.S., (1975). *The use of non-metallic piston rings as a solution to scuffing, with particular reference to reciprocating compressor experience.* Proceeding of Piston Ring Scuffing Conference, Institution of Mechanical Engineers, London, 13-14 May 1975, pp 15-23.

Winter, D. (2005). *Biomechanics and motor control of human movement, 3rd edition.* Hoboken, NJ: John Wiley & Sons Inc.

Yap, D., Megaritis, A., & Wyszynski, M. L. (2004). An investigation into bioethanol homogeneous charge compression ignition (HCCI) engine operation with residual gas trapping. *Energy and Fuels, 18 (5). pp. 1315-1323.*

Zhou, N., Xie, H., Zhang, Y., Chen, T., & Zhao, H. (2007). Study on control strategy of fully variable valve actuation for HCCI/SI dual-mode gasoline engine.

Neiranji Xuebao/Transactions of CSICE (Chinese Society for Internal Combustion Engines), 25(5), pp. 396-401.

Zhu, M., Liu, Y., Lin, Z., & Peng, X. (1995). *Engineering Thermodynamics*. Beijing, China: Tsinghua University Press. ISBN 7-302-01721-2/TK.18.

Appendix A Review of two-stroke engines

The proposed engine uses two-stroke engine cycle for its simplicity and ease of implementation in miniature scale, compared to four-stroke cycle. Also, free-piston engine requires two-stroke cycle since one powering stroke is needed in every reciprocation of the free-piston, for the engine to continue running. In this chapter, two-stroke cycle engine is reviewed, and its characteristics and design related to the present project are discussed.

Appx. A.1 Engine cycles: Two stroke & four stroke

Most of internal combustion engines run on either a two stroke cycle or a four stroke cycle. The sequences of generalized four stroke and two stroke cycles are illustrated below.

A four stroke cycle (Figure Appx. 1) consists of intake, compression, power and exhaust stroke. In intake stroke, the intake valve opens, thus fresh charge is drawn in while piston moves down. Near bottom dead center (BDC), both intake and exhaust valve close. Then piston moves up to compress the charge to a high pressure and temperature, which is compression stroke. The power stroke is initiated by some sort of ignition, and high pressure inside the cylinder pushes the piston down while doing work. When piston approaches BDC again, exhaust valve opens, and the exhaust is expelled while piston moves up.

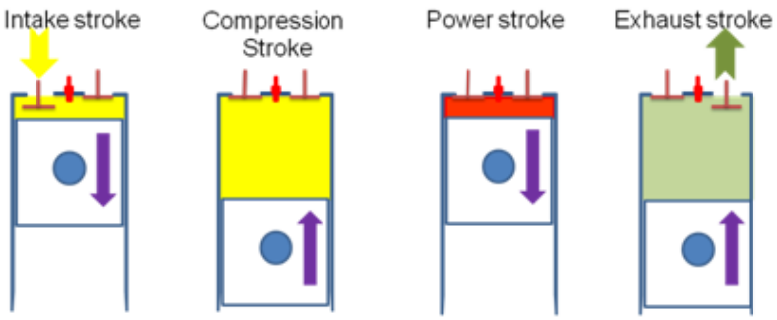

Figure Appx. 1 Four stroke cycle

In a two stroke cycle (Figure Appx. 2), piston moves down and up once, while undergoing four processes: power, blow down, scavenging and compression. The piston moves down after the internal combustion occurs near TDC, while work output is observed on the piston. At some point, the piston uncovers the exhaust port, and high pressure exhaust gas rushes out, which is called 'blow-down'. Soon afterwards, transfer port is also uncovered by the piston. The fresh charge, which is supercharged by some means, enter the cylinder and pushes the exhaust in the cylinder out through exhaust port. The scavenging continues until both intake and exhaust ports are covered by the upwards moving piston. Then compression of in-cylinder charge occurs as piston keeps moving upwards.

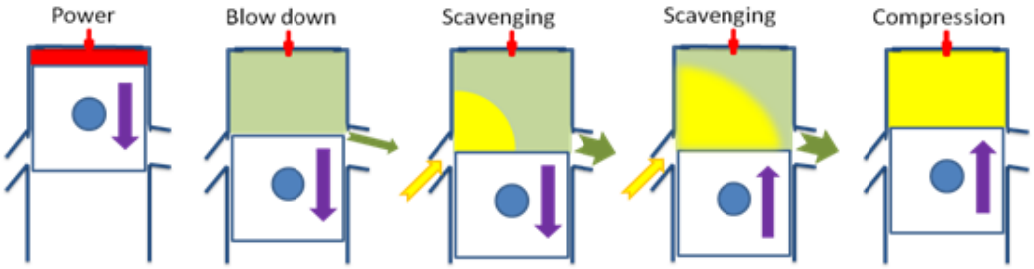

Figure Appx. 2 Two stroke cycle

Appx. A.2 Two stroke engine charging methods

Since the scavenging period occurs while both transfer port and exhaust port are open and the in-cylinder pressure is usually higher than atmosphere, it is required that the fresh charge supplied at scavenge port should be higher pressure than atmosphere. Charging methods include crankcase compression, separate scavenge pump, and special designs like stepped piston and double-piston engine.

In a crankcase compression engine, fresh charge is compressed in the crankcase by the underside of the working piston while all ports are closed. When transfer port is open, pressurized charge rushes into the cylinder through scavenge passages. This concept has the great advantage of simplicity and is preferred for gasoline engines, especially small size engines.

For crankcase compression engine, there needs to be a mechanism of inducing air while the piston moves up and creates a vacuum in the crankcase, and trapping the air inside crankcase when the piston is pressurizing the crankcase. Rotary valve and reed valve systems are the most common designs.

Rotary valve

Figure Appx. 3 shows a case using rotary drum integrated into the crankshaft, which is a common design for model engines. When the crankshaft drives the piston up, creating lower pressure in the crankcase, simultaneously the radial cut-out intake port faces the air intake, and fresh charge is drawn inside the crankcase. After the crankshaft rotates further and the intake port is covered, fresh charge is trapped in the crankcase and compression can begin.

Rotary valve can enable asymmetric induction period. This optimized asymmetric intake phase can result in maximized performance at certain working condition.

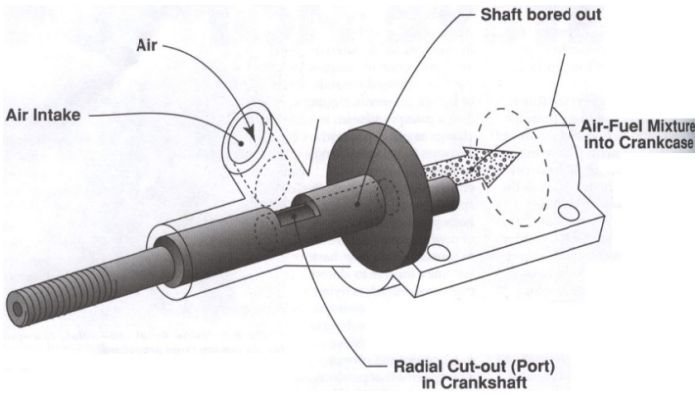

Figure Appx. 3 Rotary valve induction system (Gierke 2007)

However, this configuration is not suitable for this project since rotary component is absent in free-piston linear engine.

Reed valve intake system

Reed valve is a check valve driven by pressure difference. A check valve works as a one-way flow device to control the fresh charge intake into the crankcase, as shown in Figure Appx. 4.

When the piston moves up and creates negative gauge pressure in the crankcase, the reed valve is opened by this pressure difference, and fresh charge can subsequently flow in. After TDC the piston moves down and compresses the crankcase charge. This compression causes a pressure rise which quickly drives the reed to closed position, and fresh charge is thus trapped inside the crankcase.

One of the advantages of reed valve system is that opening and closing are according to the demands of the engine. If properly designed, the reed valve is more efficient throughout its practical speed range. The main disadvantage is that, to allow optimum size reed, a large valve is needed and it takes more space than a rotary valve.

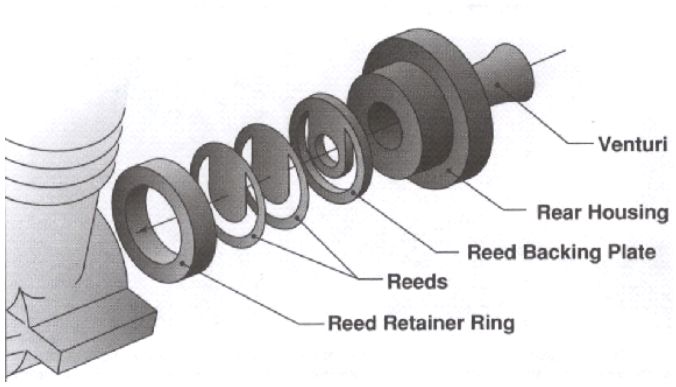

Figure Appx. 4 A typical model engine reed valve induction system (Gierke 2007)

In this project, the crankcase compression and reed valve induction configuration was preferred for optimization of simplicity and feasibility.

Appx. A.3 Two stroke engine scavenging systems

There are several different schemes for replacing exhaust with fresh charge in scavenging period, including cross, loop and uniflow scavenging, as illustrated in Figure Appx. 5.

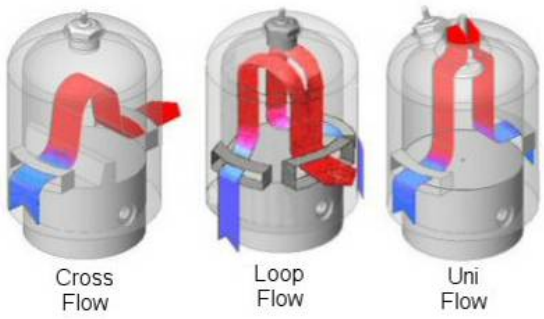

Figure Appx. 5 Scavenging systems of two stroke engines (Gierke 2007)

Cross flow scavenging system has the advantage of simplicity and low manufacturing cost, while suffering poor scavenging at high throttle opening and high speeds, thus with limited application. Loop flow scavenging has relatively good scavenging at all speed and load, with a moderate manufacturing cost, thus is seen in

most small and medium size two-stroke engines. Uniflow scavenging has best scavenging, while penalizing by requirement of additional poppet valves or synchronized opposed piston design, both of which increase complicity and manufacturing cost drastically. As a result, this is often used in large-bore low speed CI two-stroke marine engines.

In this project, loop scavenging is preferred because of its acceptable performance and simplicity. Implementing additional valves are expensive and extremely difficult at miniature scale, which discouraging uniflow scavenging configuration.

In scavenging process, charging efficiency is defined as

$$\eta_c = \frac{\text{mass of delivered charge retained}}{\text{swept volume} \times \text{ambient density}}$$

The denominator is the reference mass related to engine displacement size. Charging efficiency is the indication of how well the cylinder is refreshed with new fuel air mixture after the scavenging.

Delivery ratio is defined as

$$\text{DR} = \frac{\text{mass of delivered charge through transfer ports}}{\text{swept volume} \times \text{ambient density}}$$

Thus delivery ratio is the indication of how much mixture is used through the transfer ports to refresh the cylinder. Some of those delivered charge was retained, counted in the charging efficiency calculation, while some of the charge goes directly out of the exhaust port, i.e. short-circuiting charge. The difference between delivery ratio and charging efficiency is the retention efficiency η_r, which describes how much of delivered charge is retained inside the cylinder:

$$\eta_r = \frac{\eta_c}{\text{DR}}$$

Appx. A.4 Implications of two stroke engines in this project

The intrinsic problems with simple crankcase scavenged two-stroke engines i.e. emission, noise and dirtiness are of concern for this project.

To address these problems, first of all, new approaches should be tried to reduce noise and emission, such as low pressure drop silencers, optimized scavenging and low-odor, non-toxic fuel such as dimethyl ether (DME). Also, alternative applications which have lower Noise, Vibration and Harshness (NVH) and emission requirements than human assistive devices are sought. One of the possible applications is robot application. Current state-of-the-art robot such as HONDA ASIMO robot only has about 30 minutes of battery life. If a hydrocarbon-fuel-IC-engine-fluid-power based power package is used instead of battery-motor package, much longer run-time would be expected due to much higher power density.

Appendix B Prototype hardware problems

In this section, various practical problems encountered during prototype gen II testing are briefly discussed. Major hardware problems included (1) inconsistent starting; (2) rapid wear and piston scuffing; (3) fatigue and failure of several components. Causes of these problems are discussed and possible solutions are proposed in this section.

Appx. B.1 Piston-cylinder clearance, and piston scuffing and wear

Model aircraft engine piston and liner

The prototype gen II utilizes piston and liner from 'AP Hornet .09' model aircraft engines. Material of the piston is hyper-eutectic aluminum alloy, with high silicon content in the alloy for lubricity. The cylinder liner is brass, plated with a thin layer of chrome. This combination of material is known as 'ABC' in model engine industry, short for aluminum piston, brass liner plated with chrome. Dimensions of five model aircraft engine 'ABC' or 'ABN' (aluminum piston, brass liner plated with nickel) type pistons and liners are listed in Table Appx. 1, which shows that nearly all of them have negative clearance around top dead center (TDC) position, and taper off towards bottom dead center (BDC), when the engine is at room temperature. As a result, model aircraft engines are tight to turn over TDC position when they are cold starting. This isn't an issue for model aircraft engine as brutal force is used to turn over crankshaft during start up, and the momentum of crankshaft and flywheel would overcome the tightness during warming up. As the engine warms up, top of liner gets hotter than bottom, thus the heat expansion counters the liner taper, resulting in straight bore and good seal against the piston.

Engine	**Brodak 049**	**AP 09**	**OS 10LA**	**OS 25AX**	**OS 46LA**
Nominal bore (mm)	10.16	12.5	13.44	18.0	23.0

Piston dia (mm)	9.967	12.487	13.399	17.973	22.964
Bore at TDC (mm)	9.970	12.479	13.396	17.971	22.979
Bore at BDC (mm)	9.985	12.520	13.421	18.001	23.005
Liner taper (mm bore increase per m stroke)	1.495	3.417	2.016	1.875	1.413

Table Appx. 1 Dimensions of pistons and liners of model engines at room temperature

The negative tolerance around TDC was a problem for a free-piston engine during starting, as there was no brutal force to overcome the tightness at TDC to achieve needed compression ratio; the only force available during starting up was from the rebound spring, which was not enough to overcome the tightness of negative clearance and achieve high enough compression ratio.

Efforts to find optimum piston-cylinder clearance and finish

To address the negative clearance problem with the chrome plated brass liner, sanding and reamer machining were used to bring the clearance to an appropriate positive value. It should be noted that after sanding or reaming, the piston cylinder fit was good for cold starting. But after the engine warmed up, top of liner got to high temperature resulting in too loose clearance fit, causing inconsistent sealing.

Sanding the top part of the AP .09 engine cylinder liner to 12.51 to 12.52 mm diameter seemed to yield acceptable friction level near TDC while providing good enough sealing between piston and cylinder for starting up and several minutes running. However pistons were found to scuff easily with sanded down cylinder liner. Some scuffed pistons are shown in Figure Appx. 6.

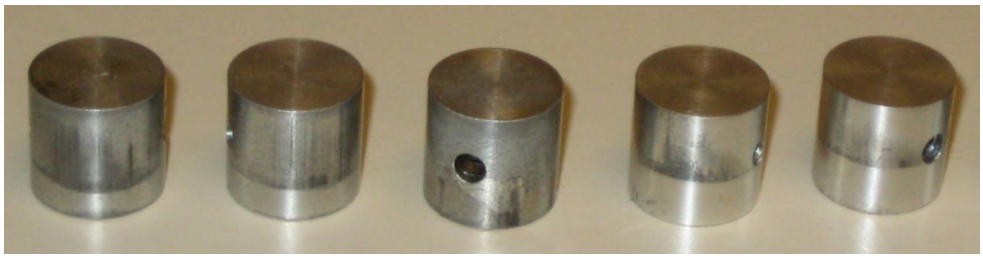

Figure Appx. 6 Some scuffed pistons from running with sanded down cylinder liner in prototype

According to Murray (1975), a smooth surface finish with less than 0.5 μm R_a (the arithmetic average of the absolute values of roughness) is needed to avoid scuffing. Sanding the chrome surface with sand paper proved to be too rough and caused the scuffing. To address this, reaming were attempted with different size reamers of 0.0005 inches (0.0127 mm) increment. The 0.4925 inches (12.510 mm) reamer were found to work well with engine side cylinder liner, and the 0.4930 inches (12.522 mm) reamer were found to work well with compressor side cylinder liner. The reamed chrome surface reduced the scuffing and increased piston life, enabling longest continuous run time of 6 minutes. A example of evenly worn piston with reamed cylinder liner is shown in Figure Appx. 7. However scuffing and piston-cylinder seal deterioration were still present and prevented longer run time. Piston life was found to be 5 to 6 minutes running time at best in the prototype.

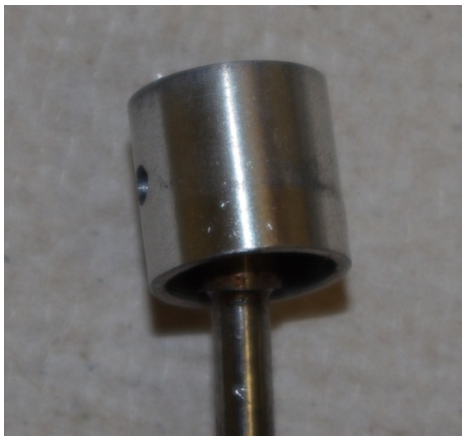

Figure Appx. 7 An evenly worn piston with reamed cylinder liner in prototype

Proposed solution to piston cylinder clearance and scuffing issue

The same material piston and cylinder liner might work better. If cylinder liner is chrome or nickel plated aluminum, the expansion factor of liner and piston can match up better, might result in more consistent seal with cold and hot engine. Some model engines use this combination of material, such as the Brodak .049 MKII RC engine as listed in Table Appx. 1. In those engines, cold engine piston – cylinder liner clearance is positive. There is less clearance change between cold and hot engine thus not needing the negative clearance in cold engines, like the ABC material combination.

Furthermore, PTFE (Polytetrafluoroethylene, or Teflon) material could be good candidate for eliminating compressor side piston scuffing. According to Wilson (1975), filled-PTFE material had been used in reciprocating compressor piston rings with success in both lubricated and non-lubricated condition. If compressor side piston of the prototype is custom made with filled-PTFE and run in non-lubricated condition, considerably better seal could be expected compared to current metal to metal seal. Suggested useful continuous temperature limit of these filled-PTFE material are 150-160 degrees Celsius (Wilson 1975), and as a result this material is not suitable for engine side because of plastic deformation of the material when exposed to higher temperature.

Appx. B.2 Fuel delivery during start up

A major reason of the prototype's inconsistent starting up was the inconsistent fuel delivery during starting up. In-cylinder pressure trace of a typical starting up effort is shown in Figure Appx. 8. In the first five failing attempts (the five groups of spikes before the bulk of high pressure continuous running pressure traces) the

engine fired for two or three cycles but fuel air mixture delivery was not sufficient to keep the engine running. On the sixth attempt in the figure, the fuel air mixture supply was just right to supply enough fuel air mixture during starting up for continuous running. The prototype went through many failed attempts before it could make each of its continuous runs, making starting up the prototype a random act.

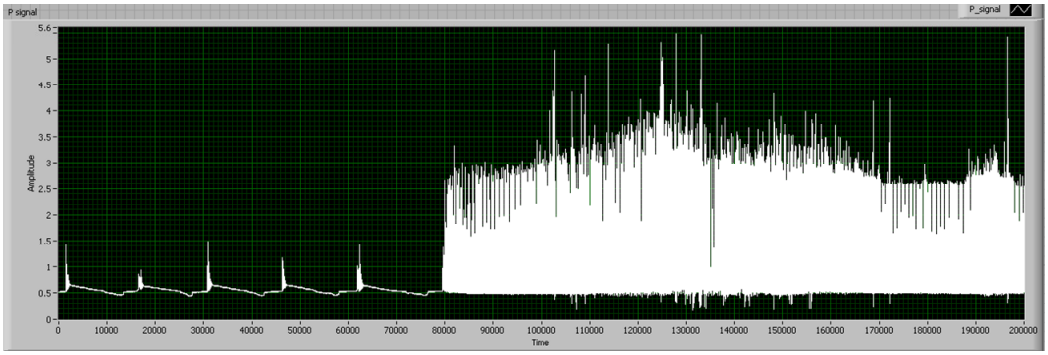

Figure Appx. 8 In-cylinder pressure trace of a typical starting up effort of the prototype

A model aircraft engine carburetor is shown in Figure Appx. 9. Due to its miniature size, the carburetor only has a metering nozzle to regulate fuel flow, lacking other fuel flow regulation devices such as a float bowl or pulsing diaphragm in a full size engine carburetor. In a model aircraft, fuel tank liquid surface level is about the same as the carburetor. When the engine starts, fuel is drawn into the air flow as air flows through the carburetor with velocity.

When the free-piston engine compressor prototype was starting up, air flow through the carburetor was not strong enough to draw fuel, due to the single starting cycle nature of free-piston engine starting. As a result, the fuel tank had to be raised to force feed fuel through metering nozzle into the carburetor Venturi, so that during starting up enough fuel would mix with air flow.

Figure Appx. 9 Model aircraft engine carburetor as used in the prototype

The problem with this 'force feed' set up was that the prototype flooded up easily with several failed starting effort, as fuel flowed continuously during failed starting attempts. When the prototype got flooded, mixture became too rich to start. This delicate balance between 'not enough fuel during starting' and 'too much fuel floods the engine' was a major reason why starting up the prototype was quite random and inconsistent.

Possible ways to address this problem includes; (1) pressurized gaseous fuel might work better in that fuel air mixture doesn't depend heavily on air flow velocity. A proper designed pressurized gaseous fuel carburetor might be able to ensure correct air fuel ratio during starting up of the prototype. (2) A more sophisticated carburetor design with a buffer chamber with air fuel mixture might work to ensure fuel air supply during starting up.

Appx. B.3 Rubber bumper fatigue and crack

As discussed in the energy balance shown in Figure 6-16 in chapter 6, in strong cycles, excess energy could present which was not absorbed by the compressor or the rebound spring. This excess energy was in the form of kinetic energy, meaning that the piston assembly was not slowed down enough towards BDC, risking metal

to metal collision between piston assembly and compressor block. An early testing of prototype bent connecting rod handle from metal to metal collision as shown in Figure Appx. 10.

Figure Appx. 10 New (left) and bent (right) connecting rod handles

To address this issue rubber bumpers were designed to cushion the collision in the case of piston over-stroking, as discussed earlier in chapter 6. However, these bumpers still suffers fatigue problem. During starting up the compressor was not loaded, yielding strongest collision onto the bumper. The rubber bumpers were found to survive through one or two starting up at most, as shown in Figure Appx. 11.

Figure Appx. 11 Several cracked rubber bumper in the prototype

Possible solution to the rubber bumper fatigue include (1) replacing the rubber with a stiff spring. Spring does not absorb much energy, but will return most of the

energy to the next cycle's compression process; (2) designing a separate air spring chamber just to stop the piston assembly before metal to metal collision.

Appx. B.4 Compressor valve fatigue

The prototype compressor check valves were fabricated from thin stainless steel foils. They suffered fatigue problems and would crack after minutes of run time, as shown in Figure Appx. 12. The fatigue and crack was due to three reasons: (1) a valve stop was not designed for this reed check valve resulting in too much valve travel; (2) the design of the output check valve resulted in a spot of concentrated stress which initiated the cracking; (3) some lubrication oil and fuel leaked into the compressor during running, resulting in fluid flow out through the output check valve, exaggerating valve deformation.

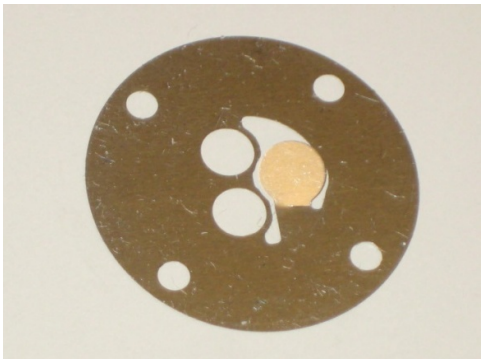

Figure Appx. 12 A cracked compressor output valve

Solution to this problem includes (1) A valve stop needs to be designed for this reed check valve; (2) valve needs to be re-designed to avoid stress concentration; (3) The compressor piston should be custom fabricated from filled-PTFE material and run dry, so that no lubrication oil or fuel would go through the output check valve.

Appx. B.5 Spring sag

The rebound spring was found to shrink about 0.1 inches after running, as shown in Figure Appx. 13. The spring length was found to stay in the sagged value quite well after 10 minutes accumulated running time. As a result, the spring fatigue was probably not affecting the prototype performance considerably other than slightly decreased rebound energy after the spring sagged.

Figure Appx. 13 A new rebound spring (left) and one with 2 minutes run time (right)

Appendix C List of materials and parts in experiments

Listed below is a table of some materials and parts used in experimental studies in this thesis project for future references.

Description	Notes	Material and part used
Laser triangulation sensor	Used in prototype testing for measuring piston position. Speed up to 40k Hz	MTI Instrument LTC-120-20-SA
In-cylinder pressure transducer	Optic type pressure transducer. M3.5 thread for miniature size sensor head	OPTRAND AutoPSI-TC sensor, model D22255-Q
Adjustable pressure maintaining aluminum relief valve	Used to maintain and adjust reservoir air tank pressure for steady state running	. McMaster part number 4783K51
Piston, cylinder liner sleeve and carburetor	These off-shelf components were used in prototype	AP Hornet 09 R/C engine
Model engine reed intake valve	This reed intake valve was used to control intake into crankcase. Valve housing was custom designed.	COX TeeDee 049 engine
Prototype rebound spring	Rebound spring in prototype. Grounded ends.	Century Springs Corp, part number 71932S
Prototype compressor check valve stainless steel foil stock	Various thickness stainless steel foil were ordered to EDM cut check valves. 0.004 inches thickness seemed to work best	Ordered by UMN EE machine shop, most probably from McMaster
Prototype double jaw crankcase seal	Fabricated from PEEK material which is a good composite bearing material	Same as above
Prototype tungsten dead weight	Fabricated from tungsten alloy rod stock	High-Strength Durable Tungsten, Mcmaster P/N

		8279K24
Reamer	Used to machine out cylinder liner sleeve for positive clearance with piston	High-Speed Steel and Cobalt Steel Chucking Reamers, McMaster P/N 8803A72
Prototype compressor output pipe air check valve	Used to prevent leak from reservoir air tank pressure through compressor high speed check valve	Plastic Check Valves with Barbed Tube Fittings and Buna-N Seal, McMaster P/N 6079T56
Small air reservoir	0.1 liter small reservoir. Was be too small resulting in rapid pressure change and engine stalling	FESTO CRVZS-0.1 P/N 160233
Prototype test fuel	Model glow ignition engine fuel, methanol based	SIG Champion glow fuel, 25% nitro content
Prototype glow plug	Off-shelf model aircraft engine glow plug	McCOY glow plug, model MC-59
Prototype rubber bumper rod	60a durometer rubber rod. Cut to appropriate length	McMaster P/N 9027K112
Prototype compressor head bolt	M2.5x20 mm, socket head	
Bolts for compressor block to engine block	M2x0.4x10 mm, pan head	
Bolts for carburetor block	M2x0.4 bolts	
Encoder disk	Used for crankshaft angle measurement during model aircraft engine testing	US Digital, HUBDISK-1-100-315-I and
Encoder module	Encoder module to use with the encoder disk	US Digital Transmissive Optical Encoder Module HEDS-9140-C00
Helical beam coupling	Used to couple test model engine crankshaft to dyno brake	Helical beam clamp-on shaft coupling, McMaster P/N 2463K305
Dual-load angular	Used to support torque arm	McMaster P/N 6680K12

contact ball bearing	during crankshaft engine testing	
Hysteresis dynamometer brake	Used to put load on model aircraft engine's crankshaft during testing	Magtrol Inc. HB-50M hysteresis brake
Variable DC power supply	Used to supply variable current to the hysteresis brake for torque adjustment	Tektronix PS 281 DC power supply
Data acquisition card	Desktop computer PCI interface data acquisition card with connector panel	National Instrument PCI-6143
Digital bench scale	Used to measure torque from the torque arm during model engine testing	McMaster P/N 1760T9
NEMA 34 face-mount brushless DC motor	Used to motor the prototype for motoring testing at various adjustable speeds. 1/3 hp, 3450 rpm, integrated speed control	McMaster P/N 7200K3
Trapezoidal tooth urethane timing belt	Used to connect two pulleys of 3:1 teeth ratio to motor a model engine to various speeds up to 10000rpm	McMaster P/N 1679K33
Acetal Pulley for XL-Series Timing-Belt	60 teeth and 20 teeth pulleys to construct 3:1 ratio drive from the NEMA motor	McMaster P/N 57105K33 and 57105K18

Appendix D Pictures of test benches

Figure Appx. 14 is a picture of the model aircraft engine test bench shown as a line drawing in Figure 4-2.

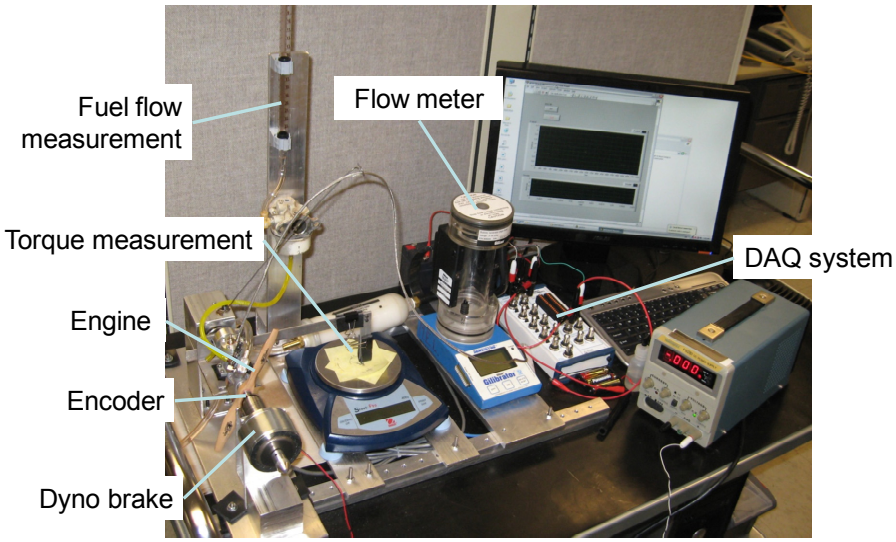

Figure Appx. 14 Model engine test bench

Figure Appx. 15 is a picture of the model engine motoring test bench shown as a line drawing in Figure 4-3.

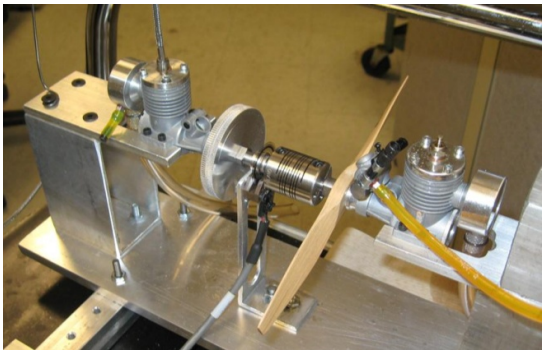

Figure Appx. 15 Picture of model engine motoring bench

Figure Appx. 16 is a test bench built for testing whether the prototype compressor worked. An electric motor was used to motor a model engine at high speed, with the prototype compressor mounted on the model engine block.

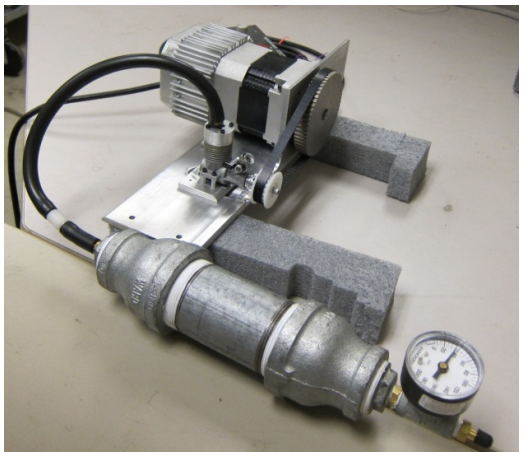

Figure Appx. 16 Prototype compressor testing apparatus

Figure Appx. 17 is a picture of the prototype experimental testing apparatus shown as a line drawing in Figure 6-9.

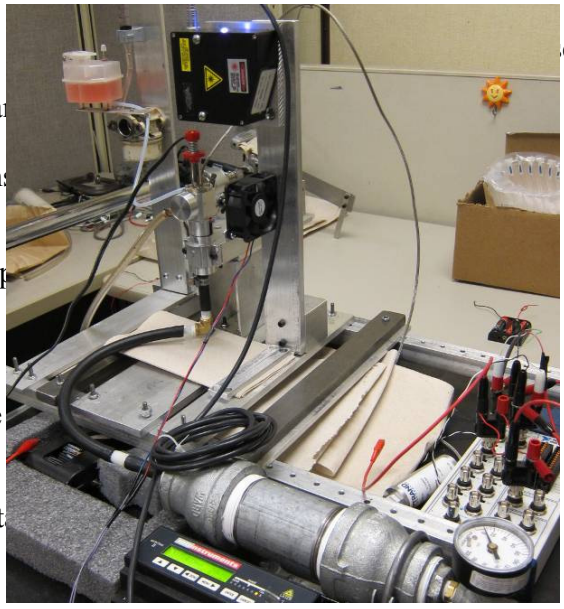

Figure Appx. 17 Prototype experimental testing apparatus

Figure Appx. 18 is a setup for testing the prototype in a standalone package. The fuel tank and the engine compressor prototype were mounted on an aluminum stand. The fuel and engine compressor package weights about 700 grams. Some FESTO L shape fittings were used so that the pipes could rotate at any angle while maintaining good seal. Although the amount of fuel in the small tank was estimated to be good for 40 minutes run time based on fuel consumption rate, the prototype only managed to achieve about 6 minutes continuous run time due to wear and sealing problems.

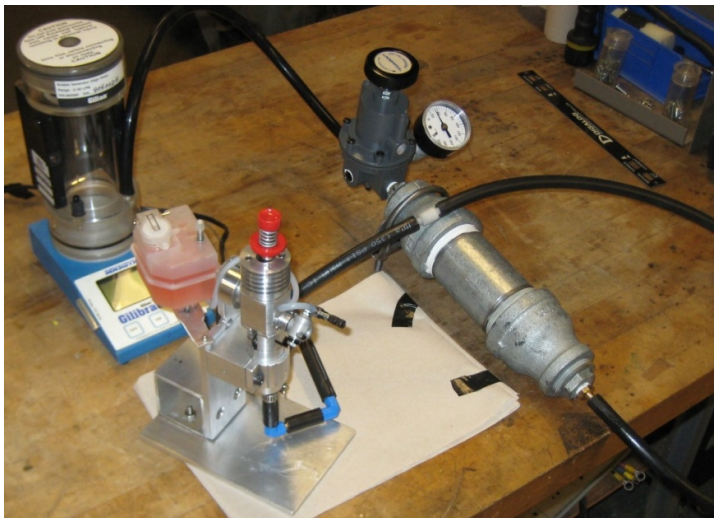

Figure Appx. 18 Standalone testing of prototype

Appendix E Prototype standard operating procedure

For reference purpose, the standard operating procedure for starting and testing the miniature free-piston engine compressor prototype is described in this appendix section.

Appx. E.1 Standard operating procedure: background:

The miniature HCCI free-piston engine compressor is a prototype being developed to provide 10W of compressed air for human scale pneumatic devices such as orthosis, robots and power tools. The prototype utilize free-piston configuration. The engine piston is not connected to a crankshaft to convert its reciprocating motion to rotary motion. Instead, it's directly connected to the compressor piston which extracts useful work. As a result, the pistons motion is determined by force balance instead of mechanical constraint. The downward motion of the pistons is driven by the engine cylinder mixture combustion and expansion, while the upward motion is mainly driven by the rebound spring force.

Various instruments are used to characterize the prototype operation. A high bandwidth, high resolution laser triangulation sensor is used to measure piston position (MTI Instrument, model LTC-120-20-SA). A small optical pressure sensor was used to measure in-cylinder pressure (OPTRAND, model D22255-Q). Fuel flow rate is measured by a graduated cylinder, connected to the engine through a float bowl of a big carburetor to maintain constant fuel pressure at the engine carburetor intake. Engine intake air flow rate is measured by a bubble flow meter (Gilibrator). The compressor output was connected to a 530mL air tank through an additional check valve to prevent slow leakage through the compressor output valve. Air tank pressure is read visually on a pressure gauge.

The prototype test bench is mounted on a lab cart and can be moved when necessary.

Appx. E.2 Standard operating procedure: experimental Procedures:

The procedures for running the miniature free-piston engine compressor prototype are described below.

- Prototype rebuilding

As the prototype is still in early stages of development, it needs a rebuild before every start.

1. Disassemble the prototype.
2. Replace the connection rod handle rubber bumper with new rubber rod bumpers (cut from 1/8 inch O.D. 50a rubber rod).
3. Inspect engine piston wear. If there are obvious scuff marks on the piston, replace with a new piston (off-shelf aluminum piston from AP 09 model aircraft engine).
4. Inspect metal rebound spring. Replace if the spring free length shrinks to less than 1.6" due to fatigue (original length 1.75").
5. Inspect compressor intake and output reed check valves. Replace if deformation is observed.
6. Inspect connecting rod, starting handle and compressor piston for deformation. If any of them are bent due to metal-to-metal collision, appropriate measures need to be taken.
7. Inspect glow plug on the engine side for carbon deposit. Make sure the platinum wire glow orange or red when connected to 1.5V DC.
8. Lubricate the pistons with oil, and assemble the rebuilt prototype.

- Test bench initiation

1. Power on computer and load measurement VI file in LabVIEW.
2. Power on the laser sensor (12V DC). Make sure the laser points at the starting handle. Adjust the sensor body mount if necessary.
3. Power on the pressure transducer (12V DC).
4. Fill the graduated cylinder with glow engine fuel. Fuel level in the graduated cylinder will drop to fill the big float bowl carburetor. Fill up until the level is around the top of the graduated cylinder.

5. Open the prototype engine carburetor needle valve to 4 turns. Pinch the fuel line to get rid of air bubbles. When the fuel line is filled with fuel, close the needle valve.
6. Connect the glow plug adapter to the prototype engine glow plug.
7. If air intake flow rate is measured, connect piping and prepare the bubble flow meter.
8. Connect prototype engine compressor side output port to the air tank.

- Engine Startup

1. Connect 1.5V DC supply to the glow plug adapter.
2. Turn the engine carburetor to 4 turns.
3. Cycle the piston using the starting handles, to fill the crankcase with fuel air mixture. After a few cycles, occasional explosion can be felt on the starting handle.
4. Pull the starting handle to the fully compressor position and suddenly release, to initiate the first cycle. The prototype might fire for several cycles and stall. After several tries, the prototype should start successfully.
5. After the prototype starts running, the glow plug power supply can be disconnected.
6. Watch and adjust the air tank pressure. It should not exceed 7 bar gauge.

- Normal Shutdown

Close the engine carburetor needle valve. The prototype will stall immediately.

- Emergency Shutdown

The prototype emergency shutdown has not been implemented yet. A solenoid shut off valve in the fuel line leading to the carburetor could be designed to function as emergency shutoff switch.

Appx. E.3 Standard operating procedure: hazard Identification:

Chemical: Glow model engine fuel

Glow model engine fuel consists of 55% methanol, 25% nitromethane, 20% lubrication oil. It is dyed to red/orange color.

Methanol

Physical-Chemical Properties

- CAS# 67-56-1
- Molecular formula CH3OH (Methanol)
- Molecular weight 32
- Form Liquid
- Solubility Soluble in water
- Volatility Volatile
- Other _____

Toxicity

- Acute effects Toxic
- Chronic effects _____
- Local effects _____
- Systemic effects _____

Nitromethane

Physical-Chemical Properties

- CAS# 75-52-5
- Molecular formula CH3NO2
- Molecular weight 61
- Form colorless liquid
- Solubility _____
- Volatility No
- Other _____

Toxicity

- Acute effects N/A
- Chronic effects _____
- Local effects _____
- Systemic effects _____

Appx. E.4 Exposure Assessment:

Route

- Inhalation: It is possible that engine exhaust fumes or calibration gases may leak into the laboratory room and be inhaled by inhabitants.
- Skin/eye absorption Fuel spill
- Accidental ingestion Fuel spill
- Accidental injection _____

Duration

- frequency _____
- length _____

Appx. E.5 Control Plan:

- Always wear safety glasses in the lab. Normal eyeglasses are acceptable if no engines are operational in the laboratory room.
- Only run in well ventilated room that can handle the exhaust fumes. Use exhaust fans when possible.
- Wear ear protection when engine is operating or if other experiments are running in the laboratory room.
- No eating or drinking in the lab.
- Wear nitrile gloves when handling used engine oil or fuels